Design and Realisation of a Monitoring System for Wire-Arc Additive Manufacturing

Xu, Fangda

Award date:
2020

Awarding institution:
University of Bath

Design and Realisation of a Monitoring System for Wire-Arc Additive Manufacturing

Fangda Xu

A thesis submitted for the degree of Doctor of Philosophy

University of Bath

Department of Mechanical Engineering

November 2019

Abstract

Additive manufacturing (AM) has been growing at a significant rate over the last ten years. During this period, the process has moved from the prototyping of plastic and metal components to the generation of the industrial parts used in actual products. The major focus of AM has predominantly been related to powder-bed complex components, but the use of direct energy deposition (DED) processes is now becoming widely prevalent. This thesis focuses on research related to a DED process namely wire arc additive manufacturing (WAAM) and specifically the monitoring of the WAAM process for large scale components.

The aim of this research is to define and realize a monitoring framework for the WAAM processes which can be generically applied to different WAAM machines. Based on this aim a framework and monitoring system has been generated consisting of 3 sub-systems namely, Environment Monitoring Sub-system, Heat Monitoring Sub-system and Bead Geometry Monitoring Sub-system. These three sub-systems contain a suite of sensors that provide the ability to monitor oxygen level, argon gas flow rate, arc voltage, arc current, temperature of the part and geometric profile of the top and the side of the WAAM parts produced.

A set of three experiment has been devised to test the performance of the WAAM monitoring system. These evaluate the effectiveness of the system with validation of the voltage and current collected from the sensors, monitoring the process data and monitoring of the geometric shape of the WAAM part produced. This showed that the monitoring was able to precisely represent the WAAM process and provide a geometric accuracy of 0.01mm.

The WAAM monitoring system developed in this thesis has been shown to have the ability to monitor, record and analyse the major output of the WAAM processes. The system has been shown to provide rapid feedback at 5Hz that makes it possible to monitor the WAAM process in real time with the generation of repeatable high quality parts.

Acknowledgements

I would like to express my gratitude to Dr Vimal Dhokia for his continuous encouragement, insightful comments and for his patience. His guidance and motivation helped me all the way through this research for this PhD's thesis

I would also like to express my deepest thanks to Professor Stephen T Newman for his enthusiasm, inspiration and endless supervision. He has been patient with me all the way long through the development of this work and without his guidance this work would not have been possible.

I would also like to extend my thanks to all those who provided collegial guidance over the years especially in AMPS team. Chloe Cunningham, Dr Laura Asensio Dominguez, Dr Alborz Shokrani and Dr Joseph Flynn.

In addition, I would like to thank the following staff for their support from Airbus, namely Andrew Henstridge, David Steer and Stephen Porter; Cranfield University namely Dr Anthony McAndrew, Dr. Paul Colegrove , Dr. Jiaoluo Ding and Prof. Stewart Williams; Prof. Junqiang Wang from Northwestern Polytechnical University; Dr. Jiarui Lin and Dr. Linghui Yang from Tianjin University; , Dr. Tao Wang from Beijing Institute of Technology; Dr. Nan Yu from University College Dublin and Dr. Yingtao Tian from Lancaster University.

Finally, I would like to thank my family, specifically both my Mother and Father for their continuous support throughout my life and career.

Contents

List of Abbreviations

AM	Additive Manufacturing
B&W	Babcock And Wilcox Co.
DED	Direct Energy Deposition
DoF	Degrees of Freedom
DIC	Digital Image Correlation
EBF3	Electron Beam Freeform Fabrication
FEA	Finite Element Analysis
FFT	Fast Fourier Transform
GMAW	Gas Metal Arc Welding
GTAW	Gas Tungsten Arc Welding
HiVE	High Value Engineering
ILC	Iterative Learning Control
ICP	Iterative Closest Point
MAT	Medial Axis Transformation
PAW	Plasma Arc Welding
PBF	Powder Bed Fusion
PCL	Point Cloud Library
RAPOLAC	Rapid Production of Large Aerospace Components
RUAM	Ready to Use Additive Manufacturing
SEM	Scanning electron microscope
SMAW	Shielded Metal Arc Welding
SMD	Shaped Metal Deposition
TEM	Transmission electron microscopy
TS	Travelling Speed
WAAM	Wire Arc Additive Manufacturing
WFS	Wire Feed Speed
X-ray CT	X-ray Computed tomography

List of Figures

List of Tables

Chapter 1

Introduction

Over the past 30 years, Additive Manufacturing (AM) technology has been continually developing. From its original applications using polymers for prototype parts, it is now being used as a process for generating near net shaped metal components with increasing levels of complexity. These new AM processes enable components to be designed and manufactured with complex internal structures from snake like ducting to highly dematerialized lattices (Hussein et al. 2013).

Today, AM has the largest growth rate of any manufacturing process with predictions of its value estimated to be over $30 Billion by 2022 (Wohlers Report, 2016). In metal AM, the most common form is powder bed fusion (PBF) technology, which accounts for the large majority of components produced. However, new forms of metal AM technology are still emerging, especially in the area of Direct Energy Deposition (DED) (Frazier, 2014). This thesis focuses on research related to an emerging DED process namely, Wire Arc Additive Manufacturing (WAAM) which is rapidly evolving as a new method to manufacture large scale structures.

WAAM has been developed from welding technology. It uses a welding torch as a heat source to melt metal and deposit metal layer-by-layer to produce a part. This process is a very complicated process that incorporates physical changes, chemical reaction, high-temperature material phase change, heat induced stress etc. Thus, to develop a reliable and consistent WAAM process which is ready-to-use level is not trivial. Irregular distortion, lack of fusion and porosity are commonly reported issues in WAAM. These defects are only a part of all challenges in the WAAM process. In order to tackle these problems, it is vital to be able to

sense the defects, to record the process and to develop a method to understand and quantify the problems during the process. This prompts the need for robust process control and monitoring framework for WAAM.

The aim of this research is to explore methods to monitor the WAAM process, create a generic monitoring framework and implement a monitoring system to identify defects and layer deformations during the WAAM part building process.

1.1 Context for the Research

The research reported in this thesis has been carried out by the author while being employed as Research Assistant for 3 years on two Innovate UK funded research projects namely RAWFEED – Rolling Assisted Wired Feed Direct Deposition for Production of High Value Aerospace Components (RAWFEED, 2016) and the OAAM – Open Architecture Additive Manufacturing project (OAAM, 2019). During these projects the author's research was undertaken on a WAAM HiVE machine based at Cranfield University (Bedford) and Glenalmond group ltd (Glasgow) (described in chapter 5) away from the University on an intermittent basis with the overall projects' goal to enable the machine to produced quality assured WAAM components.

1.2 Structure of the thesis

The rest of this thesis is organized as follows. Chapter 2 provides a comprehensive review of WAAM together with process monitoring and control literature. Chapter 3 describes the scope of the research with research boundaries, a research aim and objectives. Chapter 4 describes a framework for the design of a monitoring system for WAAM, with chapter 5 describing the realization of the actual system based on this framework. A series of experiments using the WAAM monitoring system are presented in chapter 6, with analysis of results from the

monitoring system. Chapter 7 discusses the various aspects of the research in comparison to the state-of-the-art. The final chapter provides the conclusions and areas for future work.

Chapter 2

Scope of Research

2.1 Introduction

This chapter introduces the major research issues existing in WAAM monitoring and defines the aim and objectives of this research. The latter part of the chapter defines the research boundaries and the research gaps.

2.2 Research Aim

The aim of this research, as stated in the introduction, is to explore methods to monitor the WAAM process, create a generic monitoring framework and implement a monitoring system to identify defects and layer deformations during the WAAM part building process.

2.3 Research Objectives

(i) To comprehensively review the state-of-the-art in the wire arc additive manufacturing processes, and its monitoring & control methods.

(ii) To identify the requirement for a WAAM monitoring system for large-scale component manufacturing.

(iii) To specify, design and realise a WAAM monitoring system for a large-scale WAAM machine.

(iv) To evaluate the WAAM monitoring systems through a series of experiments on an industrial WAAM machine to enable consistent geometric and quality assured part manufacture.

(v) To identify the WAAM monitoring performance measures and compare these through the results from a set of WAAM experiments outlined in section 6.2.

2.4 Areas of Investigation

(i) Review of the WAAM literature: A review of the WAAM literature will be undertaken firstly to identify and clarify the major WAAM processes and their capabilities. This will be then expanded to focus on the monitoring and modelling of the WAAM process. The final part will report industrial WAAM systems in order to generate a critique and identify research gaps in WAAM process monitoring.

(ii) Specification and design of a WAAM monitoring framework: Based on the literature the requirements for process monitoring will be explored and a framework specified and proposed to identify the performance indicators which influence the WAAM process. The goal of this framework is to provide a generic structure that can be applied to any WAAM machine and process.

(iii) WAAM Process Monitoring System: Based on the framework a monitoring system will be realized and implemented onto a WAAM machine. It is expected that the system will consist of multiple sensors based on the key performance indicators identified in the framework.

(iv) WAAM monitoring system evaluation: A number of test experiments will be devised to evaluate the performance of the WAAM monitoring system so that it generates appropriate results consistently with the WAAM process. The experiments will aim to test the system's performance and capability.

(v) Experimental Evaluation: The WAAM monitoring systems overall performance will be evaluated from a number of experiments through building of example WAAM parts. These experiments will be used to identify inaccuracies in the deposition process

together with other possible process errors. A comparison of the results from the WAAM system will identify relationships between the various monitored sensors and should provide enable rapid feedback on the WAAM process.

2.5 Research Boundaries

The research is related to several areas, as shown in Figure 2-1 The rectangle shows the relevant research areas namely: additive manufacturing process, heat source, monitoring parameters and complexity of part geometry. The inner circle shows the core boundaries for this research.

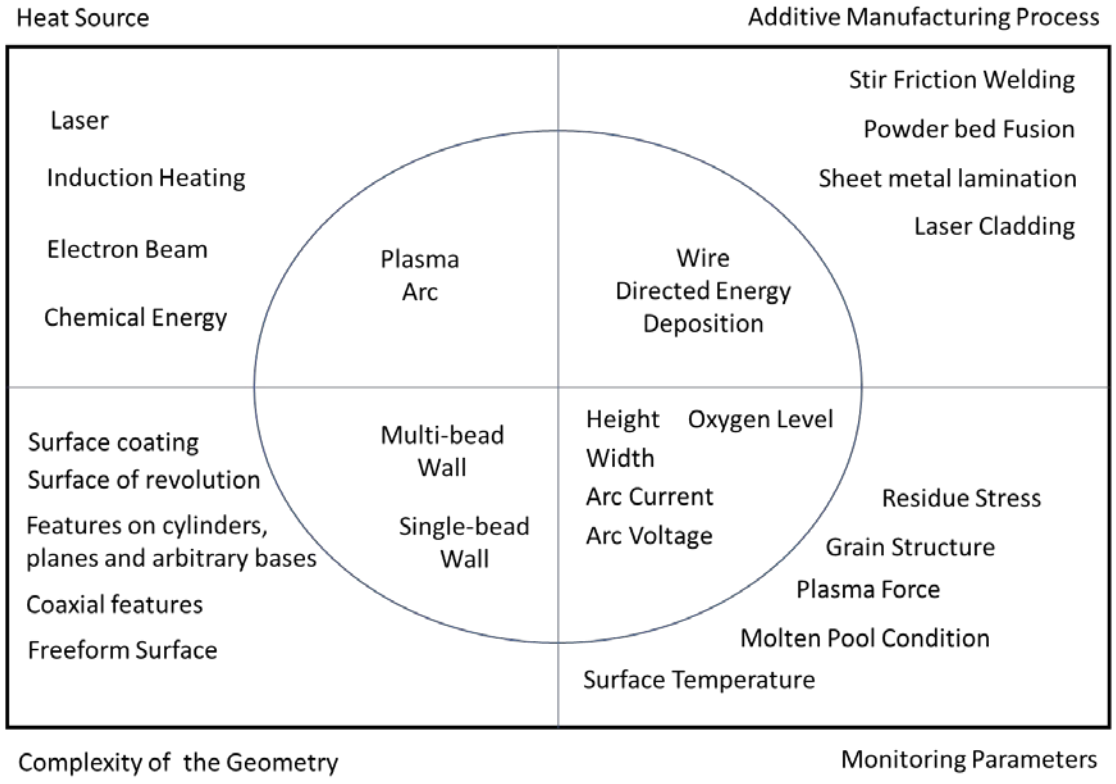

Figure 2-1Research Boundary

i) Additive manufacturing processes

This research is only focused on DED processes, and more specifically with wire feedstock. However, some ideas in this research also are learnt and adapted from other processes such as, laser cladding, stir friction welding, GTAW and GMAW welding, etc.

ii) Heat Source

In the Wire-DED processes, there are three major recognized heat sources, namely laser, electron beam and plasma arc. The wire arc additive manufacturing is based on plasma arc heat source. These three heat sources have their own advantages disadvantages. The laser has a high power density and is easy to control. However, its heat transfer efficiency might be a deficiency on some high reflective metals such as aluminium and copper (Taminger and Hafley 2003). Electron beam has been used for additive manufacturing since 2007, but the process requires a vacuum chamber to work in. Compared to these two processes, plasma arc has relatively less limitations as it is able to work in the open atmosphere (with local protection gas for the purpose of anti-oxidization of parts being printed).

iii) Complexity of the Geometry

This research focuses on the multi-bead wall and single-bead wall. This kind of 2.5D extraction geometry provides a simple environment for process monitoring. Process monitoring for other complex geometry will be developed in further work.

iv) Monitoring Parameters

This research focuses on the relationship between WAAM process parameters and the WAAM part geometry. The welding torch condition and parameters related to it are not monitored. The molten pool condition is also excluded from this research.

2.6 Research Gaps

The emergence of WAAM has the potential to provide industry with the capability to produce large parts rapidly and at low cost when compared to traditional manufacturing methods. Nevertheless, current WAAM systems are still heavily reliant on user expertise, know-how and human selected parameters. This is due to a lack of knowledge on the process input and output.

There is a need for a new method to inspect, analyse and control the WAAM process. AWAAM monitoring system will enable consistent part generation increasing the quality of build geometry.

2.7 Research Methodology

The following methodology illustrated in Figure 2-2 consists of three stages undertaken during the research process. These stages are described in the thesis section numbers shown on the Figure 2-2.

The first stage after undertaking a literature review of WAAM, is to define the objectives of the WAAM monitoring system in this thesis (section 4.2), and to analyse the WAAM process(section 4.3) in order to identify the critical monitoring parameters that influence the accuracy of the built WAAM parts(section 4.4). In addition, the monitoring level needs to be determined, as it may affect the system performance and the corresponding cost (section 4.5). Based on these parameters a process monitoring framework has been proposed to enable real-time monitoring of the WAAM process during each layer deposition (section 4.6). The output of this chapter is the design of the WAAM monitoring system.

The second stage is the design of this process monitoring system, an implementation on a real machine. The WAAM platform that has been used is introduced and analysed in section 5.2. The sensor selection is discussed in Section 5.3, and the hardware setup of the complete multi-sensor monitoring system is introduced in section 5.4. The technical detail on how to process the signals and data is introduced in section 5.5.

The final stage introduces the results and evaluation of the multi-sensor system. Three experiments are designed to validate and evaluate the performance of the system. The aims of these three experiments are introduced in section 6.2. The experimental results and the subsequent analysis are introduced in section 6.3, 6.4 and 6.5. This overall methodology has

been completed and the individual elements discussed in chapter 7 and conclusions outlined in chapter 8.

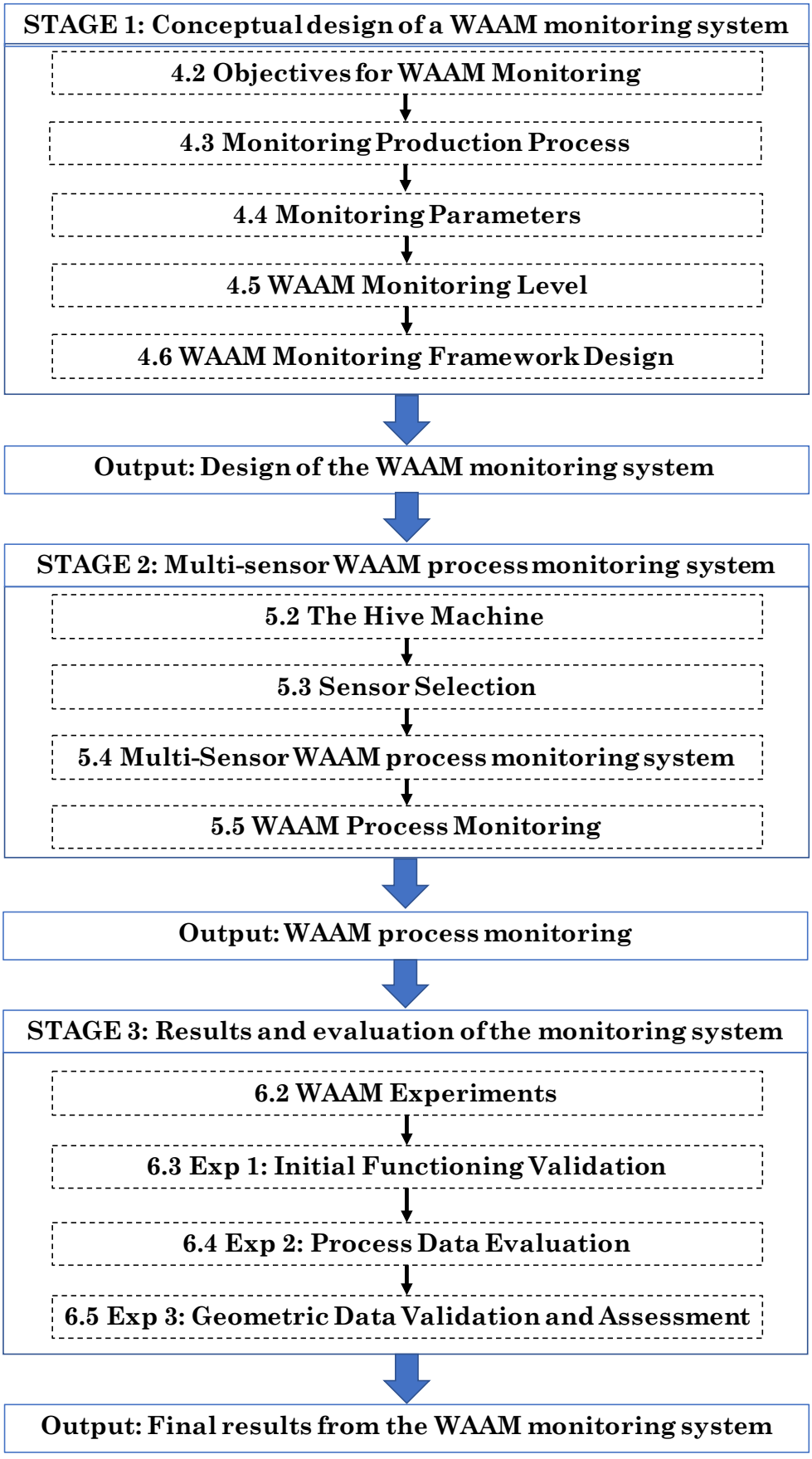

Figure 2-2 Research Methodology

Chapter 3

Literature Review on WAAM

3.1 Introduction

This chapter provides a review of the literature related to Wire-Arc additive Manufacture (WAAM). It consists of 6 major sections. The first section is an introduction, and the second section provides an overview of the WAAM processes, followed by a brief history of WAAM. Section 4 focuses on the challenges in WAAM monitoring and control with section 5 providing industrial developments in WAAM, with the final section providing a critical review of the WAAM literature.

3.2 WAAM and Relevant Processes

BS ISO/ASTM 52900 (BSI, 2015) classifies additive manufacturing into seven types. For these seven types, four of them can be used for metal, namely Binder Jetting, Sheet Lamination, Powder Bed Fusion (PBF) and Directed Energy Deposition (DED). The other three types, namely VAT Photopolymerisation, Material Jetting and Material Extrusion are mainly used for polymer printing. WAAM belongs to the Direct Energy Deposition (DED) family. By definition, DED is a series of processes using focused thermal energy to fuse and melt metal feedstock whilst being deposited (BSI, 2015). Depending on the form of the feedstock, DED is categorized into powder-DED and wire-DED.

Wire-DED mainly has three types of heat source, namely laser based, electron-beam based and arc based. Arc-based wire-DED is also termed as wire arc additive manufacturing (WAAM). These three types of techniques originate from welding techniques and use the principles of welding to generate a melt pool. However, their working requirements and energy

transfer efficiencies are different. Laser-based wire-DED is the most widely adopted due to its precision (Ding et al. 2015). The main weaknesses of Laser based wire-DED is the high price of the high-power laser source and the low energy transfer efficiency (less than 10%) (Unocic and DoPont 2004). For some highly reflective materials, such as copper and aluminium, the energy efficiency of the laser-based process could be as low as 2% (Taminger and Hafley 2003). In 2007, researchers at NASA Langley Research Centre invented a new technique named Electron Beam Freeform Fabrication (EBF3), the only e-beam wire-DED process till now, which is able to fabricate reflective material with high energy usage (Taminger et al. 2004). The inventors, Taminger and Robert (2004) claimed that EBF3 is able to achieve 95% power efficiency, and nearly 100% feedstock consumption efficiency. However, EBF3 also has its own weakness. Due to the intrinsic property of e-beam heat source, EBF3 is limited to run in a vacuum chamber. This makes EBF3 less flexible. In addition, the EBF3 machine is relatively expensive due to the high price of its high-power electron beam source.

The machining margin for WAAM is 5mm, in which 3mm for roughing and 2mm for finishing. For forging, the designer often specifies a envelop of 5mm-10mm due to the occurrence of surface effect in the forging process such as oxidization and surface stress (Thomas and Gilbert 2014). In addition, the lead time for forging could be longer than 10 months to 20 months, whereas WAAM processes could finish in several weeks.

WAAM, as a welding based wired DED process, is a considerable largely promising deposition technique due to its simplicity and high efficiency of metal transfer. It applies a generic arc welder as its heat source to melt metal wire and to deposit metal on a substrate. DuPont and Marder (1995) conducted a series of experiments and found that the power efficiency of arc welding varies between 40% to 90%. Considering the relatively low cost of the general arc welding system (around £30k, by Williams, et al. 2015) and the high-power efficiency, WAAM is regarded as a promising player in wire-DED.

3.3 Brief History of WAAM

WAAM is known as a method of using welding techniques to construct metal components. The first time people proposed this kind of idea was in 1920, when an American named Baker (1920) proposed a method of making metal decorative components with welding in his patent (Baker 1920). As shown in Figure 3-1, Baker showed two demonstration metal receptacles made with hand-held shielded metal arc welding (SMAW). At that time, Baker already realized that this technique would enable a wide range of metal design and manipulation.

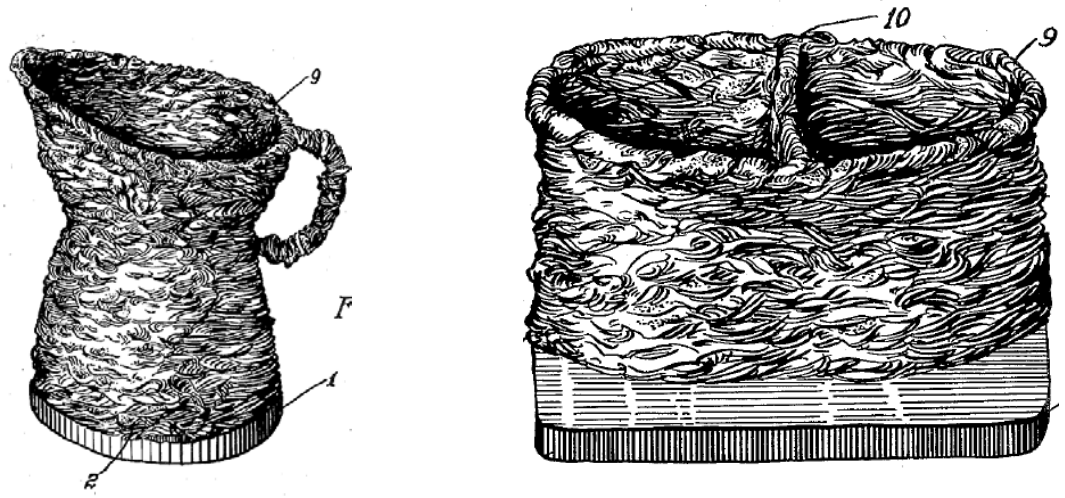

Figure 3-1 Deposited Metal Receptacle Made by manual welding process (Baker 1920)

In the 1980s, Babcock and Wilcox co. (B&W) made a great effort in WAAM which was then termed as Shape Melting. The major contribution of B&W was on temperature control and automation of the shape melting process. (Ayres et al. 1988, Doyle et al. 1989). They successfully produced asymmetrical parts under active vapor cooling control. At that stage, they had realized that without temperature control, there would be a negative effect on part distortion, microstructure and residual stress.

In around the 1990s, Spencer et al.(1998) from Nottingham University proposed a concept named 3D welding. At that time, these authors had found that 3D welding was able to build large parts with excellent mechanical properties. However, they also noticed that excessive heat input had a large impact on produced parts in terms of surface finish, distortion

and final shape. They pointed out that simple temperature control can help improve surface finish and the final shape.

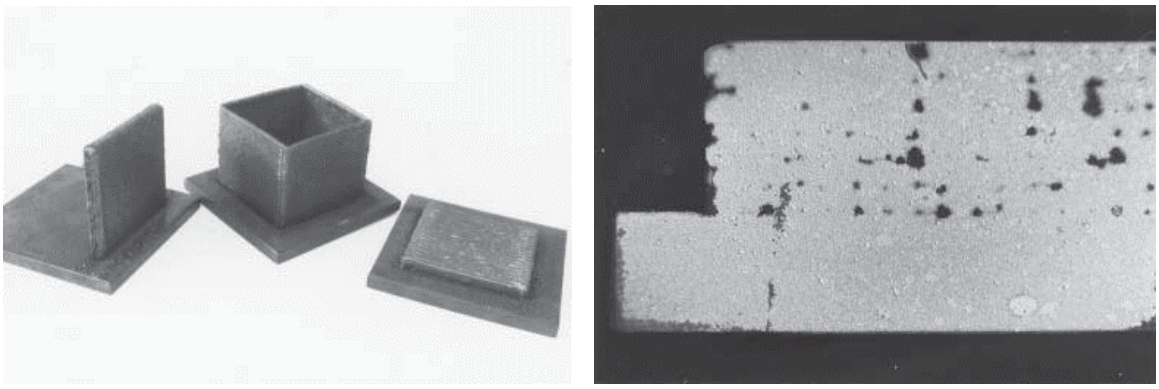

3-2(a). Vertical wall, hollow box and horizontal test parts
3-2(b). Lack of fusion in a steel part with beads produced side-by-side

Figure 3-2 3D Welding Part (Spencer et al. 1998)

More recently, welding based Metal additive manufacturing has received significant interest from industry and academia. In 2007, a research consortium led by the University of Sheffield Advanced Manufacturing Research Centre with Boeing won a €4.5 million European project, namely Rapid Production of Large Aerospace Components (RAPOLAC). They were responsible for developing a laboratory level technique namely shaped metal deposition (SMD) to a higher level. SMD is just another name of WAAM. In the project, Baufeld et al. published a series of papers (Baufeld et al. 2010, 2011a, 2011b) on revealing the relationship between grain microstructure and part mechanical property. As shown in Figure 3-3, stress and strain curves of Ti64 tensile test under different orientation, heat treatment have been provided. They found that the ultimate tensile strength of a Ti64 part varies between 936 and 1014 MPa, depending on orientation and location of the specimen. In addition, the authors also undertook a high-cycle fatigue test for WAAM built Ti64part in 2011. The maximum stress applied varies between 750MPa and 913 MPa, and the WAAM parts fails after $10^5 \sim 10^8$ cycles depending on the location and heat treatment ccondition. In Baufeld et al. (2010), the authors claimed that a wire arc additive manufactured part can reach comparable properties to cast and wrought part

in terms of strength and ductility. In addition, the authors concluded that parts built by additive layer manufacturing are able to meet the requirements for space and aerospace industries.

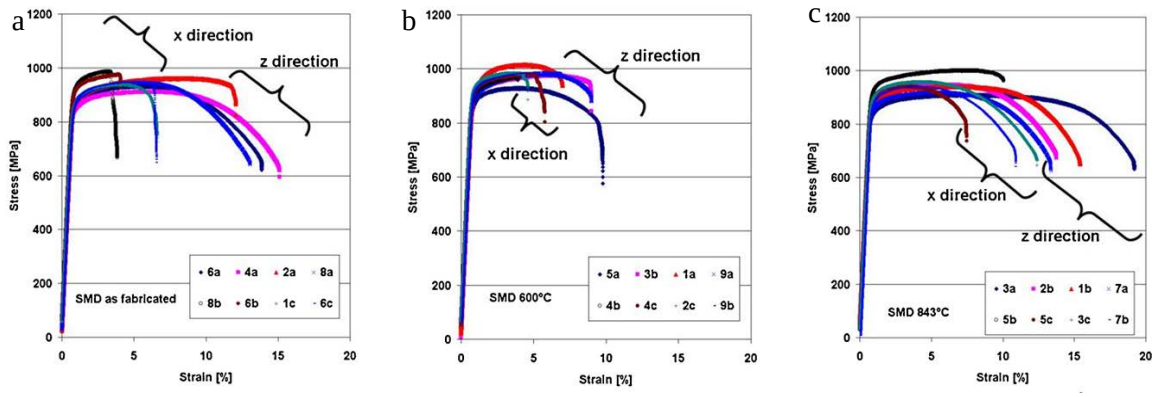

Figure 3-3 Stress–strain curves of WAAM part in the as fabricated state(a), after heat treatment at 600℃(b) and 843℃(c) (Baufeld et al. 2011)

In 2007, Cranfield University gained an EPSRC project namely Ready to Use Additive Manufacturing (RUAM) project. Under this project, Ding (2012) undertook research on WAAM simulation. She invented a new fast finite element analysis (FEA) simulation method for stress distribution simulation during WAAM process. In addition, Almeida (2012) made a survey on how process parameters affect the product quality. In 2014, Martina (2014) finished his PhD on rolling assisted wire arc additive manufacturing and proved that rolling during the WAAM process can decrease the distortion, refine the grain size, and improve homogenous properties of the part.

From 2014, Airbus entered this area and started an Innovate UK project with 3 partners including University of Bath, Cranfield University and Delcam Plc. The name of this project is Rolling Assisted Wire Feed Direct Deposition, with the aim to validate the feasibility of using rolling assisted WAAM to build up aerospace part (Xu et al. 2018).

In 2017, Norsk Titanium announced that their WAAM technique achieved technology readiness level 8 and attracted much attention from the aviation industry. In that year, they gained millions of investments from Boeing and decided to build up a factory to produce parts with the WAAM technique. In 2017, Boeing and Norsk Titanium declared that their WAAM

produced parts had received FAA approval for aerospace. Thus, Norsk Titanium had proved the possibility and feasibility of using WAAM in aviation industry.

3.4 State of the art for WAAM Process

3.4.1 WAAM System

Typically, a WAAM system consists of four parts, i) an arc welder, ii) a motion platform, iii) a wire feeder, and iv) a PC or an integrated control board (Ding et al. 2015). Additionally, in order to prevent the part from oxidization, either a sealed chamber with protection gas or a localized shielding gas device might be applied. Furthermore, in order to monitor and control the system performance, a monitoring system is required.

3.4.2 WAAM Categorization

3.4.2.1 Heat Source Category

Three types of welding technology are commonly applied in the WAAM process, namely gas metal arc welding (GMAW), gas tungsten arc welding (GTAW) and plasma arc welding (PAW) (Ding et al. 2015). These three types arc welder require the application of high voltages between the electrode and workpiece to generate a sufficiently high temperature plasma arc to melt the metal. The three types of arc welder are illustrated in Figure 3-4. In Figure 3-4a, Gas Metal Arc Welding (GMAW) welder nozzle uses consumable metal wire as one of its electrodes. Metal wire is fed into the molten pool, and later consolidated on the base plate or lower layer. To avoid oxidation in the melt pool area, the shielding gas is inserted and carried through the outer casing tube around the nozzle as detailed in Figure 3-4a.

In Figure 3-4b & Figure 3-4c Gas Tungsten Arc Welding(GTAW) and Plasma Arc Welding (PAW) welders apply inconsumable tungsten electrodes and separately inserted feedstock. Apart from the feeding pattern, the GTAW welder is essentially the same as the GMAW welder. PAW can be considered as an upgraded version of GTAW. It applies an extra

outer tube inserting gas to constrain the high temperature plasma torch. Through this way, PAW is able to achieve a higher power density and high temperature torch, which is estimated to be higher than 11000K, whereas GTAW and GMAW torches are in the region of 7000K (Wu et al. 2014). To avoid the deposited metal becoming oxidized in the high temperature environment, all three types of welding methods insert a shielding gas around the torch as shown in Figure 3-4.

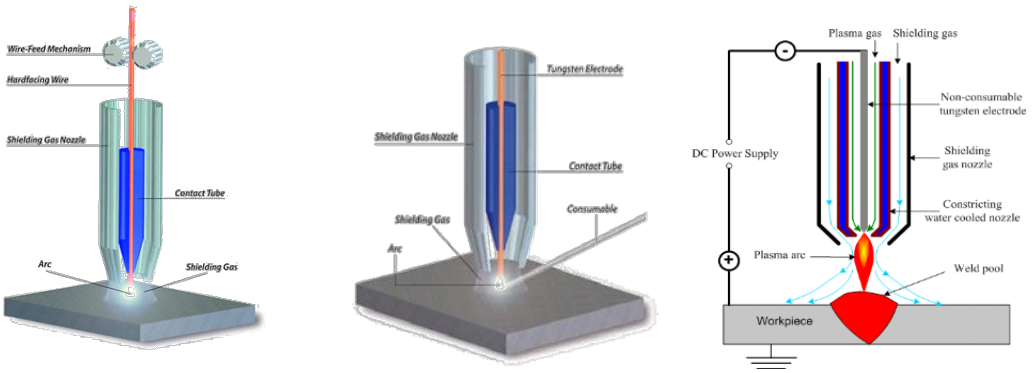

3-4(a) Gas Metal Arc Welding 3-4(b) Gas Tungsten Arc Welding 3-4(c) Plasma Arc Welding

Figure 3-4 Heat Sources for WAAM Process

3.4.2.2 Process Parameters Category

From a production viewpoint, WAAM can be considered as an extension of the welding technique, which naturally inherit welding properties and fatigues which makes welding monitoring methods a possible option for WAAM monitoring. Węglowski (2012) adapted the classification of weld monitoring to WAAM monitoring, as shown in Figure 3-5. For a WAAM monitoring system, there are two types of methods/parameters. The first type of parameters are traditional parameters which are monitored in most welding-related applications, including arc voltage, arc current, wire feed rate, welder moving speed and shielding gas flow. These parameters are associated with the system itself instead of the part. For example, arc voltage and arc current are used to monitor the heat input condition as demonstrated by the research undertaken by DuPont and Marder (1995). The shielding gas flow is used to ensure that the inert gas is enough to prevent the part from oxidation. The welder moving speed and wire feeding rate are used to monitor the deposition rate per minute (Xiong *et al.* 2017).

From the point of ensuring part quality, monitoring of the traditional parameters is not enough, as these parameters are only related to the machine condition. None of these parameters are associated with the part condition or environmental condition. As the heat accumulates and the environmental conditions alter, defects may begin to emerge and accumulate without being picked up or notified. Therefore, other methods are induced to monitor the part condition, namely acoustic signal monitoring, X-ray radiation, optical measurement, and thermal measurement as shown in Figure 3-5.

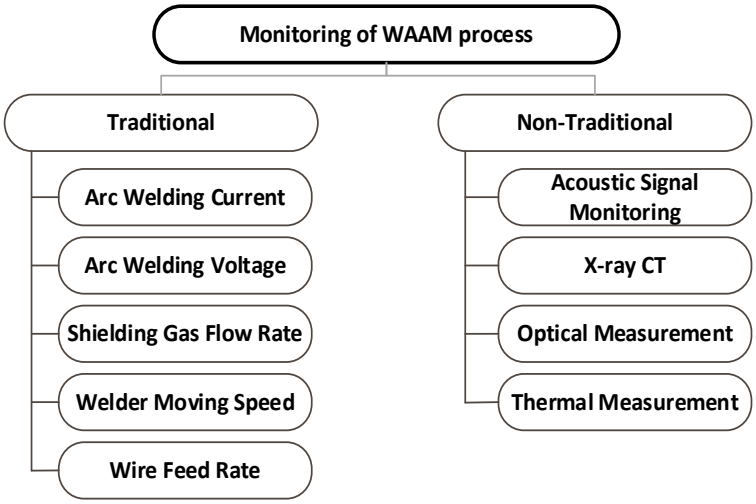

Figure 3-5 Monitored parameters and methods in WAAM
(Adapted from Węglowski, 2012)

3.4.3 Defects and its causes in WAAM process

The WAAM process suffers from a variety of defects in the process and out of the process. The defects have been summarised and illustrated in Figure 3-6. As shown in Figure 3-6, defects are categorised based on 6 reasons, namely material, process parameters, design, environment, operational error, and intrinsic property of the process. The major defects come from improper process parameters and operational error. Defects like lack of fusion, excessive heat input, an uneven gap between the welder and part commonly occur in the WAAM process, as WAAM still needs human adjustment in each layer. Process monitoring, process control and other automation techniques may help to decrease the occurrence of defects. Design experience and know-how is also an important for WAAM process. Incorrect path planning could lead to

defects collision of the part and welder, and in turn cause a lack of fusion or inclusion defect. Thin substrates (i.e. less than 20mm) may crack in the process because of the high residual stress generated in the process. Moreover, the intrinsic properties of the process also could cause defects. In the welding pool area, the arc is relatively unstable in terms of its position, as the mixed plasma gas, shielding gas and surrounding evaporation gas may cause deflection, and splashing metal beads. In addition, with constant input parameters when depositing a layer, the process has a tendency to generate a jump and valley at the beginning and the end of the layer (Xu et. al., 2018). This effect may seriously decrease the accuracy of the part after layers accumulation. In addition, the material properties such as porosity, grain size and micro morphology of the material are also important to the WAAM process. Like all other manufacturing processes, the environmental factors also affect the WAAM process. Oxygen concentration level, vibration level and ambient temperature can all have an effect the quality of the part.

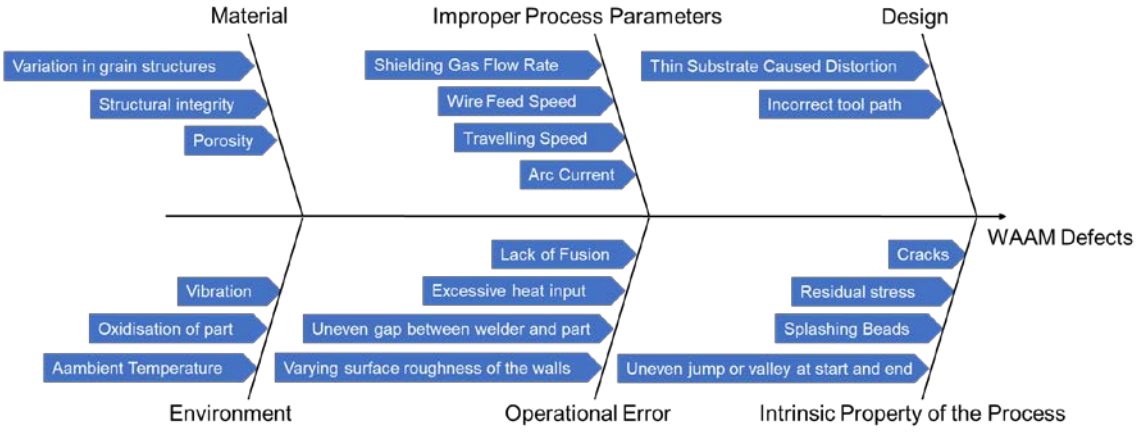

Figure 3-6 Fish bone diagram for cause of defects in WAAM process

3.4.4 Process Parameter Modelling

WAAM is a complicated process with numerous parameters that affects the stability and the quality of the process. Researchers often monitor the welding process through measuring parameters such as voltage, current, gas flow, temperature, sound intensity level. Traditional

welding monitoring monitors arc voltage, arc current, welding speed, wire feed speed and gas flow rate (Węglowski et al. 2012). These parameters are still the basic parameters in WAAM monitoring, as mentioned in Bonaccorso et al. (2009), Xu et al. (2018).

Moore et al. (2003) systematically introduced a physical model of GMAW. Specifically, they introduced the physics of the arc, heat transfer model, cooling rate model, melting rate model, arc transfer mode and metal transfer dynamics model. Moore et al. also induced the INEEL/ISU (Idaho National Engineering and Environmental Laboratory (INEEL)/ Idaho State University(ISU)) model to unify all above models.

In 2011, Anzehaee and Haeri(2011) summarized and simplified a mathematical model based on the previous work done by Moore, Naidu, and Tyler (1997), Thomsen (2004) and Planckaert, Djermouneand Richard (2010). Their model was a fifth order non-linear state space model for GMAW process as shown in Equation (1). They applied a model predictive control strategy for voltage and current control in the welding process and achieved a comparable performance to a proportional–integral (PI) controller, which proved the effectiveness of their model.

$$\dot{X}_1 = X_3 - (\frac{c_1}{\pi r_e^2} X_2 + \frac{c_2 \rho}{\pi r_e^2} X_1 X_2^2)$$
$$\dot{X}_2 = \frac{1}{L_s}(U_2 - (R_a + R_s + R_L) X_2 - V_0 - E_a(l_c - X_1))$$
$$\dot{X}_3 = \frac{1}{\tau_m}(k_m U_1 - X_3)$$
$$R_L = \rho \left[X_1 + 0.5 \left(\frac{3X_6}{4\pi\rho_e} \right)^{1/3} + X_4 \right]$$

The state and input variables are defined as follows:

$X_1=l_s$	stick out(m)
$X_2=l_a$	welding current (A)
$X_3=S$	welding wire speed (m/s)
$X_4=X$	droplet displacement (m)
$X_5=\dot{X}_4$	droplet velocity (m/s)
$X_6=m_d$	droplet mass(kg)
$U_1=V_{arm}$	motor armature voltage(v)
$U_2=V_{oc}$	open circuit voltage(v)

$l_c = CTWD$ contact tip to work piece distance(m)

Martina et al. (2012) investigated the working envelope and defects using plasma arc welding (PAW) as the heat source for WAAM. They initially selected three factors, namely wire feed speed (WFS), travelling speed (TS), and current (I), as the inputs of a response model. Through a series experiments, they concluded a working envelope for PAW based WAAM process. As shown in

Figure 3-7, the proper working envelope is in the blue area, and Martina et al. explained that the upper limit of the WFS was due to the hardware limit, and the lower limits of the TS and the WFS were due to the need for high deposition speed. In addition, they found that when the TS was too high, it may induce the humping phenomenon (A1, A2, A3). When the current was low, the insufficient heat input may lead to incomplete melting (area B3, B4), in the contrast when the heat input was too high, the bead shape became non-uniform (area B1, B2).

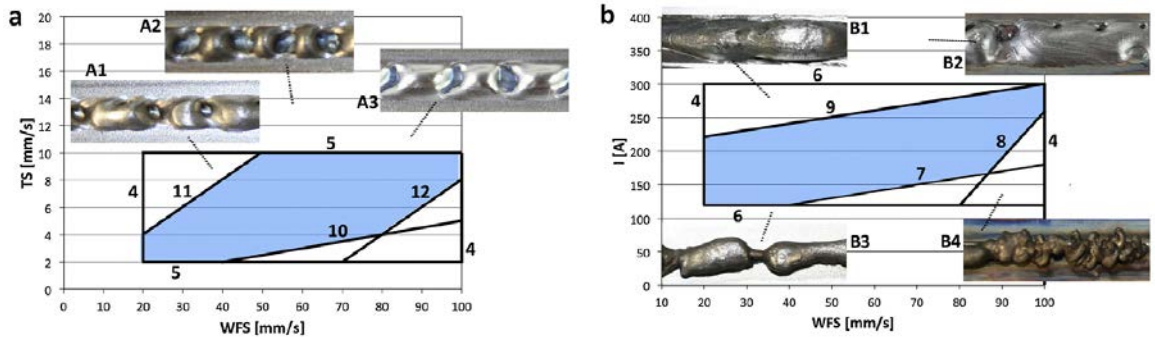

3-7(a) WFS-TS working 3-7(b) WFS-current working

Figure 3-7 WAAM working envelop & defects (Martina et al. 2012)

3.4.5 Shape Monitoring and Control

WAAM is widely regarded as a promising candidate for producing large aerospace components due to the low material usage. In the aviation industry, the material usage is also termed as buy-to-fly ratio, which stands for the weight ratio between the billet and the final part. As mentioned by Thomas et al. (2014), for some complex geometry part the buy-to-fly ratio may reach 20:1,

and even for simple geometry, this ratio can reach 8:1. A high buy-to-fly ratio leads to high machining cost and material cost. According to a report by Williams and Martina (2016), WAAM produced near net-shape part can reach a buy-to-fly ratio ranging between 5:1 ~ 2:1. However, there is a trade-off between deposition speed and buy-to-fly ratio at the highest deposition rate (10kg/h), the buy-to-fly ratio may be intolerant. However, this can be overcome through the development of the monitoring and control system, where with precise control over the layer shape, the buy-to-fly ratio will decrease.

Escobar-Palafox et al. (2011a, 2011b) provided an overview for the shaped metal deposition (SMD) process (alternative for WAAM). They introduced their motion platform which consists of a KUKA KR16 robot and a DKP400 turntable as shown in Figure 3-8a. In order to monitor the process, a range of equipment was installed, including a Redman weld vision camera, a Systech oxygen monitor, a Triton AMV4000 weld monitor, two Raytek pyrometers, 12 thermocouples a microphone, a CCD camera and a thermal camera. With this equipment, Bonaccorso et al. (2009, 2011a, 2011b) developed an arc welding monitoring system as shown in Figure 3-8b. This system was able to monitor all arc voltage, arc current, arc sound, arc light, wire feed speed and travelling speed. They also applied a control algorithm on this system.

They recognized that it was difficult to obtain the layer height directly with optical sensor due to the interference of high temperature and intensive light. Therefore, they used arc voltage as an indicator of the part height because it is directly related to arc length, and arc length is proportional to layer height when the torch height was fixed in the z-axis. In addition, they adopted a linear control model to control the layer height. As shown in Figure 3-8c, WF stands for the wire feed rate, and V-Vref stands for the arc voltage error. The voltage error varies as the distance between welding tip and part surface varies. The wire feed rate runs at its working point, and it would vary linearly to voltage error to compensate low part surface. The trials

shown in Figure 3-8 proved the effectiveness of this simple control strategy. Though the minimal difference between the controlled part and manual parts cannot be easily observed by naked eye as shown in Figure 3-7.

3-8(a) SMD motion platform

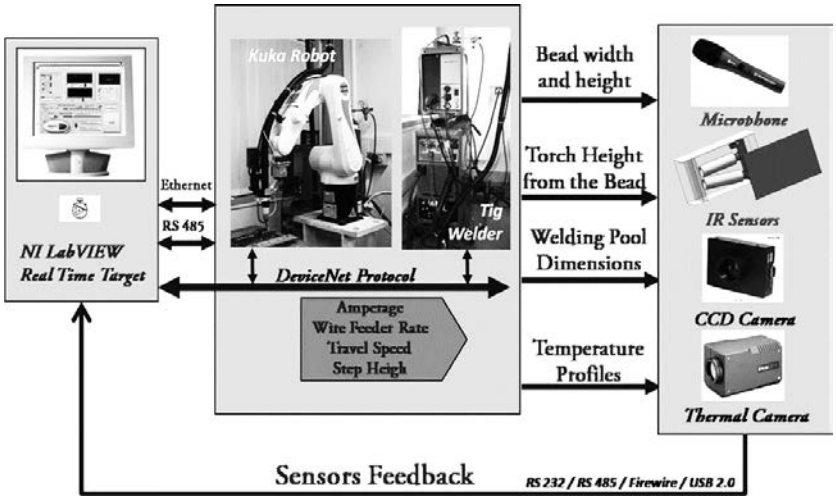

3-8(b) SMD Sensor System

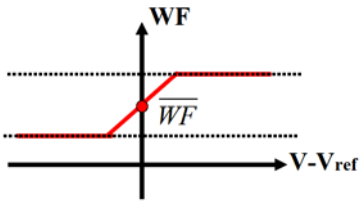

3-8(c) linear control strategy for SMD process

3-8(d) Comparison between manual SMD and controlled SMD

Figure 3-8 Shape Metal Deposition System Diagram (Bonaccorso et al., 2011a)

Monitoring the height and the width is always a key issue in WAAM monitoring. Zhang et al. (2006) invented a mathematical model for reconstructing a welding bead shape from a 2-D image. Two 2-D images of two welding beads under different welding parameters, are shown in Figure 3-9a,b. The authors reconstructed the bead shapes as shown in Figure 3-9 c, d. To validate the accuracy of their model, the authors built a man-made standard circular bead part and compared the mathematical model with the standard part. The final results showed that their model could achieve an average accuracy of 0.11mm.

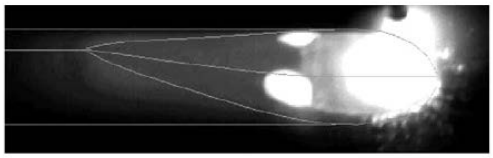

3-9(a) Bead Image 1

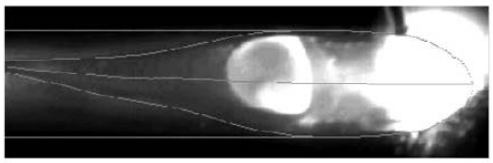

3-9(b) Bead Image 2

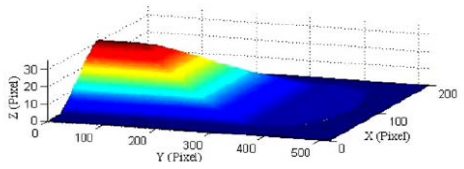

3-9(c) Reconstructed Bead Geometry 1

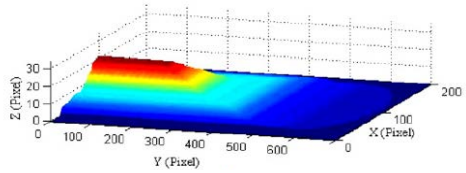

3-9(d) Reconstructed Bead Geometry 2

Figure 3-9 a mathematic model for reconstructing a welding bead (Zhang et al. 2006)

In 2003, Saeed and Zhang (2003) introduced a novel dot-matrix reflection method to monitor the welding bead shape. In the successive ten years, they developed and improved this method, and published a series of papers Saeed et al. (2004, 2007) and Zhang et al. (2013, 2015). Essentially, they utilized a laser source to project a dot matrix on the surface of the bead. Due to high directional property of the laser, the dot matrix would be reflected on the imaging plane as shown in Figure 3-10a, whereas the arc light would only diffuse on the background. Nevertheless, these authors mounted a band pass filter on the camera to reduce the interference of the arc light. Subsequently, by applying a mathematic algorithm invented, a 3-D model was generated as shown in Figure 3-10b,c.

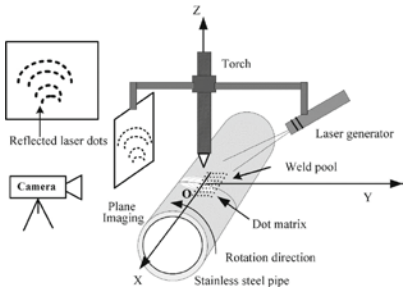

3-10(a) Dot Projection Setup

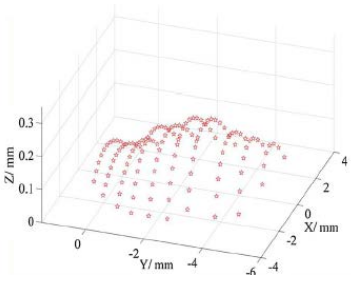

3-10(b) reconstructed result

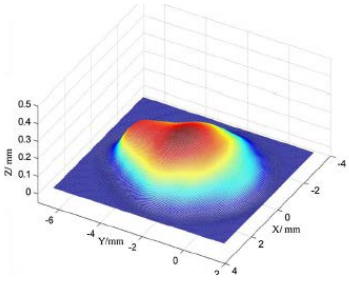

3-10(c) reconstructed model

Figure 3-10 A reflected dot monitoring system (Saeed and Zhang 2003)

Xu et al. (2012) developed a method using arc voltage signal to track part height. In the arc welding area, they identified that the arc length has a linear relationship to arc voltage. The authors designed an experiment to fit the arc length and arc voltage relationship. As shown in Figure 3-11a, they set a decreasing height path for the welder and the original arc voltage signal is shown on the side. In order to extract the feature of the arc voltage variation, the author applied a threshold and extracted the signal, as shown in Figure 3-11b. Subsequently, they applied a moving average filter, wavelet filter and anti-impulse interference moving average wavelet filter to filter out the noise, and finally the authors fitted the linear equation for the voltage and the arc length. They tested the fitted equation against a test case, and found that the model could achieve an accuracy of 0.236 mm.

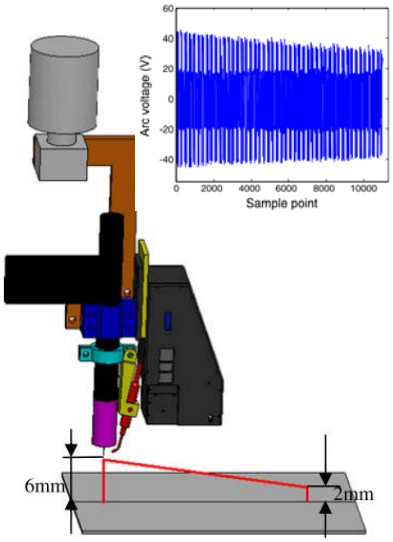

3-11(a) Experiment Setup

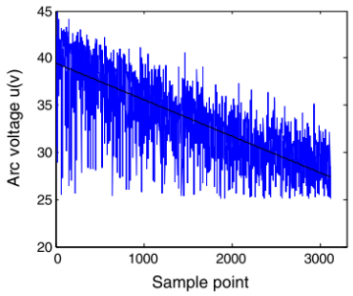

3-11(b) original arc voltage signal

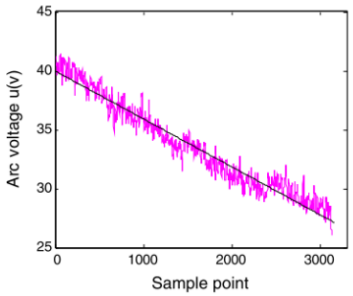

3-11(c) moving average filtered signal

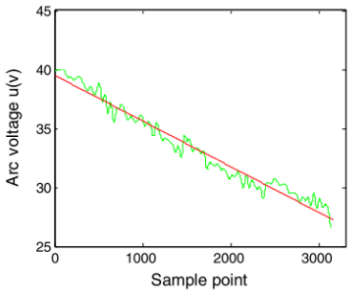

3-11(d) wavelet filtered arc

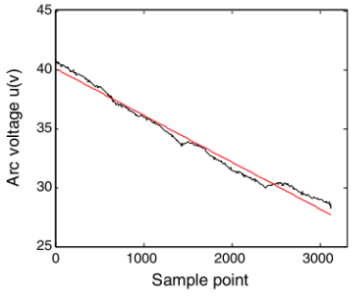

3-11(e) anti-impulse interference moving average based on wavelet filter

Figure 3-11 Height to Voltage Relationship (Heralic et al. 2012)

Heralic et al.(2012) reported on a laser metal-wire deposition height control strategy with an advanced iterative learning control(ILC) algorithm as shown in Figure 3-12a. As shown in Figure 3-12b, the blue and the black line stands for the height variation at 10th layer and 35th layer under ILC control, and the red line is the height variation for open loop control. It is obvious that their ILC strategy minimized height deviation in a large extend. The key idea of ILC is that if a system repeatably conduct a task, the performance of the system could be improved from the previous experience, where WAAM as a layer-by-layer process is suitable for the case. In addition, a common problem for WAAM is that it is not easy to measure the height and the width of the part during process because of the intensive heat and light around the torch area. In this paper, Heralic et al.(2012) applied an intermittent measurement method to overcome this issue. As shown in Figure 3-12a, they mounted a laser profilometer on a linear drive unit, and they move it down when needed and it was retracted at other times.

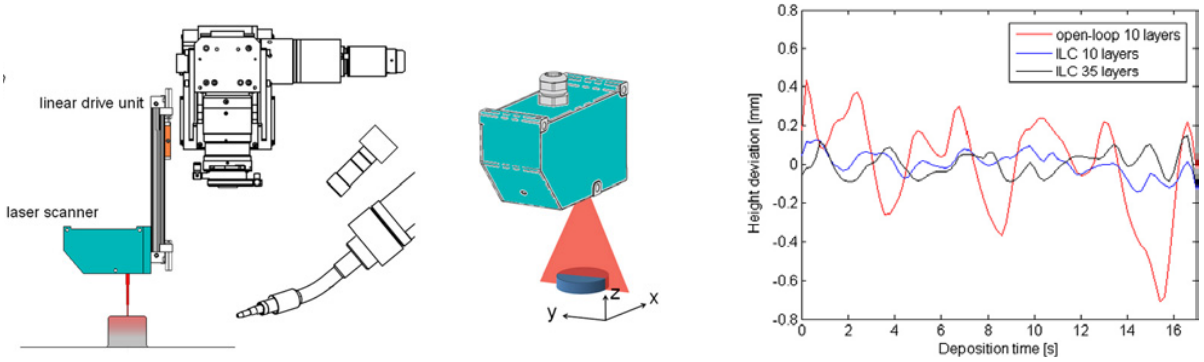

3-12(a) Laser metal-wire deposition monitoring setup

3-12(b) Height Variation Under different strategy

Figure 3-12 laser metal-wire deposition with iterative learning control (ILC) height control (Heralic et al. 2012)

Kissinger et al.(2019) reported a coherent range-resolved interferometric (CO-RRI) technique to measure the height of the part. The schematic set up and the enclosed interrogation unit are shown in Figure 3-13a,b. The device is equipped with a 5 mW 1550 nm diode laser source, which emits a sinusoidally wave at a modulation frequency of 49 kHz. The light returned by the part is captured by the photo detector. The authors used a field programmable gate

array(FPGA) board to process the signal and achieved a measurement frequency of 100Hz. As shown in Figure 3-14a, this sensor head is attached to the GMAW welder, and it is able to measure the height of the part under bright light generated by GMAW welder. The measurement results for the height of a wall from layer 1 to layer 12 are shown in Figure 3-14b. The author did not explicitly report the accuracy of the sensor. According to the result in Figure 3-14b, the accuracy is estimated to be better than 1mm.

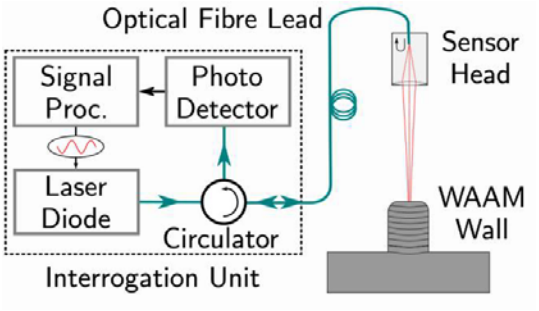

3-13(a) An illustration of the optical measurement setup

3-13(b) A picture of the fully-enclosed interrogation unit

Figure 3-13 Height Measurement Sensor using Interferometric Techninque (Kissinger et al. 2019)

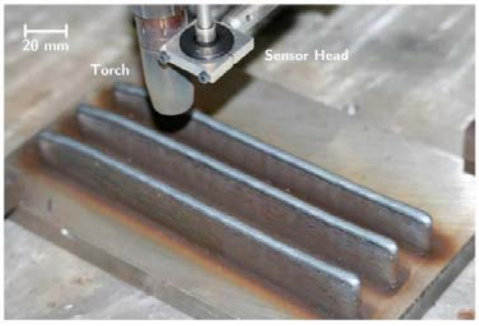

3-14(a) Measuring Part Height using Interferometer

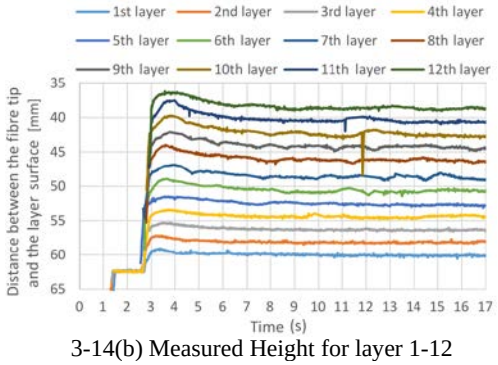

3-14(b) Measured Height for layer 1-12

Figure 3-14 Height Measurement Result using interferometric sensor (Kissinger et al. 2019)

Font Comas et al. (2016) developed a passive imaging system to measure the width of a part for plasma arc welding process. The experiment setup is shown in Figure 3-15a. The relative position of the torch and the camera is fixed, and they are all mounted on a moving panel of the CNC machine. The welding pool are is monitored by the camera and the width extraction algorithm is shown in Figure 3-15b. The authors achieved 0.05 mm accuracy for width

measuring during the process.

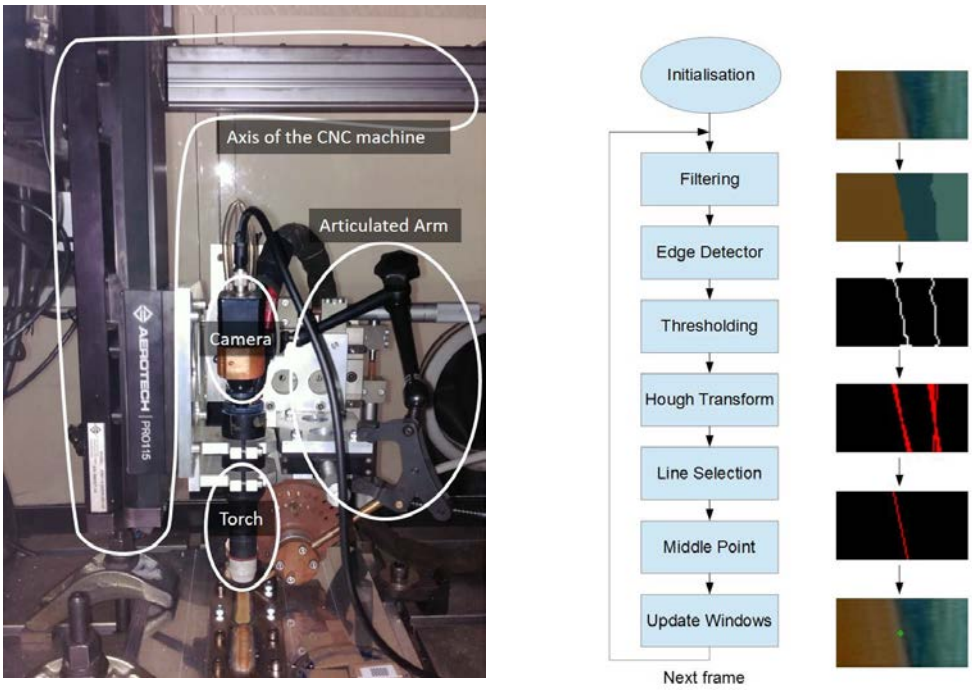

3-15(a) Experiment Set-up 3-15(b) Width Extraction Method

Figure 3-15 Passive Visual Monitoring System (Font Comas et al. 2016)

3.4.6 Bead Geometry Models for Process monitoring

As a basic problem, Ding et al. (2015) investigated the bead cross-section profile. He compared three different empirical bead models as shown in Figure 3-16a. Based on his experiments and fitting result, he proposed a multi-bead model termed a tangent overlapping model which surpassed the performance of the traditional flat-top overlapping model as shown in the Figure 3-16b. The core idea behind the flat-top overlapping model is shown in the Figure 3-16c. The area of triangle BEC should be equal to that of triangle AED. In addition, they assumed Line CB is tangent to the parabola. The result shows that Ding's flat-top overlapping model fits the real results extremely well, and it surpassed the traditional flat-top model.

Table 3-1 Bead Models (Ding et al. 2015)

Models	Model Function	Bead Height	Bead width
Parabola Model	$y = ax^2 + c$	c	$2\sqrt{-c/a}$
Cosine Model	$y = a\ \cos bx$	a	π/b
Arc Model	$y = \sqrt{a^2 - x^2} + b$	a-b	$2\sqrt{a^2 - b^2}$

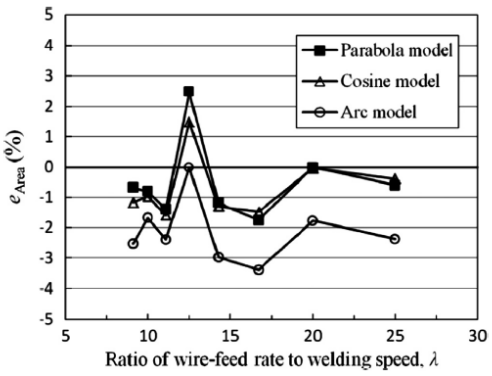

3-16(a) Area error percentage of different profile model

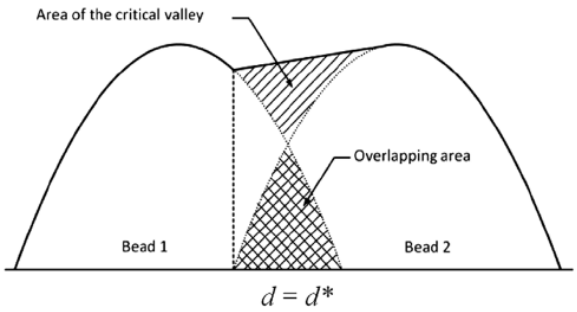

3-16(b) Geometric model for multi-bead part

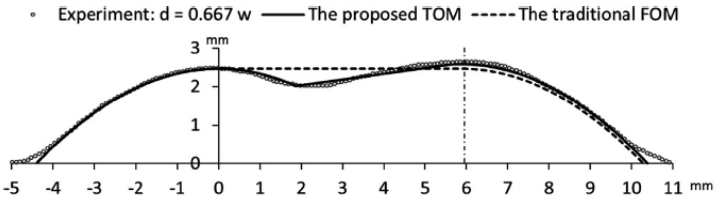

3-16(c) Geometric model for multi-bead part

Figure 3-16 Multi-bead model (Ding et al. 2015)

Ding et al.(2015) did not discuss which parameters affected the profile. However, this is another major area for geometry control. Xiong et al. (2010 and 2011) wrote two papers for WAAM in-process monitoring control. They applied two customised cameras to monitor the height and width respectively and1 applied similar algorithm to extract the height and the width of the red hot bead from the corresponding camera as shown in figure. In addition, they applied two different strategies to control the height and the width. For height, an adaptive controller was applied. For width, they applied a single neuron controlled and realized varying bead width ranges between 6mm to 9mm. They also proposed that WAAM is a non-linear process that can be described by the second order Hammerstein process (Ding et al. 2011).

Doumanidis and Kwak (2001, 2002) wrote two papers on WAAM monitoring and control. They applied a traditional active structural light measurement solution for measuring the height of the part. In addition, the authors also used an Infrared camera to monitor the

temperature distribution. The biggest contribution of the authors is that they realized the process is a dynamic process and tried to use system identification for the recognition the system. The authors applied the first order system model and the system followed the geometric shape of the bead well. In addition, the author applied a control algorithm on its system which reflected good performance. (Doumanidis and Kwak 2002)

Han et al. (2018) firstly applied a control algorithm for the multi-layer multi-bead WAAM process. As shown in Figure 3-17, two different control strategies were applied to control the height and the width. It should be noted that the authors used a line-structured laser sensor to obtain the profile in real-time where there is a difficulty to obtain the profile under intensive heat and light. However, the authors did not explicitly describe how they used their line-structured laser sensor to detect the height and the width in real time. As shown in Figure 3-17, the cross-section of parts showed an improved consistency of the width of the part with the control algorithm.

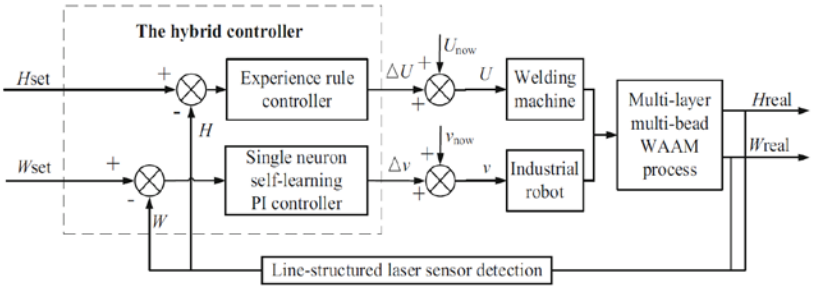

3-17(a) Multi-layer Control Algorithm

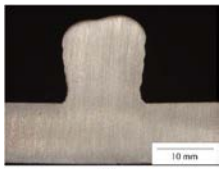

3-17(b) Open Loop Result

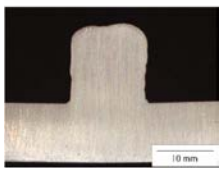

3-17(c) Controlled Result

Figure 3-17 Schematic diagram of a multi-layer WAAM control system (Han et al. 2018)

In Almeida (2012), the author analysed the process with a full parameter analysis with a batch of experiments. This research was mainly based on multi-variable linear regression. From this point of view, it's helpful to gain a general sense of how those parameters affect the process. However, it is not helpful in automated process control, as the WAAM process is a highly

dynamic process, whereas the multivariable linear regression is a static analysis process.

Lü et al. (2010) undertook an experiment for controlling the weld pool size with a model-free adaptive control (MFC) algorithm. The authors developed a complex three-light-path visual system to monitor the weld pool in three directions, as shown in Figure 3-18b. Based on the obtained image, they extracted the width of the weld pool. Subsequently, to control the weld pool width, they selected welding current and wire feed speed as the input of the control algorithm, and they successfully achieved an accuracy of 0.42~0.45mm.

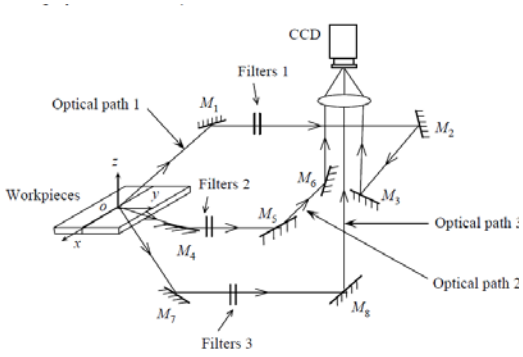

3-18(a) Schematic diagram of a multi-camera monitoring system

3-18(b) Combined monitoring image from different viewpoint

Figure 3-18 Multi-Camera Monitoring System (Lü et al. 2010)

Geng et al. (2017) developed a model to predict the layer height and width based on response surface methodology. The authors applied welding current, wire feed speed and travelling speed as input, and the layer height and width as output to fit a multi-linear regression model. As shown in Figure 3-19a, the authors fitted a response surface of the height with respect to wire feed speed and peak current. They found that their model could predict the bead height and width with maximum error of 4.5% and 7.1% respectively, as shown in Figure 3-19b.

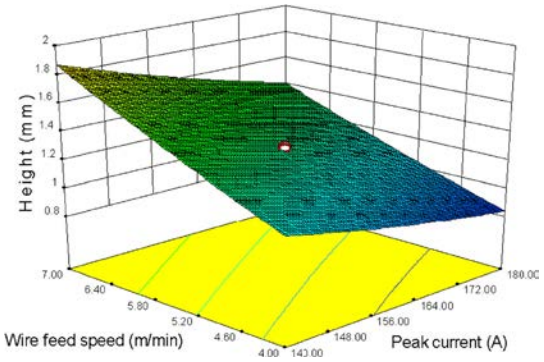

3-19(a) Response surface of the height with respect to wire feed speed and peak current

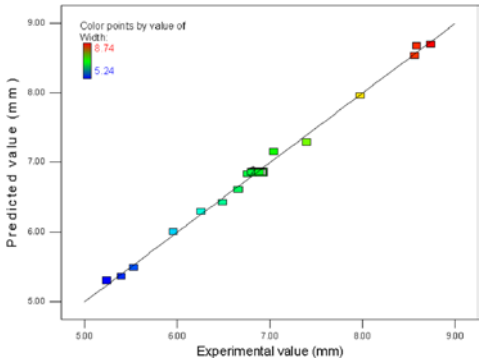

3-19(b) Predicted Height Value with respect to experiment Value

Figure 3-19 Response surface of the height with respect to wire feed speed and peak current (Geng et al. 2017)

In GTAW based WAAM, the wire feed position with respect to the arc affects the actual deposition quality especially for joint position. As shown in Figure 3-20a, due to the deviation of the intended wire position, the part generated a gap defect. Geng et al. (2017) undertook a research on the wire position in related to wire height and wire feed angle. They found that when the wire was fed with small angle 10° and with a height of 3.8mm could lead to a smooth layer appearance.

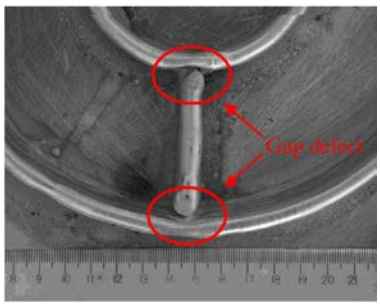

3-20(a) Gap defect caused by wire deviation caused by wire deviation

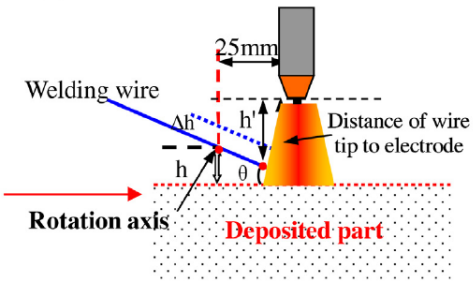

3-20(b) wire position with respect to the arc

Figure 3-20 Gap Defect Caused by Wire Deviation (Geng et al. 2017)

For the multi-pass WAAM process, the spacing between two passes is a key factor for WAAM quality. Aiyiti et al.(2011) undertook a research on the impact of the spacing distance to the quality. They found that as the increase of the spacing distance, the surface roughness would increase, in the contrast the decrease of the spacing distance may cause greater pass than

previous track as shown in Figure 3-21a, b, c. The authors thought a proper spacing distance should be determined. The schematic diagram of a multi-pass WAAM part is shown in Figure 3-22a, and in Figure 3-22b, the authors believed that when the overlapping area GDJ was equal to ADB, the spacing distance was most proper. Therefore, they derived an equation as shown in Equation (2):

$$x_D = \frac{1}{h}\left[\frac{r^2}{2}\arcsin\frac{w}{2r} - \frac{w}{4}(r-h)\right] \qquad (2)$$

Where X_D is the coordinate of the intersection point D, w and h are the width and height of the bead respectively and r is the radius of the arc as shown in Figure 3-22b.

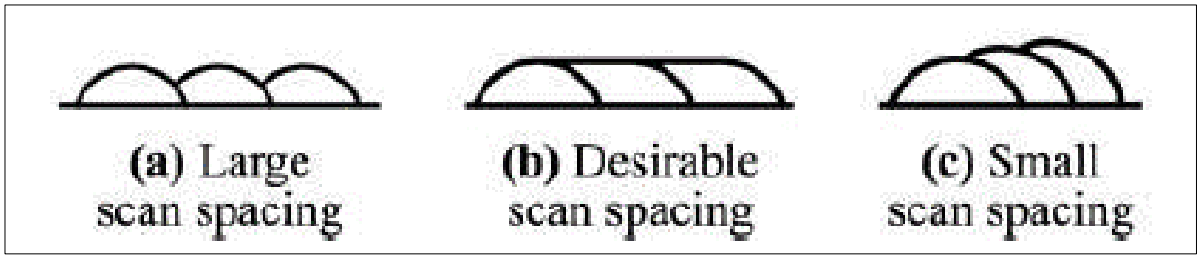

Figure 3-21 A multi-pass spacing distance

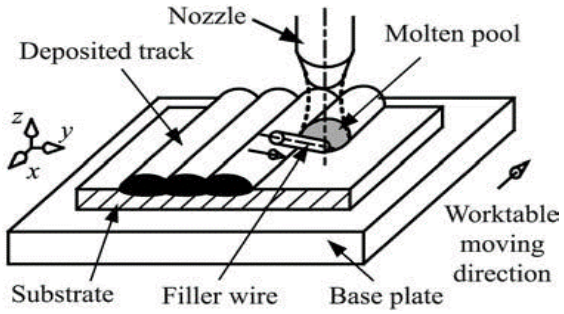

3-22(a) A schematic diagram of building up a multi-pass WAAM part

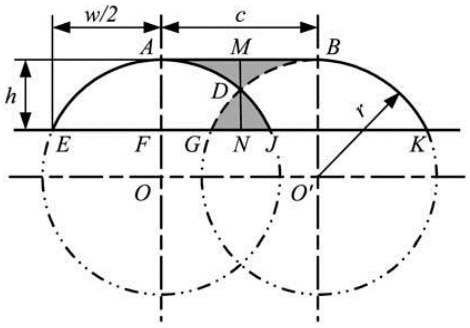

3-22(b) Geometric model for multi-pass part

Figure 3-22 Multi-pass spacing distance schematic diagram and geometric model (Aiyiti et al. 2011)

In addition, the authors found that the width to height ratio λ also had an impact on multi-pass WAAM part. As shown in Figure 3-23, when λ was lower than 3:1, it was easy to generate less melting defects.

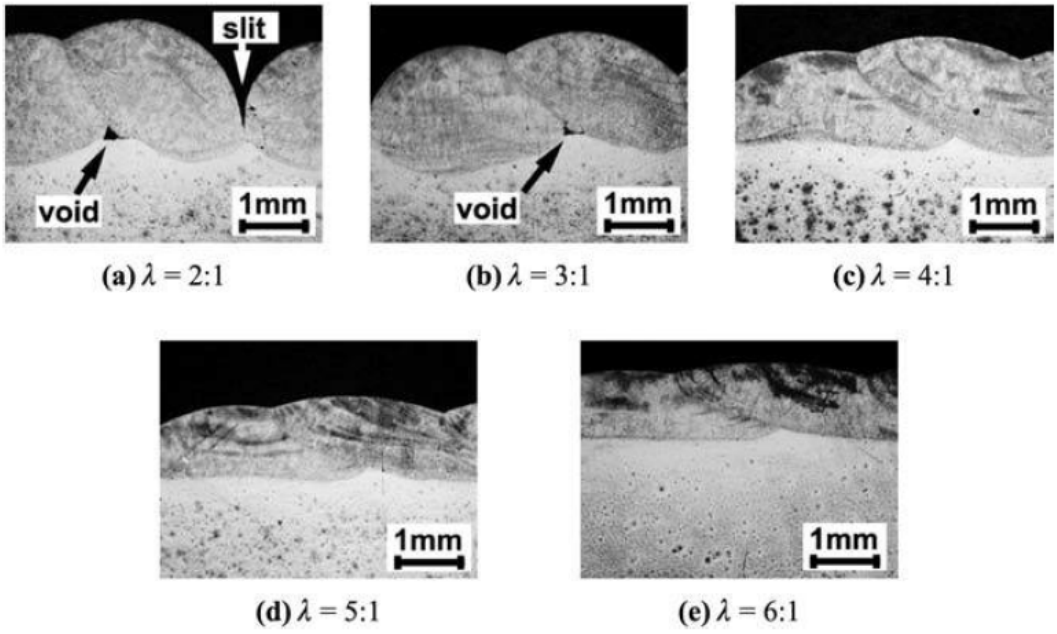

Figure 3-23 Part quality again width to height ration λ

3.4.7 Fatigue Monitoring and Control

Apart from shape monitoring, the WAAM monitoring also focuses on fatigue and problems in the whole process. Ogawa (2011 and 2012) thoroughly introduced how to visually monitor the arc welding process. To avoid the interference of the intensive arc light, he identified two methods by applying a narrow band-pass optical filter and secondly a shorter exposure time. The arc images for mild steel and SUS304 stainless steel are shown in Figure 3-24a. The left images were captured under 1/10 second exposure time which was too long with the arc area already saturated, though the electrode was clear. On the opposite side, the right images with shorter exposure time resulted in the image of the electrode almost disappearing. Ogawa (2012) also studied the arc image under different wavelengths by applying different optical filters, as shown in Figure 3-24b.

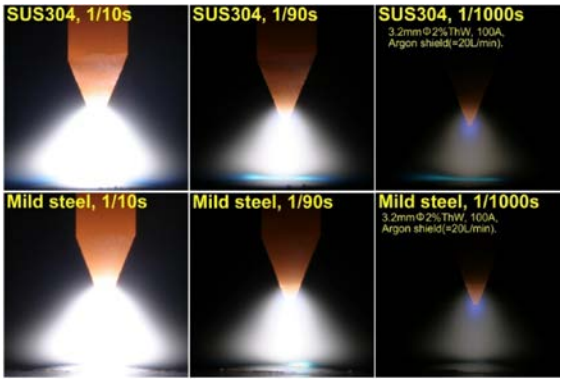

3-24(a) Argon arc images under different exposure time

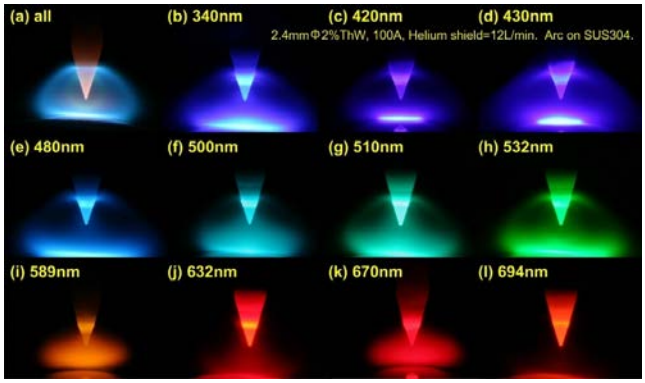

3-24(b) Argon arc images under different wavelength filter

Figure 3-24 Argon arc image under different exposure time (Ogawa 2012)

In the WAAM process, the sound generated is induced due to the energy being released in the solid materials. Wang et al. (2009) argued that the defects in the welding process should be associated with energy variation, and hence there would be a reflection on acoustic signal. They investigated the acoustic signal in the range of 20-20000Hz produced from arc welding process as shown in Figure 3-25.

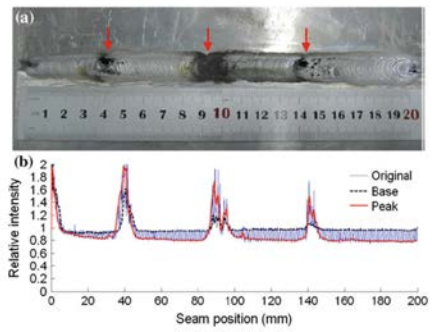

3-25(a) welding arc spectral signal against welding defects

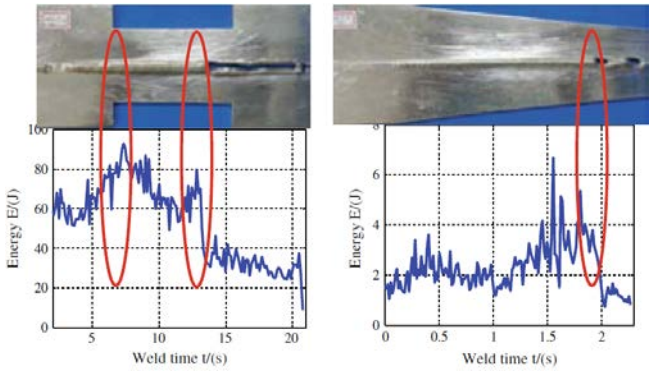

3-25(b) welding sound intensity signal against welding defects

Figure 3-25 Acoustic signal variation indicates welding defect (Wang et al. 2009)

Segerstark et al. (2017) undertook an experiment using a thermocouple to measure the temperature during a laser additive manufacturing process. They used a Type K thermocouple which has a range of -200-1200 ℃ with a melting temperature at 1400℃. To avoid the potential damage from the laser heat source, Segerstark et al.(2017) welded a small metal sheet over the thermocouple to protect it.

Wu et al.(2017) investigated the temperature variation of a WAAM part as the layers increased. In their experiment, they utilized a pyrometer to measure the surface temperature. A common drawback in use of a pyrometer is that its measurement is dependent to the emissivity of an object which will be varying as the temperature goes higher. The authors designed a calibration procedure by comparing the pyrometer's measurement to two thermocouples' measurement. As shown in Figure 3-26a, they fitted a second order curve for the pyrometer readings. Based on the calibrated readings, the authors measured the inter-pass layer temperature, substrate temperature and heat accumulated as shown Figure 3-26b. The authors also found that the bead geometry varies in the first few layers due to heat accumulation.

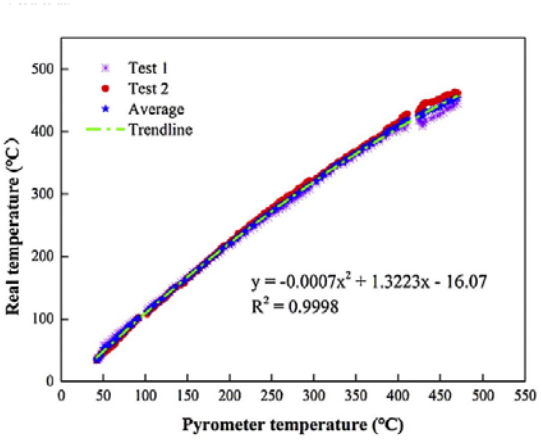

3-26(a) pyrometer measurement against thermocouple measurement

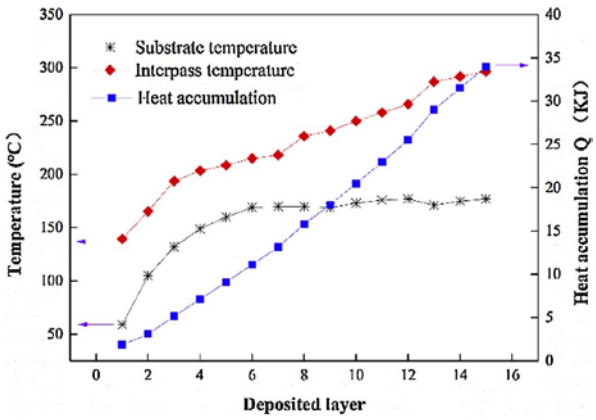

3-26(b) Inter-pass layer temperature, substrate temperature and heat accumulation

Figure 3-26 Temperature Variation of the inter-pass layers in a WAAM part (Wu et al. 2017)

Chen et al. (2016) applied a digital image correlation (DIC) algorithm to measure the strain in real-time. As shown in Figure 3-27a, they used an Infrared camera to measure the temperature in the region of interest (ROI), and a DIC camera to measure the strain. The accuracy of the DIC algorithm is in the order of the 100 um/m. (Pan et al. 2009) Due to the interference of the arc light, the authors found the noise level in this case was as high as 1000um/m, as shown in Figure 3-27b. They applied a Savizky-Golay filter to smooth the result and tried to measure the strain for a part with deliberate defects as shown in Figure 3-27c. Compared to the normal

strain curve in Figure 3-27d, the results showed an obvious difference, which suggested the potential of using DIC to detect defects in real-time.

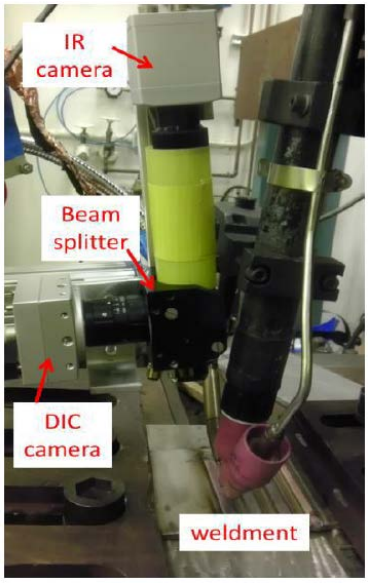

3-27(a) Experiment Setup

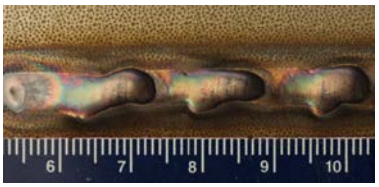

3-27(c) Deliberate Defect

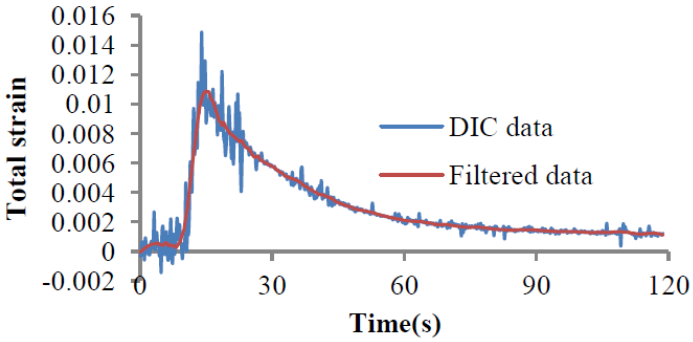

3-27(b) Savizky-Golay filtered Strain Signal in Part

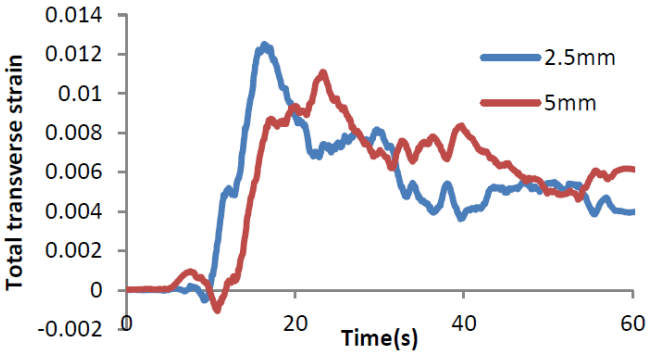

3-27(d) Normal Strain Signal in Part

Figure 3-27 In situ DIC strain monitoring equipment and results (Chen et al. 2016)

3.4.8 Monitoring of WAAM Defects and Features

Xiong et al. (2017) used WAAM to build up an inclined wall. The authors investigated the relationship between the inclination angle and the travelling speed and wire feed speed. They found that when keeping the travelling speed constant, the increase of the wire feed speed led to a decrease of the maximum inclination angle. In contrast, when keeping the wire feed speed constant, the maximum inclination angle increases along with an increase in travelling speed. They also produced thin wall geometry to prove the feasibility of using WAAM to build up parts with inclined walls, as shown in Figure 3-28.

Figure 3-28 WAAM inclined wall parts. (Xiong et al. 2017)

Kazanas et al. (2012) also investigated the possibility of building inclined walls and horizontal walls. They found that traveling speed (TS) had a large impact on building wall quality and a TS of 0.2m/min provides the best quality of the wall. After a series of experiment, Kazanas et al. proved that WAAM is able to build horizontal structure and hollow structure as shown in the Figure 3-29 a, b & c.

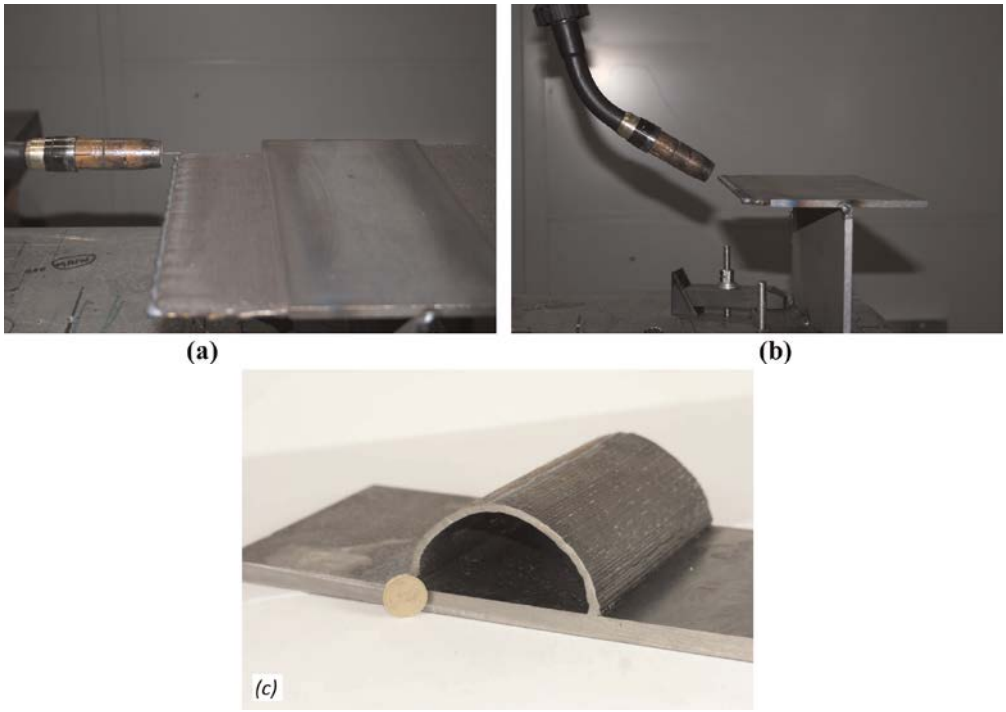

Figure 3-29 Overhang WAAM walls (Kazanas et al. 2012)

Ding et al. (2015, 2016a, 2016b) undertook a series of research on WAAM path planning. In 2015, Ding et al. (2015) proposed an algorithm for decomposing 2D geometry into convex polygons, and then an optimal tool path would be selected for each polygon. Finally, the sub-paths were connected to generate the ultimate path as shown in Figure 3-30. Ding et al. (2016a) expanded this idea into 3D geometry as shown in Figure 3-30. Here complicated geometry could be decomposed into simple sub-volumes depending on its build direction. The main aim of this tool-path was to build up the part with minimal support structures.

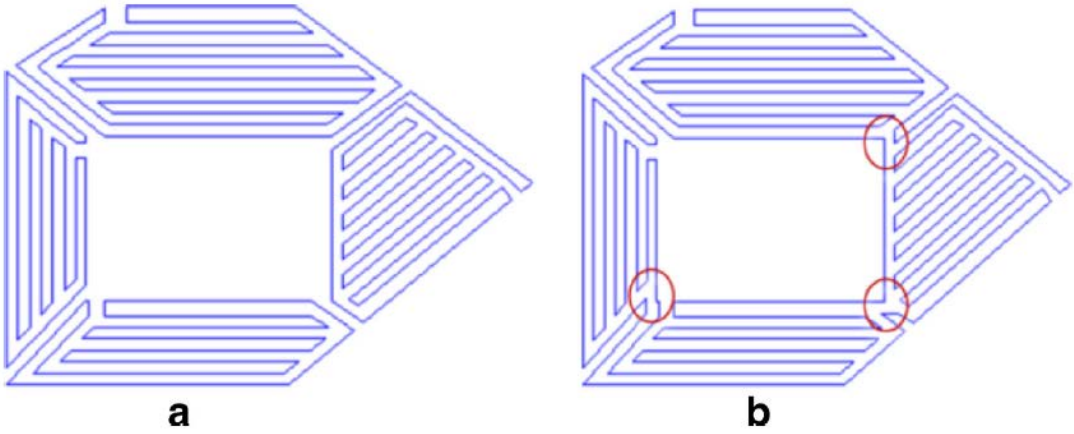

Figure 3-30 Decomposing 2D geometry and generating separate toolpath (Ding et al. 2016a)

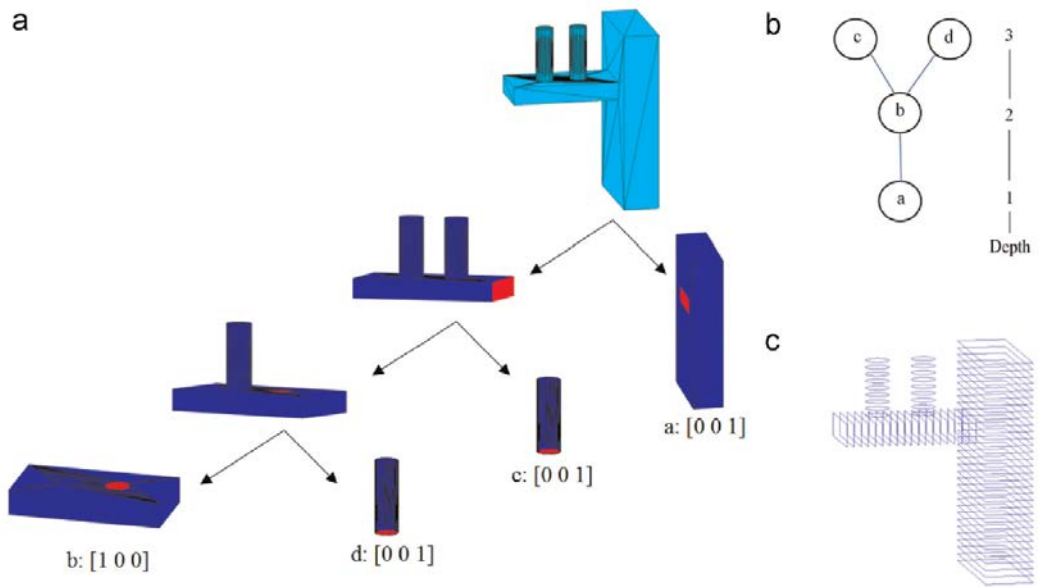

Figure 3-31 3D decomposing algorithm and generating multi-direction tool path

Ding et al.(2016b) found that there was a problem for WAAM path planning with contour-pocket path plan as shown in Figure 3-32b. Due to the width of each single pass of WAAM process, an internal gap was left inside of the part. To address this problem, Ding et al.(2016b) proposed a path planning algorithm based on medial axis transformation. The essential idea of this path planning was to extract the skeleton of a geometry and then to generate a path surrounding the skeleton, which properly conquered the internal gap problem as shown in Figure 3-32 c&d.

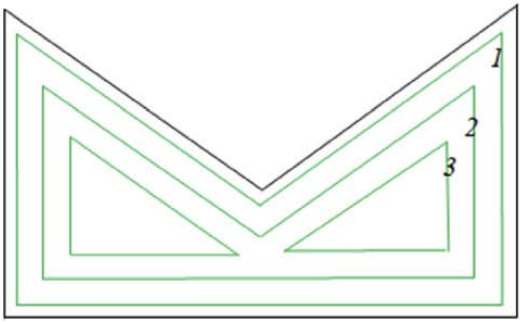

3-32(a) a contour-pocket path planning

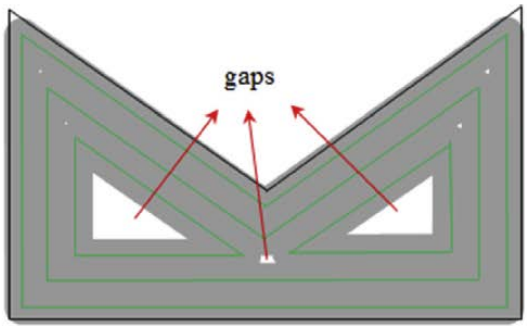

3-32(b) Internal gap in contour-pocket path

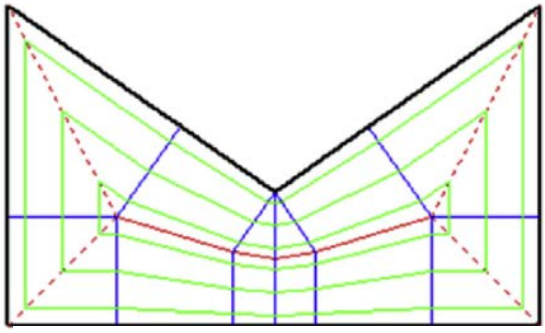

3-32(c) Medial axis transformation (MAT) for a 2-D geometry

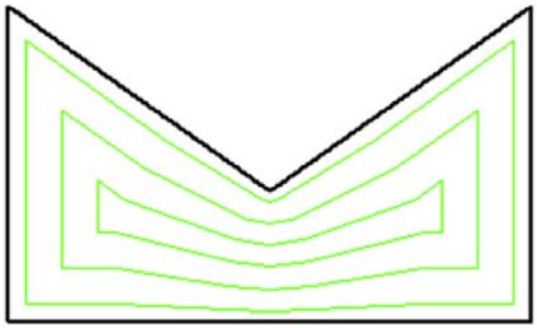

3-32(d) a path planning strategy based on MAT

Figure 3-32 A comparison between coutour-pocket path planning and MAT path planning (Ding et al. 2016b)

Distortion and residual stress are common phenomenon that existed on WAAM parts. Colegrove el al. (2013) reported a rolling method to decrease distortion and residual stress. As shown in Figure 3-33a, they mounted a roller on a WAAM platform, and used roller to roll a layer on the part after deposition. They compared the performance of three different rolling

strategies, which were rolling the final layer only, rolling after every four layers and rolling after each layer. Also, they adopted different rollers and different rolling pressure to investigate their performance. The authors found that rolling can significantly reduce the residual stress and distortion. Additionally, rolling after 4 layers had no obvious difference to rolling each layer, and the microstructure of the part got further refinement due to the pressure.

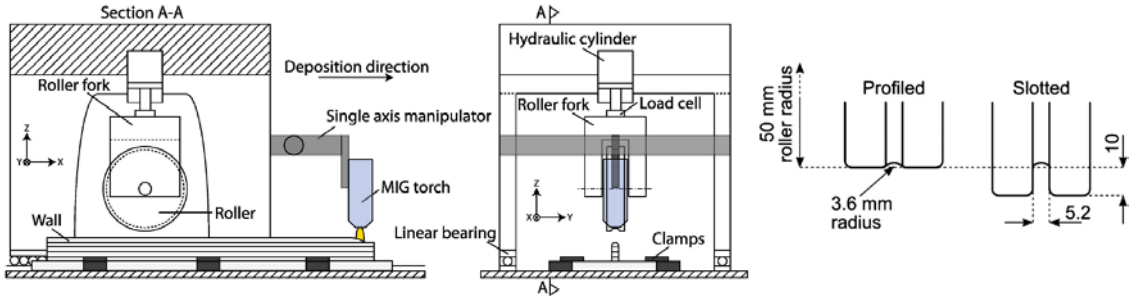

Figure 3-33 WAAM platform with rolling mechanism Right: Different rollers (Colegrove el al. 2013)

Ding et al. (2011) reported a thermo-mechanical analysis using the finite element analysis (FEA) software (ABAQUS). They developed a transient model and a static model to simulate the temperature variation and the stress variation during a simple wall building process. As shown in Figure 3-34, the simulated distortion result and the simulated temperature result both showed good alignment to the experimental result, which proved the effectiveness of the finite element analysis(FEA) model. In 2014, Ding et al. reported a computational efficient model which can save on computational time by 99%, with similar simulated accuracy compared to the original FEA model.

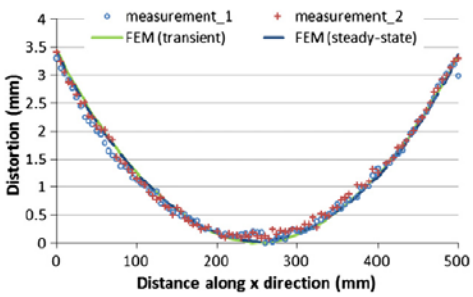

3-34(a) Finite element simulated wall distortion along the x direction against the measured result

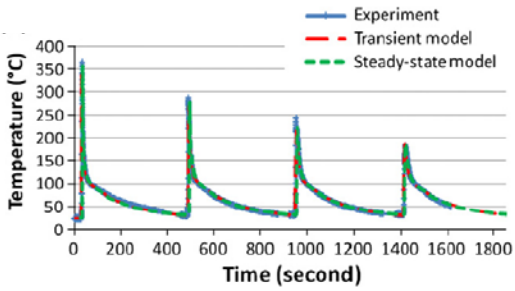

3-34(b) Finite element simulated temperature variation with respect to time against experimental result

Figure 3-34 Finite Element Simulated Stress and Temperature Against Experimental Result (Ding et al. 2014)

For the WAAM process, the part oxidation caused by heat is a common concern. Existing shielding devices have a number of shortcomes such their size that the flow turbulence can results in entrainment of the air. Ding et al. (2015) reported a new laminar flow local shielding device which may provide good shielding performance. They undertook an experiment to test the oxygen concentration level at different positions and conducted a CFD simulation to investigate its flow field. They demonstrated that their new shielding device had an improvement compared to conventional shielding gas devices.

Gockel et al. (2013, 2014, 2017) induced the process mapping method into electron beam wire additive manufacturing. They investigated how the process parameters affects microstructure and molten pool size, as shown in Figure 3-35 Gockel et al. identified beam power (P) and beam travel velocity (V) as two major process parameters. As shown in Figure 3-35 left, the molten pool area and the molten pool length to depth ratio illustrated with respect to beam power and beam travel velocity, and in Figure 3-35 right, the grain type is illustrated with respect to two major parameters.

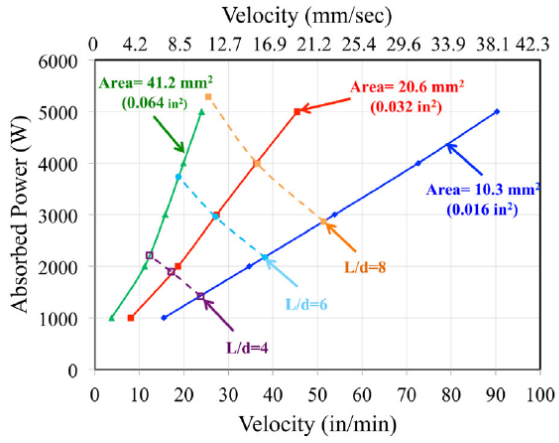

3-35(a)Process map for controlling melt pool dimensions

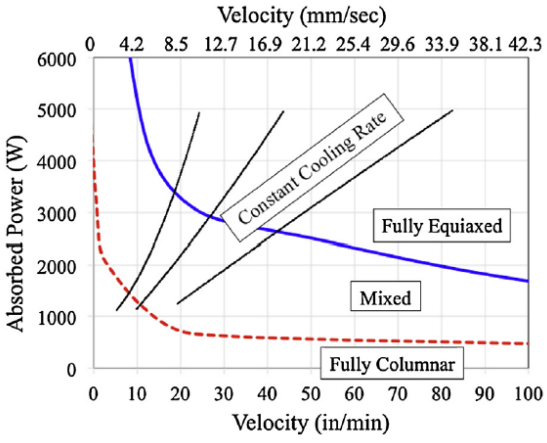

3-35(b) Microstructure process map for Ti-6Al-4V

Figure 3-35 relationship between process parameter and microstructures

Feng et al. (2012) investigated the influence of the welding speed on the droplet impact behaviour. They find out that when the welding speed was higher than 0.4m/min, the droplet would impact outside the weld pool, whereas when the welding speed was lower than this value, the droplet would impact inside the weld pool. In addition, they found out that when keeping the wire feed speed, welding current and welding voltage constant, the weld width decreased from 12.9mm to 6.3mm as the welding speed increased from 0.4m/min to 2.0m/min.

Wu et al. (2017) investigated the influence of feeding direction and feeding angle on WAAM quality. They designed a circular path that incorporates front feeding, back feeding and side feeding as shown in Figure 3-36. In addition, they investigated the wire feeding angle from 30° to 70°. Due to the interference of the torch nozzle, the wire feeding nozzle was unable to be adjusted larger than 50°. The authors rotated the torch nozzle and the wire feed nozzle simultaneously when the feeding angle was larger than 50°. As shown in Figure 3-37, the front feeding and side feeding was able to provide a good quality whereas the back feeding was not able to provide continuous welding. The authors found that when feeding the wire at 60°, the deposition quality was better than 50° and 70°.

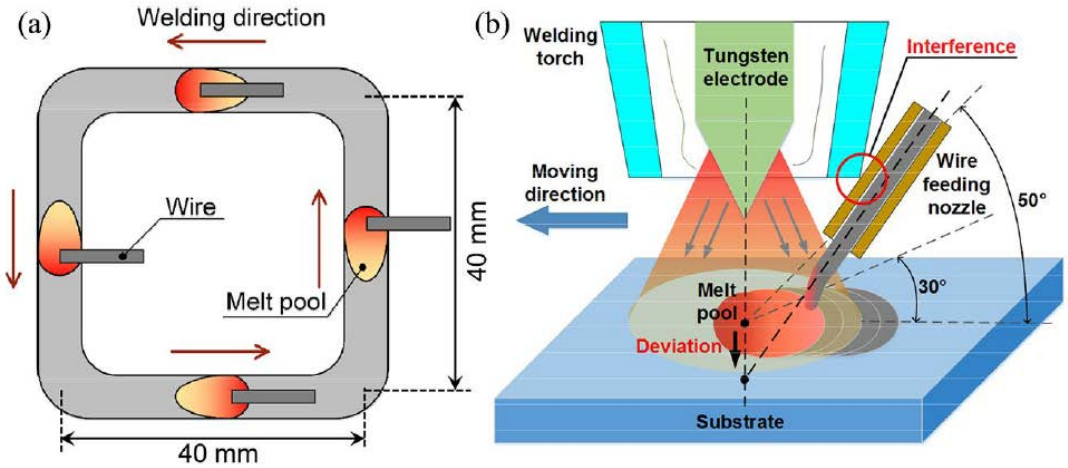

Figure 3-36 Feeding Direction Feeding Angle (Wu et al. 2017)

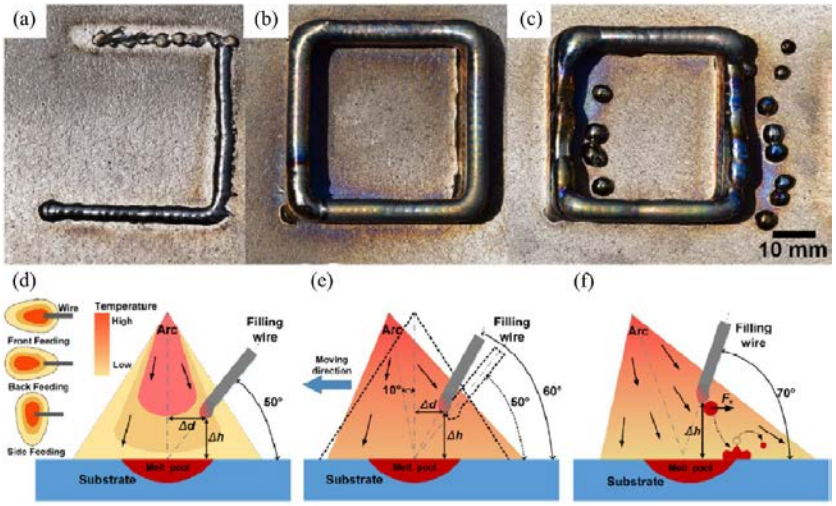

Figure 3-37 Deposition Performance against Feeding Direction (Wu et al. 2017)

In the WAAM process, the feedstock wire may deviate from the expected straight direction. Zhan et al. (2017) reported that in the worst case, this may cause wire jamming and defects on the part. The authors developed an online monitoring algorithm to detect the deviation of the stick out wire. They used a colour welding camera to capture images of the stick out wire and applied the Hough transform to detect the wire in the image automatically. Subsequently, they applied an image processing algorithm to obtain the deviation angle of the wire. As shown in Figure 3-38, the deflection of the wire is a common phenomenon, with the wire possibly deflecting to around 15 degrees. The authors did not provide a solution to correct this deflection, but it can be corrected with further development of mechanical structures or motion platforms.

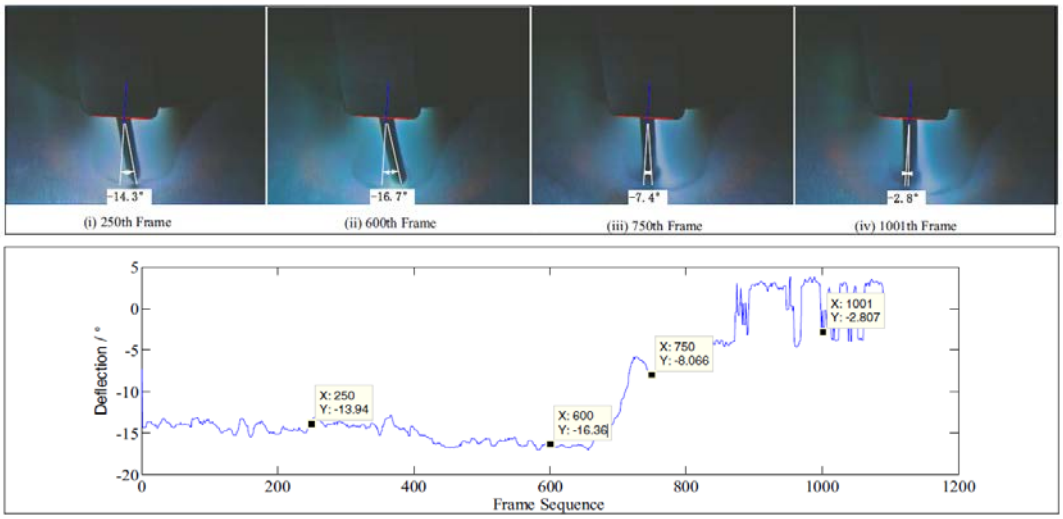

Figure 3-38 Wire Deflection Monitoring by Camera (Zhan et al. 2017)

The material properties of a part are critical as they affect the parts mechanical performance. For WAAM parts, the process parameters largely affect the properties of residual stress, the material grain size, the grain orientation etc. (Martina et al. 2015).

Cooling Rate and Thermal Gradients can largely affect the material grain size and it structure. WAAM monitoring is referred to the WAAM process parameters monitoring. It is basically used to address the WAAM defects by investigating the relationship between process parameters and its output. Since WAAM monitoring is an extension of welding monitoring, therefore the basic monitoring parameter set is similar to the welding monitoring, including welding voltage, welding current and shielding gas flow etc. However, WAAM is normally used to build a complex part with multiple layers rather than joining. It brings in new challenges for WAAM, such as excessive heat and distortion etc. To address these issues, researchers around world tried different methods to tackle these problems.

Wu et al. (2017) investigated the influence of the molten pool on microstructure and tensile strength properties. They built up a series of WAAM parts with different molten pool width's ranging from 7mm to 22mm by adjusting the wire feed speed. They found that the macrostructure of the Ti-6Al-4V part changed from columnar grains to equiaxial grains as the increase of the width of the molten pool. They also found that the ultimate tensile strength of the part decreased as the increase of the width of the molten pool. Wu et al. (2017) argued that the decrease of the strength is due to the much coarser α-lath within larger β grains.

3.5 State of the art in Industrial WAAM systems

Norsk Titanium is the leading company in the area of WAAM (Norsk, 2018). In 2015, Norsk Titanium achieved the TRL-8 certificate (Technology Readiness Level). The highest level is TRL 9, representing the technique has been proved mature in operation. TRL 8 represents the technique has been proved in test and demonstration. Afterwards, Boeing invested Norsk to

develop their technique specifically on aerospace parts. In April 2017, Norsk got the FAA certificate which enables their WAAM parts to be used in an actual commercial aeroplane (Norsk, 2017). Figure 3-39 Shows a Norsk plasma based WAAM machine which is able to produce high quality aerospace parts using a WAAM process termed rapid plasma deposition.

Figure 3-39 Norsk Titanium MERKE IV Machine (Norsk Titanium, 2017)

Sciaky is an American company which founded in 2005 (Sciaky, 2018). It was originally working on Electron Beam wire additive manufacturing. Recently, they joined the industrial competition in wire arc additive manufacturing due to the similarity between electron beam based and arc based wire AM. Figure 3-40 (Sciaky 2018) shows the use of a 5-axis system including X, Y, Z, part tilt and part rotation to enable highly flexible shaped WAAM part manufacture.

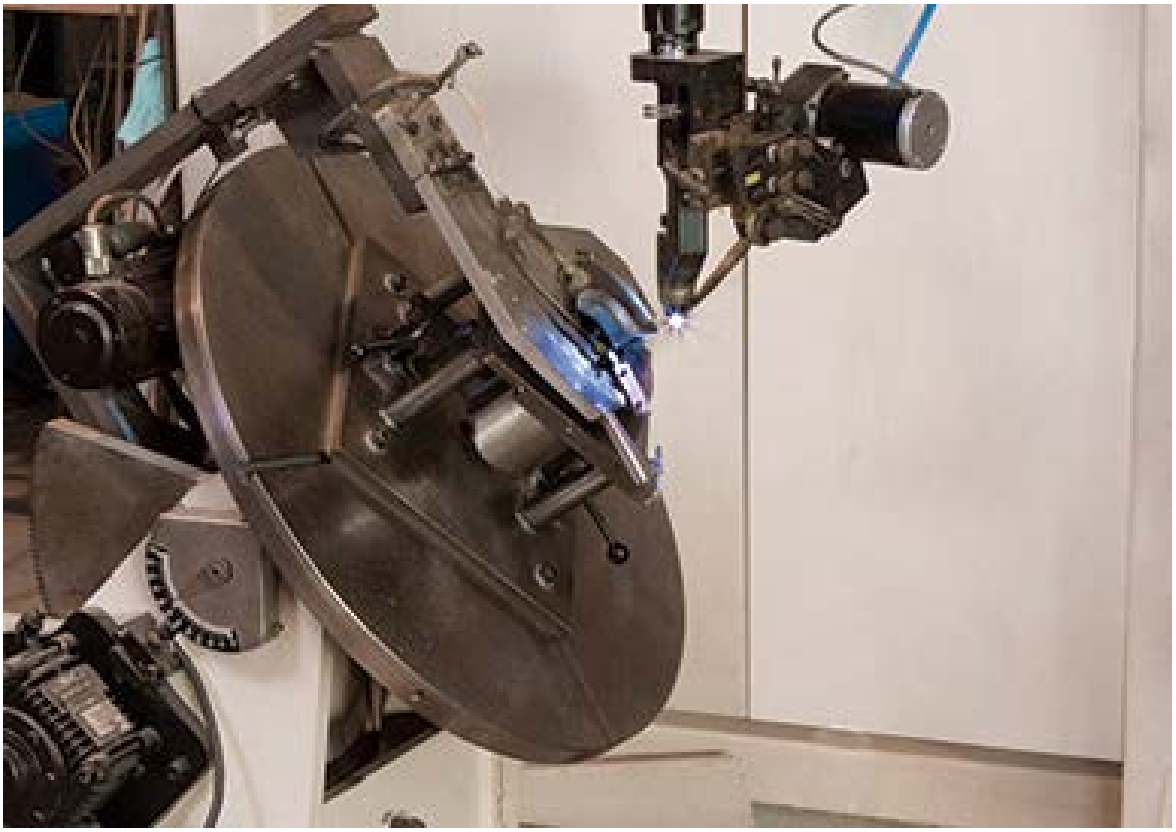

Figure 3-40 Sciaky AcuWeld 1000 System (Sciaky 2018)

Mazak released their Variaxis j-600/5X AM machine in 2018(Mazak 2018). The machine is capable of both additive and subtractive operations interoperable, this enable raw material including castings and forgings to have materials added and removed interchangeably on one platform. At present the machine is limited to WAAM using steels and Aluminium alloys.

Gefertec GmbH is a German WAAM company founded in 2015, released a number of plasma based WAAM machines(Gefertec, 2017) . As shown in Figure 3-41, they claim to provide a complete solution for creating large parts with their 3DMP WAAM process chain. The company claims that with their 3DMP process, the production cost could save up to 60% compared to conventional process.

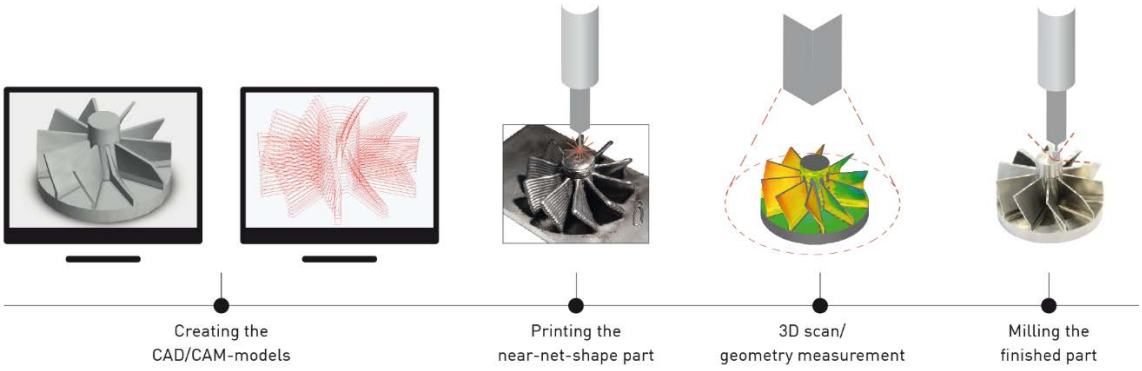

Figure 3-41 Gefertec WAAM Process Chain (Gefertec GmbH, 2017)

3.6 Critique

WAAM is an emerging technique among wire-fed AM techniques. Compared to WLAM and EBF^3, the unique feature of WAAM is that it uses an arc-based welder as the heat source. Arc-welders, as conventional metal jointing tools, has been developed for more than 40 years. Applying the welder into additive manufacturing has a natural advantage as significant research has been carried out in this area. Ding *et al.* (2015) has summarised a list of research teams in this area. Due to different background and motivation, different research groups are applying different energy sources for WAAM.

In the sections above, issues listed in Table 3-2 have been reviewed and discussed. The author is targeting the geometric accuracy of the WAAM part. Hence, layer height and layer width are selected as the key parameters. Moreover, the WAAM part is also very susceptible to the heat induced distortion. Therefore, layer temperature has also been selected. In addition, the WAAM process input are recorded as well, namely arc voltage, arc current, wire feed speed, and travelling speed.

Table 3-2 Reviewed Topic in Chapter 3

• Parameter Envelop	• Layer Width	• Layer Height
• Layer Temperature	• Arc Voltage	• Arc Current
• Weld Pool Condition	• Acoustic Signal	• Fatigue Level
• Heat Accumulation	• Strain	• Inclined Angle
• Wire Reflection	• Colling Rate	• Thermal Gradient

From the shape control perspective, the accuracy of the geometric shape and the deformation level are the key issue for WAAM process. The accuracy of geometric shape refers to the accuracy of the height, the width, and also the waviness of the part. In the WAAM process, increasing accuracy of these quantity is not only by adjusting parameters, but also by overcoming defects (such as inclusion and lack of fusion) and by investigating the physical and metallurgical principle. Currently, the waviness on the side of WAAM part is ± 0.2mm (Ding et al. 2015). The demand for high accuracy near net shape part is from three area, namely the process stability, the machining requirement and the material property requirement.

For WAAM process stability, though current accuracy has been achieved ± 0.2mm, this accuracy was realized under full human supervision (Ding et. al., 2015). Currently, in the WAAM process, the operator needs to carefully monitor the process and to adjust it manually in each layer to realize stable WAAM deposition process. The height of each layer may be higher or lower than expected, which in turn may affect the arc length and the arc voltage. After several layers accumulation, it may finally result in inclusion, lack of fusion and other defects.

For the machining requirement, the machining margin is 5mm for each side, with 3mm for roughing and 2mm for finishing. The current accuracy satisfies the requirement for machining, but this margin may decrease with the demand of decreasing low buy-to-fly ratio components.

From the material property point of view, the grain size in the outer envelope of the part is coarser than those inside (Donoghue et al. 2013). In order to achieve better mechanical properties of the part, a coarse grain structure needs to be machined. The size of the coarse grain in the outer envelope is reported to be larger than 0.7mm (Donoghue et al. 2013).

For the deformation, it is generated by generated by repeated heating and cooling in the WAAM process. In reality, the part is deposited on a substrate, and the substrate is more than 20mm

thick and well clamped on the fixture. Therefore, the deformation is minor and not easy to be observed unless the substrate is released, though the underlying residual stress might be huge. In order to eliminate the residual stress, the part will be heat treated after the deposition. After that, residual stress is largely released, and the deformation is released as well. Therefore, the deformation is not measured in the process.

WAAM has been demonstrated as a feasible industrial process for high value large part manufacturing (Norsk 2017). However, Cranfield University also argues that WAAM still suffers from low deposition rates (i.e. 0.5kg/hr ~ 2kg/hr) (William and Martina, 2015). In addition, Manchester University published a series of papers on defects inside of the WAAM part (Colegrove et al. 2017, Ho et al. 2019). In addition, there is still a lack of mature shape control method for WAAM.

In summary, the author believes WAAM can be considered still to be on a rapid growth curve with significant further developments required. The author has identified two main problems in WAAM, namely i) mechanical properties such as part distortion and material structural integrity, and ii) shape control of the deposited parts. The mechanical properties problem comes from the residual stress generated in the WAAM parts during the process, as a lot of heat is induced within the part, with the part distorting due to uneven cooling and shrinkage rates. Shape control is a key technique to increase the buy-to-fly ratio for the WAAM parts. Currently, most WAAM processes use an open loop constant width control, which means the part is deposited without any feedback from the WAAM controller. Though deposition can be measured separately the process has to be closed through process monitoring. At present such monitoring systems have not been used for feedback to improve the shape produced or modify the WAAM layers deposited. In addition, WAAM parts mostly are near net-shape part which all need to be machined. Hence, a final CAD model for the produced part is needed. Till now, no shape monitoring system take post-processing into account.

Until now, only few authors have realized WAAM shape closed-loop control system. The system developed by Heralic et al (2015) is used for laser wire-fed system. Doumanidis and Kwak's research was made on 2002, in which their shape monitoring system was too cumbersome. Xiong et al. (2015) achieved good quality deposition in terms of the height and width control, but this method can be only used for single pass layer control. The system developed by Han et al. (2017) realized multi-pass multi-layer height control with a relatively good quality. However, all these systems are only applied in simple wall parts. For complex geometry, current control system will face a number of challenges.

Chapter 4

Conceptual Design for a WAAM Monitoring System

4.1 Introduction

This chapter describes the requirements for developing a WAAM monitoring system and provides a conceptual design of a multi-sensor framework. It consists of 5 major sections. The first section is this introduction, and the second section sets out the objectives for the WAAM monitoring system. Section 3 outlines the monitoring level for WAAM system, followed by monitoring parameters selection. Section 4 focuses on sensor selection and section 5 provides a final multi-sensor system conceptual design.

4.2 Objectives for WAAM Monitoring

To enable the design of a WAAM monitoring system the requirements of the WAAM process need to be clearly understood. The WAAM monitoring system developed in this thesis is used primarily used for research purposes.

The main purposes of this monitoring system it to:

a) Keep a comprehensive record of the whole WAAM process

b) Detect the defects that occur in the WAAM process

c) Improve understanding for the WAAM process and the cause of the defects through analysis of WAAM input and outputs.

In order to fulfil these requirements, the monitoring parameters and the monitoring frequency need to be determined. The former one, monitoring parameters, determines the sensors that

need to be used in the system. The latter one, monitoring frequency affects the system design and the sensor selection.

4.3 WAAM Production Process

Determining the monitoring parameters relies on the thorough analysis for the requirements from the whole WAAM process. This is because, from a research and development perspective, the data obtained from the monitoring system will be used for all the steps in the WAAM process. In order to fulfil the research requirement from these steps, it is vital to be clear about the research focus of the whole WAAM process. The author has summarised the WAAM production process to study the technical need for the monitoring system and is shown in Figure 4-1.

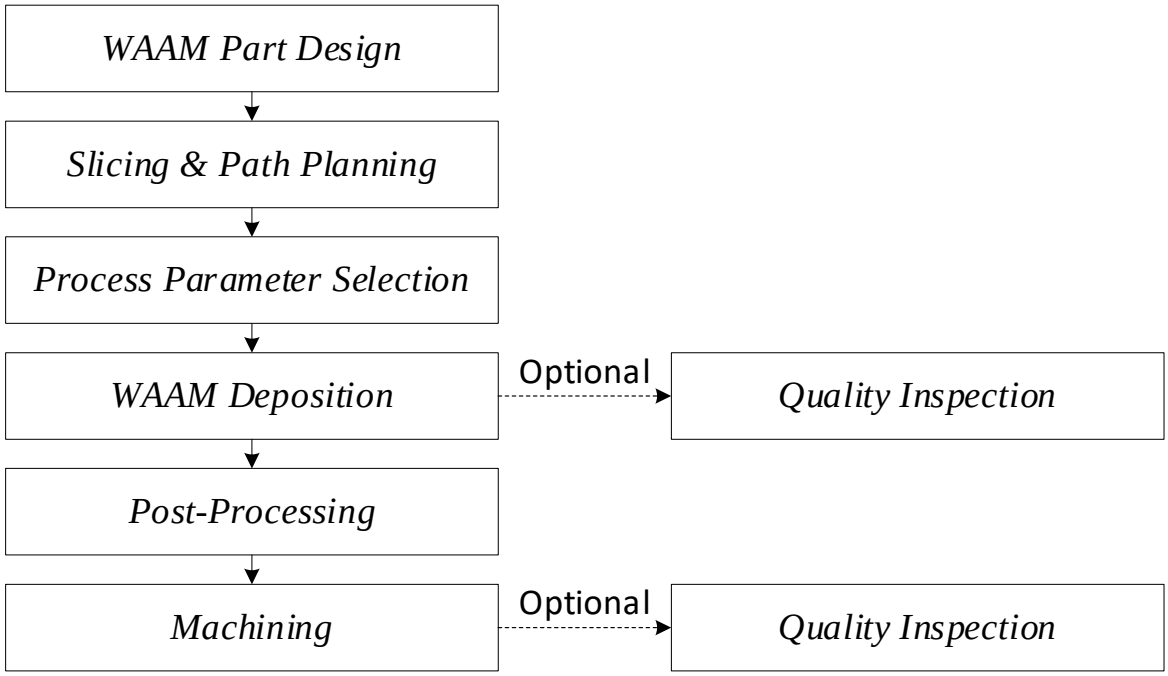

Figure 4-1 WAAM Production Process Diagram

The WAAM production process begins from the WAAM part design, followed by slicing and path planning, process parameter selection, WAAM deposition, post-processing and machining. A separate quality inspection step might be applied after WAAM deposition and machining to

examine the quality of the WAAM process and machining process accordingly. This is optional dependent on the confidence of the WAAM process and machining process. Detailed monitoring demand from the WAAM process are analysed as follows:

WAAM Part design – The WAAM part design relies on the knowledge and the limitation of the process, such as the defect-free width, maximum inclined angel, joint thickness, relationship between occurrence of defects and geometric shape etc. This knowledge cannot directly come from the WAAM process monitoring but relies on the accumulation of the monitoring data. Hence, the WAAM part design research proposes a need for the geometric shape process data monitoring, and relevant defects data monitoring.

Slicing & Path Planning – WAAM parts need to be sliced into layers and a tool path plan needs to be generated prior to deposition. Prior knowledge is required, such as the achievable layer height and layer width for different material, and defects caused by specific path patterns. This knowledge relies the accumulation of the process data and operational experience. Hence, this step requires WAAM monitoring to be able to measure the geometric data and process data.

Parameter Selection – Parameter selection relies on the understanding of the process parameters, and its influence on macrostructure and microstructure. In order to obtain the knowledge between these factors, the process parameters, geometric shape and possible microstructures need to be monitored.

WAAM Deposition –WAAM deposition is the core step in the whole production. In order to produce a defect-free, repeatable, and traceable part, all adjustable process parameters should be recorded. In the same time, the part heat, geometric and material features should also be recorded, as these factors could be developed as indicators for the quality of the part. In addition, considering health and safety issue, ambient parameters such as shielding gas flow rate, oxygen

concentration level should also be recorded.

Post-processing – For WAAM parts, heat treatment needs to be applied after completion of the deposition process to release the residual stress, and to refine the grain. This step needs little information from the process, but it requires the final condition of the part such as the part distortion, residual stress after deposition, and microstructure of the part.

Machining –WAAM generates near net-shape parts which require subsequent post-machining. Due to the irregular shape and the distortion, these parts have to be inspected and laser scanned prior to machining. The scanning process is normally a separated step after the WAAM deposition is completed. However, the scanning process could be incorporated in the WAAM deposition process, as the geometric shape data has been measured by the process monitoring system.

Quality Inspection – Quality inspection is a step similar to process monitoring. This step is a compensation for process monitoring. Since it is carried out after the deposition, further advanced and more in-depth testing could be undertaken, such as X-ray CT, SEM testing, TEM testing etc.

4.4 Monitoring Parameters for the Production Process

The requirements for WAAM monitoring come from all steps of the production process, and these requirements are predominantly related to five aspects namely, WAAM defects, the molten pool condition, part cooling rate, part geometry and working proof condition. However, these factors need to be related to measurable parameters. The following parameters are selected:

Acoustic Signal Variation – The acoustic signal indicates the energy variation of the WAAM process. The occurrence of a defect is commonly associated with energy variation (Wang et al. 2009).

Surface temperature – The surface temperature indicates the cooling rate of the part and it may affect the microstructure of the part.

Molten Pool Monitoring – The shape and morphology of the molten pool indicates the stability of the WAAM process.

Arc Current – The arc current provides the information about the heat input in the WAAM process.

Arc Voltage – The arc voltage indicates the arc length changes in the WAAM process, and indirectly reflects the height variation of the WAAM part.

Welder Travelling Speed – The welder travelling speed indicates how fast the welder travels.

Wire Feed Speed – The wire feed speed indicates deposition rate, and it affects layer height and layer width.

Part Profile – The part profile directly reflects the geometrical errors of the deposition layer and provides feedback for potential process control.

Shielding Gas Flow – The shielding gas flow indicates argon gas flow rate in the WAAM process, which is used to ensure an appropriate welding environment

Oxygen Concentration Level – The oxygen concentration level indicates the oxygen level around the molten pool area in order to ensure that the metal part is sufficiently isolated from oxygen.

4.5 WAAM Monitoring Level

The WAAM monitoring level refers to the monitor frequency of the production process. The level determines the difficulty and cost of the monitoring plan. The difficulty for WAAM monitoring mainly comes from the severe environment around the molten pool area. During the deposition process, the temperature around the plasma torch may reach over 4000℃, together with intensive light emission, electromagnetic interference, chemical reactions and

physical changes. In order to avoid these problems, a common remedy is to monitor the part after deposition. According to the monitoring frequency, the author classified the WAAM monitoring into three levels namely task level, layer level and real-time level.

Task Level - only inspects the part at the beginning and the end of the process. Sometimes, also in the middle of the process to identify problems. In this level, it is not able to rectify any problems and defects in the process, as it is not able to detect the occurrence of these issues until the inspection. The main purpose of the monitoring in level is to verify the quality of the part. In this level, most measurements are not conducted on site. Typical measurement experiments include checking by eye, material sample tensile tests, material grain size inspection etc.

Layer Level inspection is the medium level inspection plan for WAAM. In this level, the WAAM part will be measured and inspected after the deposition of each layer, with the data recorded alongside the process. Since the inspection is conducted after the deposition, layer-level inspection would not be affected by the severe welding heat radiation, electron-magnetic radiation and fumes. At the same time, the defects of each layer can be detected, traced and analysed. In addition, by applying some compensation algorithms for a part, some variations and defects in the part can be rectified in the next part layer.

Real-time level inspection is the most difficult level of inspection for WAAM. It requires the sensor to measure and monitor the information during the process in real-time. In this way, the sensors have to be able to tolerate the harsh environment around the welding torch. At the same time, a real-time control algorithm needs to be applied to avoid defects and rectify defects immediately.

4.6 WAAM Monitoring Framework Design

The author proposes an in-situ multi-sensor system framework in this section, aiming to acquire information on the WAAM process. The framework is divided into five layers as shown in Figure 4-2, namely the sensor layer, the signal layer, the feature layer, the decision-making layer and the output.

The sensor layer contains all physical devices and the signal layer collects the raw signals from the sensors. Since the raw signals cannot directly reflect what is happening in the WAAM process, an additional data processing procedure is needed. In the feature layer, data processing algorithms are applied to extract effective data which might be used as process indicators or even feedback for further process control. As shown in Figure 4-2, in the feature layer, five types of factors are illustrated namely, defects, feature data will be passed to the decision-making layer which will adjust the process parameters to improve the quality of the depositions. With each specific deposition, the online monitoring system will be modified based on each individual case.

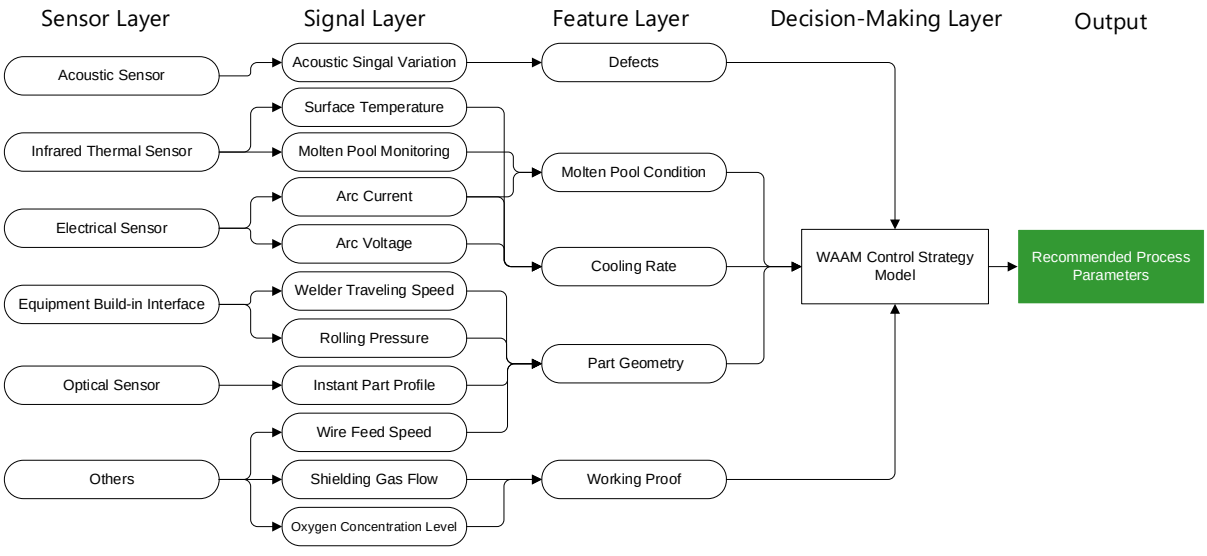

Figure 4-2 Schematic diagram of a holistic monitoring framework for WAAM

As shown in the Figure 4-2, the author summarised a four layers concept design, consisting of a physical sensor layer, signal layer, feature layer and decision-making layer. The physical sensor layer incorporates all sensors that are used in the monitoring system. The signal layer is the raw data acquired from the physical sensors. However, these signals may not be meaningful for WAAM. Therefore, a feature layer is needed, which is used to extract the indicting features from the signal layer. As mentioned above, the author argues that the cooling rate, the distortion level, the molten pool condition, the defects and the working proof are the five main features.

As a basic set-up, the sensors for process parameter monitoring required are voltage sensor, current sensor, wire feed speed sensor and welding speed sensor are the four basic sensors that most WAAM monitoring systems use.

4.7 Summary

This chapter outlines the conceptual design of the WAAM Monitoring System. It consists of

- An explanation of the WAAM production process of the equipment and process chain.
- Identification of the monitoring parameters for the WAAM production process.
- A definition and description of the various level for WAAM monitoring.
- The design and description of and WAAM monitoring framework.

The chapter also has illustrated the WAAM process chain in 6 major activities, as shown in Figure 4-1. These 6 activities namely WAAM part design, path planning, process parameter planning, WAAM deposition, part quality inspection, and machining. The final post process of heat treatment, part quality inspection and machining enable production of the final finished WAAM part. The major focus of the WAAM deposition stage is the WAAM process monitoring system which measures the process parameters and uses the feedback for potential process control.

Chapter 5

The Realization of a Multi-Sensor WAAM Process monitoring system

5.1 Introduction

This chapter describes the realisation of a process monitoring system for a large-scale WAAM manufacturing machine. This monitoring system is based on the research framework outlined in chapter 4 and provides a detailed view of the implementations and feedback monitoring the system is capable of attaining. The first part of the chapter outlines the HiVE (High Value Engineering) WAAM machine. The major aspects focus on the sensor selection and the implementation with the final on process parameter monitoring, thermal monitoring, geometric shape monitoring and laser profilometer calibration.

5.2 The HiVE WAAM Machine

The HiVE machine was originally a 3 axis Cartesian gantry platform for the friction stir welding process, with movement ranges of 10 meters in the X-axis, 5 meters in the Y Axis and 1.5 meters in the Z-axis. In 2014-2015, the HiVE machine was retrofitted to be a WAAM machine, as shown in Figure 5.1. A welding head and a pressure roller were added to replace the friction stir welding head. The addition of a pressure roller was incorporated to eliminate the distortion and to release the residual stress by applying high pressures to each part layer after deposition (Williams et al. 2015). To enable the welding head and the roller to travel in different directions, two additional rotational axes were added on the machine as shown in Figure 5.1b, where the pressure roller is termed as CR-Axis and the welding head is termed as C-Axis. They are both able to rotate 360 degrees along their axis. A shielding gas box has been

mounted on the C-Axis to avoid oxidation around as-deposited area by blowing argon gas. A Fronius plasma welder head has been used as the welder power source. The motion system and the welder system are controlled by a FANUC PLC controller. The HiVE machine was located in Cranfield University since 2015. In 2017, it was moved to Glenalmond group which is located in Glasgow. The author participated in the retrofitting job for the HiVE machine, in which he was responsible for the design and the installation for the monitoring system.

5-1(a) HiVE 5-axis gantry

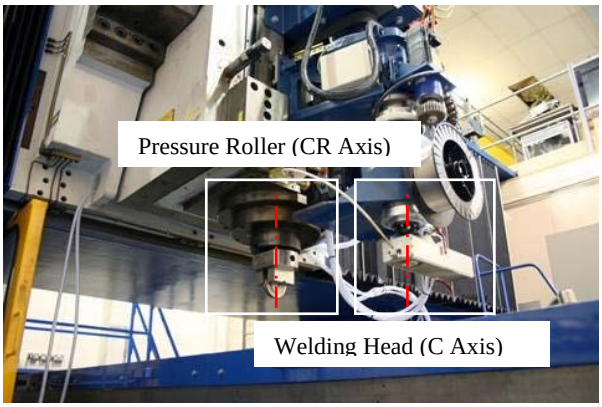

5-1(b) Deposition head and Pressure roller

Figure 5-1 WAAM HiVE machine

After the retrofitting process, a Fronius machine was installed on HiVE. As listed in Table 5-1, all adjustable parameters in the process has been listed, but some of them are only partially adjustable. For arc current, it only can be adjusted to a number of pre-set current values. Arc voltage can't be adjusted directly from the power module, but it could be adjusted by changing the welder head's position, and the arc length. The position and moving speed of all five axis, namely X axis, Y axis, Z axis, C axis and CR axis, are able to be adjusted in the real-time. In addition, the wire feed speed also can be adjusted in real-time. These adjustable parameters established a basis for WAAM real-time process control on HiVE.

Table 5-1 Adjustable Input Parameters on HiVE machine

• Arc Current	• Arc Voltage	• Arc Length
• Travelling Speed	• Wire feed speed	• X, Y, Z, C and CR axis

5.3 Rolling Procedure for WAAM

The HiVE machine was located in Cranfield University, and this research was carried out in collaboration with Cranfield University. As mentioned in Section 5.2, a roller was installed on CR axis on HiVE. This roller is used to carry out a process named pressure rolling, aiming to release residual stress in the WAAM process. Since 2013, Cranfield university has published a series of papers (Colegrove et al. 2013, 2014, Martina et al. 2014, Donoghue et al. 2016) reporting their investigations on adding rolling process in WAAM. In this pressure rolling process, each layer would be rolled after its deposition, and a pressure of 50 kN to 70kN would apply on the deposited layer to release the residual stress. According to Colegrove 2013, the stress at all location of WAAM part decreased about 100MPa, and in one of its sample, the residual stress at the top of part reduced from 600Mpa to 250MPa. In addition, they found that the rolling process could largely refine the grain size from 700um to 100um. In this research, the pressure rolling was applied after each deposition process.

5.4 Sensor Selection

5.4.1 Temperature sensor

In this research, a temperature sensor has been used to measure the temperature on the top surface. Since the WAAM process is a continuous material adding process, the top surface is always changing. Hence, a contact fixed sensor is not applicable. In terms of the contactless temperature sensor, a pyrometer and thermal camera are two types of sensor that are able to measure the object temperature from a distance.

For the WAAM process, according to temperature distribution, the part is divided into a molten pool, heat affected zone (HAZ), and base metal. The molten pool is where the material melts into liquid condition. The heat affected zone is a non-melted area that undergoes material changes under high temperature. The base metal refers to the substrate or the layer being

deposited on. Different sensors provide different methods and the ability to measure these areas. As shown in Table 5-2, thermocouples, pyrometers and thermal cameras are the most commonly used sensor in welding & WAAM applications.

Table 5-2 Temperature Sensors for Welding & WAAM Process

	Contacted/Contactless	**Principle**	**Target Object**
Thermo-Couple	Contacted	Seebeck effect	Base metal
Pyrometer	Contactless	Stefan–Boltzmann law	HAZ, Base Metal
Thermal Camera	Contactless	Stefan–Boltzmann law	Molten Pool, HAZ, Base Metal

(i) Thermocouples

The working principle of thermocouples is based on the Seebeck effect (Van Herwaarden and Sarro, 1986) The Seebeck effect refers to a phenomenon in which two dissimilar conductors under a temperature difference generate a voltage between the two conductors. The generated voltage is proportional to the temperature difference in a certain range. A wide range of thermocouples provides the ability to measure the temperature ranging from -200 ℃ to 2000 ℃. The drawback of the thermocouple is that it needs to be attached prior to the welding process.

(ii) Pyrometer & Thermal Camera

The pyrometer and thermal camera all utilize infra-red thermography to measure temperature. The pyrometer measures the temperature in a small spot depending on focal length and the distance to the target (e.g. Micro-Epsilon Pyrometer SF75 series lens has a spot size of 16 mm at a distance of 1200mm), whereas thermal cameras could measure the temperature distribution of an area. Similar to a standard camera, the size of the view area is dependent on focal length and the distance to the target. The working principle is based on Stefan-Boltzmann law, which describes that all objects that have a temperature above the absolute zero radiates energy, and the energy complies with the following equation (5.1):

$$E = \varepsilon \sigma T^4 \tag{5.1}$$

Where ε represents the emissivity, σ represents the Stefan–Boltzmann constant, and T is the temperature. It is noted that emissivity ε varies when material melts and solidifies (Zheng et

al., 2015). This phenomenon induces large inaccuracies for infer-red sensors. However, the big advantages of the contactless measurement method overweigh its disadvantages. Thus, the pyrometer was selected as the sensor type for WAAM monitoring system within this research and is described in 5.6.5.

5.4.2 Arc Current Sensor

According to the Joule's law, the energy generated by the heat source is proportional to arc current and the resistance as shown in Equation 5.2.

$$\mathrm{P} \propto I^2 R \tag{5.2}$$

In order to create and maintain a stable and consistent melting process, the current is controlled to fix at a value by the welding power. The arc current is typically in the range of the range of between 100~500 amperes. The mainstream measurement method uses a Hall-effect probes, which can measure the current with no physical interference of the system. As shown in Figure 5-2, the Hall-effect probe is able to measure the current when attached to a cable.

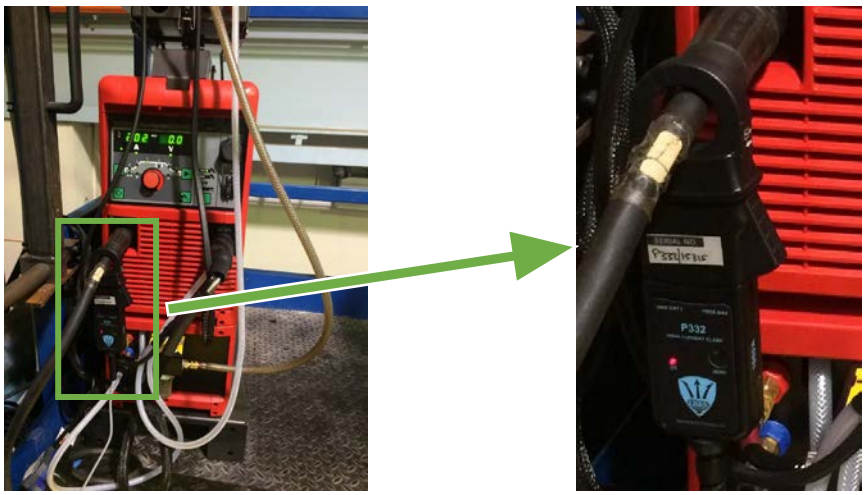

Figure 5-2 Hall effect current probe attached on a welder power module

5.4.3 Arc Voltage Sensor

The arc voltage is a dependent parameter in the welding process. According to Joule's Law

$$V = I \times R \tag{5.3}$$

Where V is the arc voltage, I is the arc current, R is the resistance of the plasma. Arc current *I* is commonly controlled by the power module and *R* is varying according to the arc length. Therefore, the magnitude of the arc voltage V varies as R varies. In other words, arc voltage is a reflection of the arc resistance or the arc length. The voltage sensor is a standard and widely used electrical measurement device. For this WAAM application, the voltage is monitored by the welding power module. In order to obtain a more reliable data, an external voltage clamp is added to monitor the output voltage variation from the welder power source.

5.4.4 Geometric Shape Sensor

As previously reviewed in section 3.4.5, 6 methods of shape monitoring methods are introduced as listed in Table 5-3. According to the discussion in sections 4.3, 4.4& 4.5, this monitoring system only needs layer level monitoring, which means the shape monitoring could be undertaken after the deposition of each layer. However, deformation is a critical problem for the WAAM process (Martina et al. 2015). In order to study the relationship between process parameters and geometric defects and distortion, it is more important to obtain the full shape of the WAAM part rather than the height or the width of the part only.

Table 5-3 Shape Monitoring Method

Method	**Height/Width/Shape**	**Monitoring Level**	**Author**
2D image shape reconstruction	Shape	Real-Time	Zhang et al. 2006
Dot-matrix projection	Shape	Real-Time	Saeed and Zhang 2003
Indirect Voltage conversion	Height Only	Real-Time	Xu et al. 2012
Coherent Interferometer	Height / Width	Real-Time	Kissinger et al. 2019
Laser Profilometer	Height / Shape	Layer/Task	Heralic et al. 2012
Camera	Height/Width	Real-Time	Xiong et al.

To quantify the deformation level, it is necessary to measure the profile of the part during the production process. For WAAM with an integrated rolling process, profile monitoring is critical for controlling the rolling pressure. Typically, a laser contactless profilometer is applied to measure the profile. When using only one profilometer on the top of the part, the side measurement information was not able to be measured accurately. In this research, active

optical signal monitoring was applied, specifically, two laser profilometers were adapted for use by the author at 90 degrees to each other as shown in Figure 5-3a for measuring a multi-layered part shown in Figure 5-3b. Post processing software was then designed and implemented to fuse the data from the two different sensors, as shown in Figure 5-3c.

For WAAM with a subsequent rolling operation, monitoring the pressure of the roller was also necessary. This enabled the rolling of each layer with different pressures according to its height. Optical signal monitoring is divided into two categories, active optical signal monitoring and passive optical signal monitoring (Xiong et al. 2013). Passive optical signal monitoring is the normal camera monitoring, whereas, active optical signal monitoring applies an external laser source to improve monitoring accuracy.

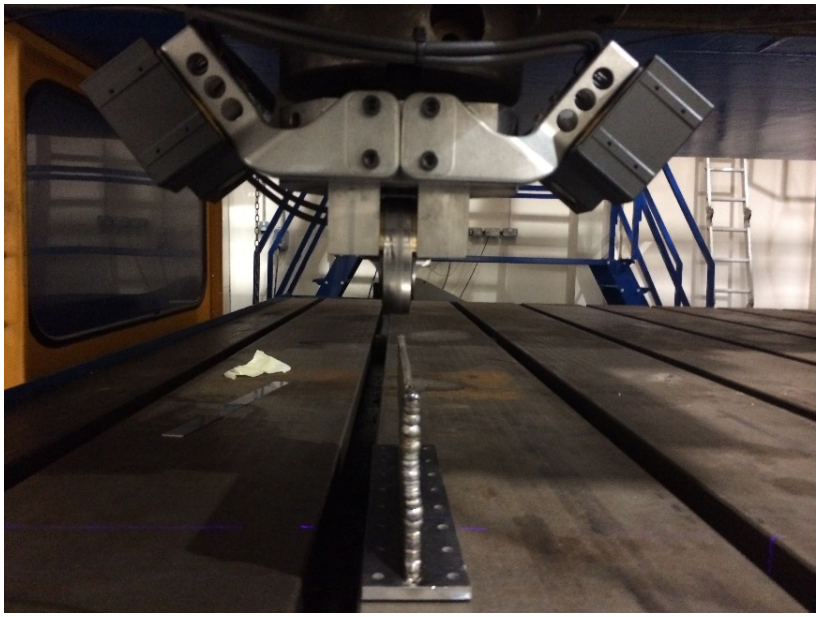

5-3 (a) Two Laser Profilometers mounted in front of the roller on HiVE

5-4 (b) A typical WAAM part to be scanned

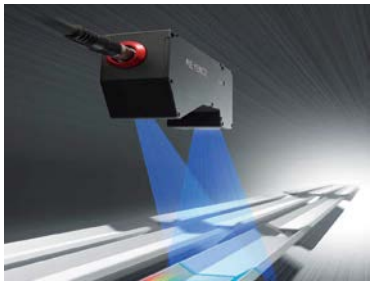

5-3 (c) A schematic diagram of Keyence Laser Profilometer

Figure 5-3 Laser Profilometer Arrangement on HiVE

5.4.5 Wirefeed Speed Sensor

Bead geometry is another factor that influences the final profile. According to Ding et al. (2013), the bead profile is dependent on the wire feed rate and welder head speed. In most applications,

the welder head speed is monitored and controlled by a CNC-controller. To monitor the wire feed rate, a wire feed sensor was attached to the machine. As shown in Figure 5-4, the sensor was passively driven by the wire to obtain an accurate reading. It should be noted that the wire was actively fed by the welder machine.

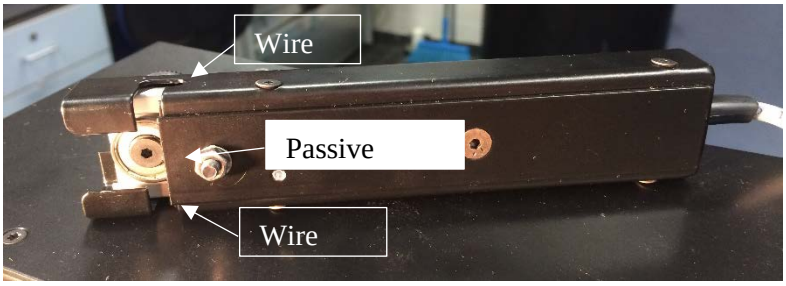

Figure 5-4 Wire feed sensor

5.4.6 Environmental sensors

With the high temperature of the WAAM heat source (typically higher than 4000 ℃), depositions can become easily oxidized. To avoid oxidation, it is necessary to blow shielding gas, normally argon, around the melt pool. In most welding and WAAM applications, oxygen concentration sensors are widely applied to ensure that the concentration level is lower than 100 *ppm* (Ding et al. 2015). To use the shielding gas economically and in the correct location, a gas flow sensor has been applied to measure the flow speed of the argon gas (litre/min), and an oxygen sensor has been installed near the welding torch.

5.5 Multi-Sensor WAAM process monitoring system

To realize a complete monitoring loop for WAAM, the author designed a system based on the conceptual design described in section 4.6. This consists of seven sensors, namely, pyrometer, shielding gas flow sensor, wire feed speed sensor, current sensor, oxygen concentration sensor, laser profilometer and rolling pressure sensor. In order to collect data from different sensors, a NI PXI Data Acquisition (DAQ) system was used as a middle layer between physical sensors and the PC. The hardware data link diagram is shown in Figure 5-5. All the sensors are

connected to the NI PXI system and then connected to the PC. The Fronius welder is connected to the FANUC PLC and the to the PC. The Fronius Welder is a welder controlled by the PLC, but also used as a sensor to measure the welding current and voltage. A detailed specification of the sensors is listed in Table 5-4.

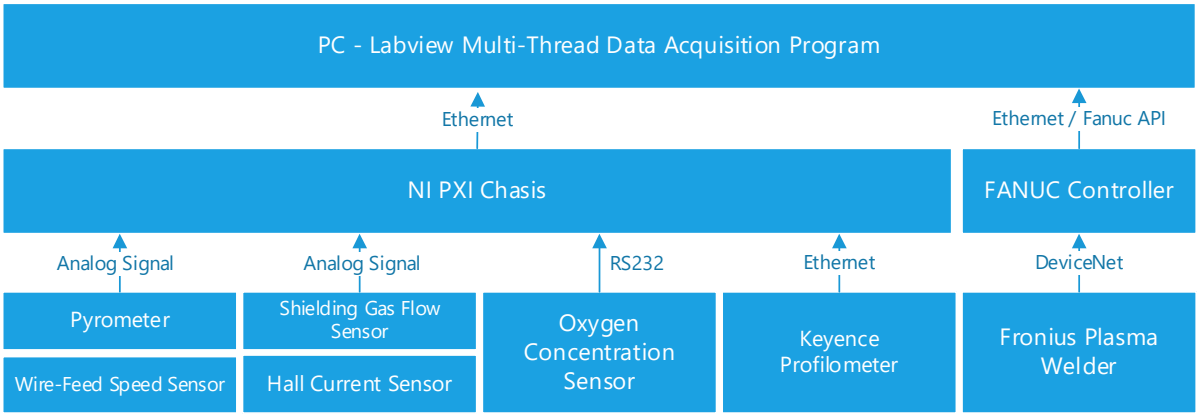

Figure 5-5 WAAM Monitoring System Data Link Diagram

Table 5-4 Sensor Manufacturer and Basic Specifications

	Type	Rated Working Range	Accuracy
Pyrometer	MicroEpsilon CTL -SF75	-50-950℃	±0.1 ℃
Wire Feed Speed Sensor	Triton	0~12m/s	±0.1 m/s
Current Sensor	Triton	0~1000A	±0.1 A
Shielding Gas Flow	Triton	0~20 L/Min	±0.25L/min
Oxygen sensor	PurgEye 500	10~1000 ppm	±1 ppm
Laser Profilometer	Keyence LJ-V 7300	-120 ~ +120 mm	±5 μm

The NI PXI data acquisition system was used as it provides extensive interfaces for different types of sensors, and numerous tools to process the feedback of the signals. As a consequence, NI Labview was applied as the option for the software implementation platform as this is the accepted way to utilize the NI PXI system. The data is collected from the FANUC controller, and the Fronius Plasma welder data was transmitted and stored in the FANUC controller. Due to the encoding method of the data, Labview was unable to read it directly from the controller, therefore an additional middleware was added to convert FANUC data to normal float type

data.

The NI Data Acquisition System (NI DAQ) provides a complete solution for different types of signal. In this system the author adopted the NI PXIe-1065 chassis and a batch of signal acquisition boards.

5-6 (a) NI PXI Express-1065 Chassis

5-6 (b) Optic fibre connection board

Figure 5-6 Data Acquisition Device

As shown in Figure 5-6, the NI PXIe-1065 chassis which includes 9 PXI slots, 4 hybrid slots, 3 PXI Express slots and 1 PXI Express system timing slot. These slots are used for different PXI boards like the board shown in Figure 5-6b. In Figure 5-6b, it is the optic fibre connection board which is used for connecting the NI PXIe system to the PC. All boards adopted by the system are listed in Table 5-5.

Table 5-5 PXI Board List

	Model	Type	Use
1	NI PXIe-1065	Chassis	Data acquisition chassis
2	NI PXI-8430/2	RS232	Collect data from oxygen concentration sensor
3	NI PXI-4300	Analog	Collect data from universal sensor
4	NI PXI-8234	Ethernet	Collect data from laser scanner
5	NI PXI-8368	Optic Fibre	Connect NI PXI to PC

The layout of the sensors on the HiVE machine are shown in Figure 5-7. The welding power control module and the NI DAQ system were positioned on top of the machine, and the sensors were installed around the welding head. This layout has been applied under the consideration that the data processing and control units should be kept away from the harsh welding environment, but still be close enough to obtain data. It should be noted that when the welding head moves, all the sensors move along with it. Thus, the sensors remain in the same relative

position to the welding head throughout the process. This enabled the sensors to provide consistent output data.

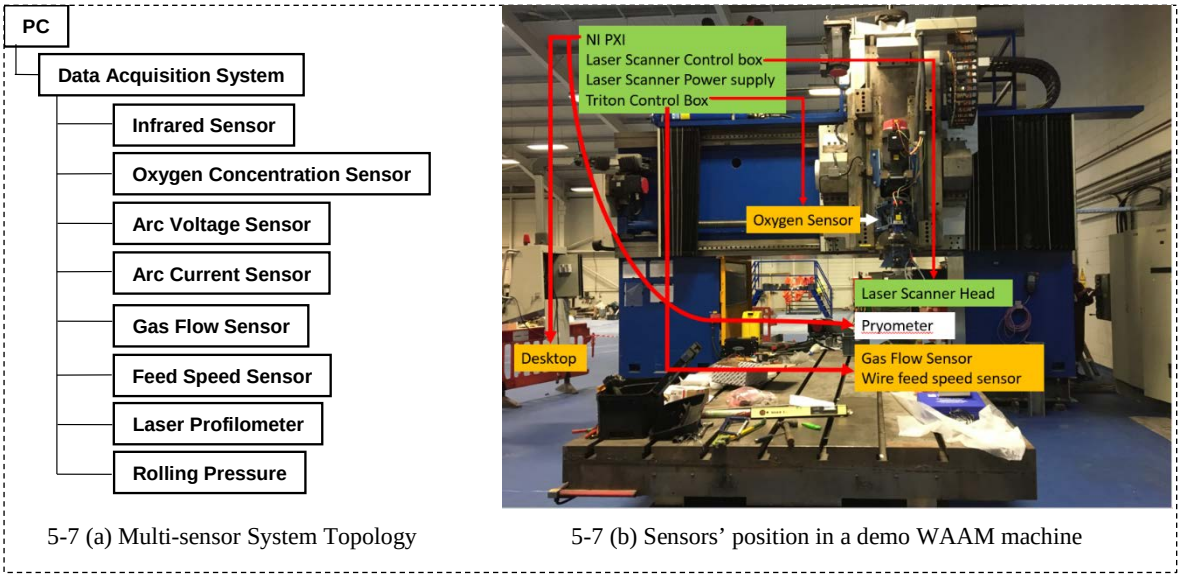

5-7 (a) Multi-sensor System Topology

5-7 (b) Sensors' position in a demo WAAM machine

Figure 5-7 WAAM Monitoring System Structure

Though all these sensors are used to analyse the WAAM process, they focus on different aspects of the system. Therefore, they have been divided into sub-systems. The three sub-systems shown in Figure 5-8 are: i) heat monitoring sub-system, ii) bead geometry control sub-system, and iii) environmental monitoring sub-system.

The heat monitoring sub-system is used to monitor heat output from the arc welder and the temperature of the melt pool. It consists of IR sensor and arc voltage/current sensor. By collecting data from these sensors, the heat input can be measured in terms of how much energy has been input through arc welding system. Variations in this would show the heat balance between the heat input induced by the arc welding system and the heat dissipated through the metal part and the environment.

The bead geometry monitoring sub-system is used to monitor the single bead size and analyse and predict the bead geometry and quality. The system gathering data includes component profile from the laser profilometers, wire feed speed from feed sensor, torch travelling speed from the NC board and roller pressure if a roller is applied. Normally, the bead

geometry system is connected to the NC-control board to generate a closed loop process control system. This is because, for a WAAM machine, controlling the bead geometry is a critical requirement as this ultimately governs the deposition quality and repeatability. The closed loop system gathers the profile data from the laser scanner as feedback and controls the wire feed speed and torch travelling speed to generate uniform beads. In addition, for the HiVE WAAM machine with the integrated roller system, control of the roller pressure is required.

The environmental sub-system is used to monitor the oxygen concentration level. It consists of the oxygen concentration sensor and the shielding gas flow sensor. During the production process, the system monitors the Oxygen concentration near the melt pool or in the chamber to ensure that the component is not affected by adverse quantities of Oxygen.

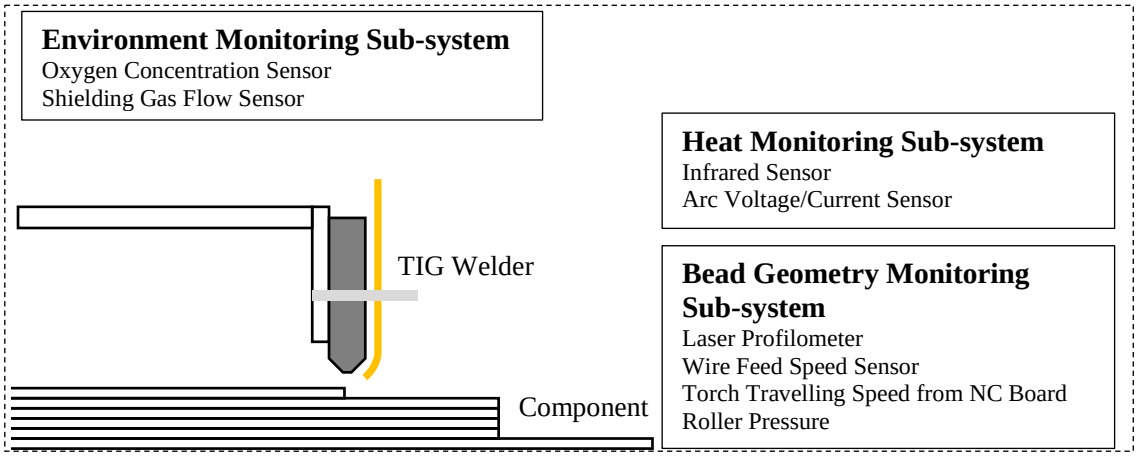

Figure 5-8 Multi-Sensor Sub-Systems

5.6 WAAM Monitoring Process

5.6.1 Monitoring Program

The monitoring program structure is shown in Figure 5-9. This program is based on Labview, and it is used to collect data, and record data from the WAAM process. The program can monitor and record all sensor data including oxygen level, temperature of the part, profile of the part, and also voltage with current of the plasma torch. The program consists of three units, namely Initialization Unit, Data Collection Unit and Data Recording Unit. The initialization

unit is used for sensor communication protocol setup and initialization. It also consists of an emergency stop function which will stop the whole multi-sensor system in case of the occupancy of any emergency or malfunction. The data collection unit consists of sub-modules for different types of data from different ports such as serial port data collection, analogue data collection and ethernet data collection and PLC data collection as reviewed in Figure 5-5 previously. The data recording unit has been created in order to integrate and fuse the data from different sensors. It records process data in the deposition process and records profile data when the part is being scanned.

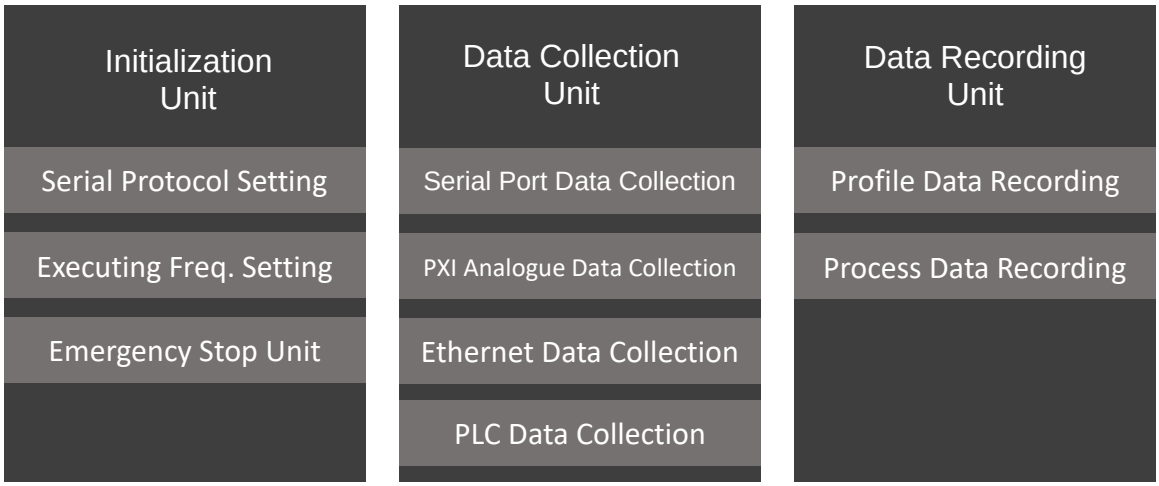

Figure 5-9 Labview monitoring program structure

5.6.2 Data format for WAAM Process

The WAAM manufacturing process for depositing a single layer is shown in Figure 5-10. For each layer, the process starts with the deposition stage, followed by rolling and profile measurement. Occasionally, in order to compare the pre-rolling and post-rolling profile, an additional optional profile measuring step is conducted before rolling as shown in the dashed box in Figure 5-10. These processes are then repeated to build up a WAAM part layer-by-layer. It is noted that in the rolling process, only the rolling load in x, y, z directions are measured and recorded, whereas the other two processes of deposition and profile measurement are the major processes that affect the quality and accuracy of the WAAM components.

Since the deposition and profile measurement process occurs in a same layer on a part, but are undertaken separately, it is necessary to unify them in the same coordinate framework so that the process data recorded in the deposition process and the profile data recorded in the measurement process can be mapped. This requires a specific data structure to unify them together.

The process data acquisition model is shown in the bottom left of Figure 5-9 and represents how the data is stored in the WAAM deposition process. Here the position information is used as a primary index in each frame of data. Every 0.2s, all process data is stored in the process data model. Similarly, the profile data of the WAAM component is stored in the geometric data acquisition model in which position information is also used as the primary key. It should be noted that the process data and the geometric data are from the same part but are measured separately. By using the position information as the primary index, to enable the connection between both acquisition systems, the deposition data and post-deposition data (geometric data) have been combined according to the absolute position information.

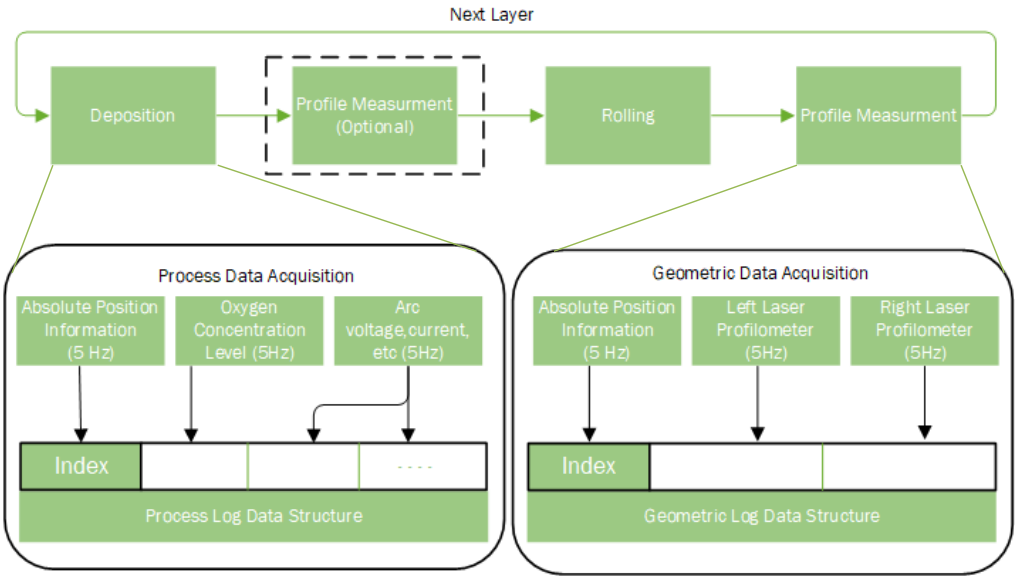

Figure 5-10 Schematic Diagram for Monitoring Process Results

5.6.3 Process parameter monitoring

In section 4.4, a series of process parameters that needed to be monitored have first been documented. These are commonly referred to as process parameters that users can adjust before and during the process. In WAAM, the process parameters are welding voltage, welding current, welding moving speed and wire feed speed (Węglowski, 2012). The monitoring process of these parameters are described below.

5.6.4 Voltage and current monitoring

Welding voltage is a factor associated to welding power, welding current and the gap between the welding head and the part. Welding voltage is not adjustable, and it is approximately linear to the gap between the welding tip and part. The author has set up a global acquisition frequency of 5 Hz, as this is the best frequency rate that the profilometer can achieve, and the author has synchronized all the sensors to gain a meaningful relationship between process inputs and outputs.

Initially, it was determined to use an external voltage sensor to monitor the welding voltage between the welding head tip and the substrate. However, it was not applicable as the welding tip moves in a large area and it needs an external mechanism to keep the sensor attached on the tip. Subsequently, the voltage reading from the welding power module was used to control the electrical parameters.

Welding current is directly related to the heat induced in the part and adjustable during the WAAM process. To avoid excessive heat input, monitoring the current is necessary. The current data was also collected from the welding machine directly through a hall current clamp attached to the main welding torch cable.

5.6.5 Thermal Signal Monitoring

The cooling rate of the part is extremely important in terms of the final mechanical properties.

This is important as it controls the grain size of the as-deposited WAAM part. Repeated uneven expansion and contraction largely influences the residual stress and distortion. Therefore, monitoring the temperature of the part is necessary. Since the melting point of the titanium is 1668 ℃, and the part is growing in the process, a contact thermal sensor is not applicable. Therefore, a contactless thermal sensor such as a pyrometer was used and is shown in Figure 5-11. This micro-epsilon pyrometer is able to monitor the temperature in a small spot (16mm) within 1200mm. The real-time data from the controller was obtained through an analogue channel on the NI PXI System. The pyrometer measuring range is from -50 ~ 950 ℃. This clearly represented an appropriate range for the WAAM process as the WAAM parts cools down quickly from more than 1668 ℃ down to 200~400 ℃ in the open air.

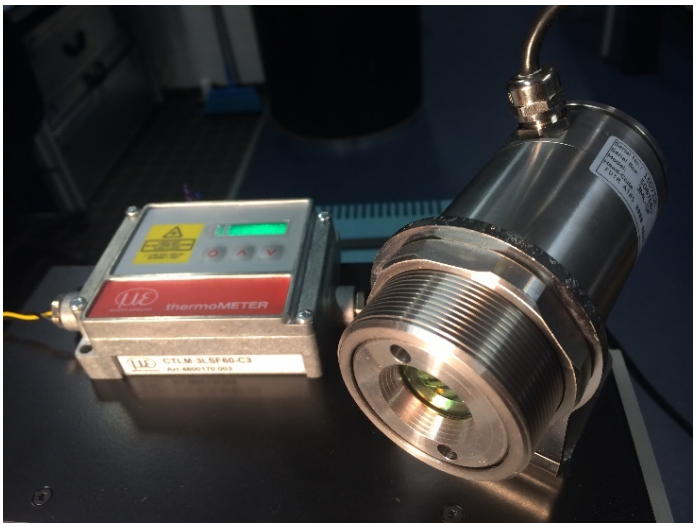

Figure 5-11 Pyrometer and Its Control Unit

5.6.6 Geometric Shape Monitoring

The raw data obtained from the laser profilometer is a batch of height data along the cross-section of the part. A typical raw data sample is depicted in Figure 5-12b. One laser profilometer can only obtain the feature from its own side due to the inclined setting of the laser profilometers (See Figure 5-12a). In order to capture a complete part shape, the data from two different laser profilometers are combined.

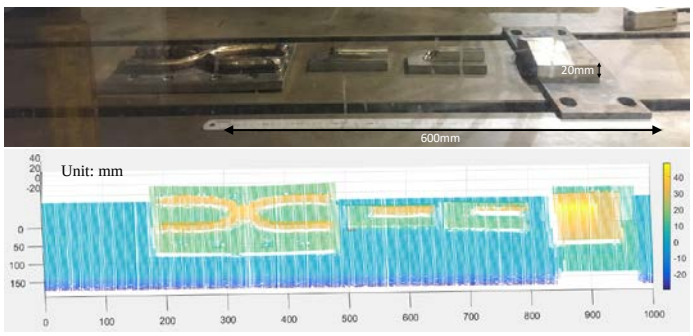

5-12 (a) Laser Scanning Point Cloud in comparison with real parts

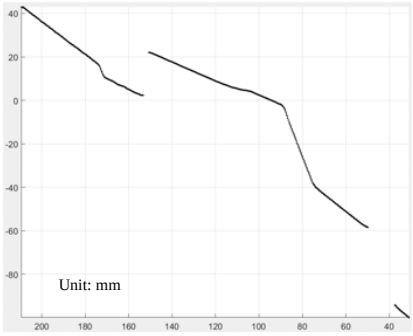

5-12 (b) a cross-section frame of data obtained by laser profilometer

Figure 5-12 Point cloud Results from Laser Profilometers

Considering the noise in the data and the inclined set-up of the laser profilometer, a series of data processing procedures are needed. The standard procedure consists of six steps as shown in Figure 5-13.

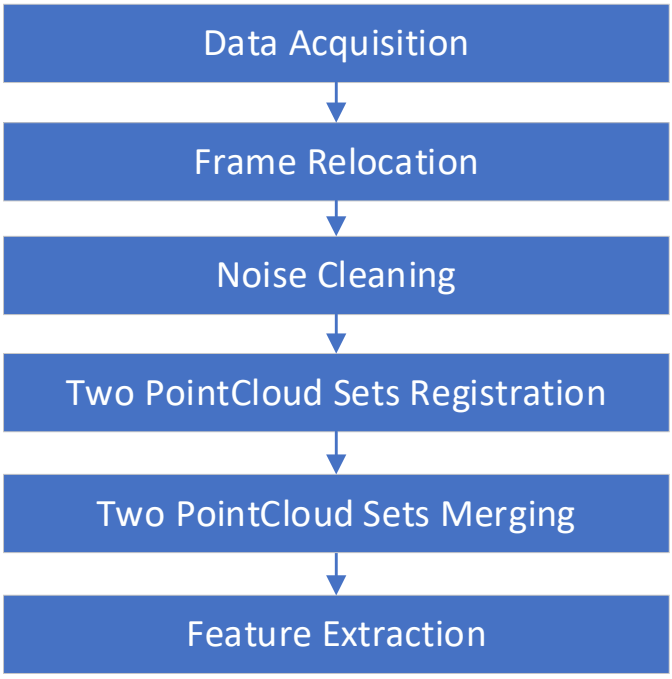

Figure 5-13 Standard data processing procedure for inclined dual laser profilometers

- Data Acquisition – Each laser profilometer scans the profile of a part and sends the data to the PC.

- Frame Relocation – The original results obtained from laser profilometers are frames of point height data without any explicated information about where these points are collected. As mentioned in section 5.6, the location and orientation information of the laser profilometer were stored with the laser profilometer results. In order generate a point cloud model, all frames are relocated according to its acquisition position and orientation.

- Noise Cleaning – With the irregular reflection form the metal surface, the raw data normally contains considerable amounts of noise data. In this research, the author applied a simple out-of-range filtering method to clean the data, which means all the height data that was outside of a certain range was filtered out. The range is manually determined with regards to the distance between the parts and the laser profilometer. Readers may refer to the Point Cloud Library (PCL) (Rusu and Cousins. 2011) for advanced data cleaning algorithm.

- Point Cloud Registration - Point cloud registration is a specific phrase in data cloud processing, which means precisely aligning two point clouds through their similar shape. The most common point cloud register algorithm is the iterative closest point(ICP) algorithm. Readers are referred to Besl and McKay (1992) for the ICP algorithm. Another method to register point clouds is to calculate the transforming matrix by precisely calibrating two laser profilometers. In this research, the calibration method is selected and introduced in Section 5.6.7.

- Point Cloud Merging – This step is to merge the point cloud results into one. As the two point clouds coincide at the middle, the point density at the middle would be higher than other area. An average point cloud filter was applied to smooth out the point density.

- Feature Extraction - The final step is to extract features such as height, width or CAD model from the registered and combined point cloud. Most commercial point cloud software is able to convert point cloud data to CAD models, such as Geomagic(2019) and Rhino(2019).

5.6.7 Laser Profilometer Calibration

As shown in Figure 5-14, two laser profilometers are positioned at different locations and in different orientations. To merge their point cloud results into a unified coordination frame, their orientation and location differences must to be rectified. Otherwise, various errors will be induced in the measuring process. The major errors that could be induced are shown in Figure 5-15. In the Figure 5-15, a demonstrate part is shown on the left, and typical errors might be induced are shown on the right. There three devised sections in the part. Section A is a pure horizontal plane. Section B is a stage with a horizontal plane. When the vertical misalignment of two laser profilometer are not well rectified, a vertical error will be generate in the scanning result. Section C consists of an edge generated by two inclined plane. If the horizontal or vertical misalignment of the two profilometers is not rectified, the scanning error will be reflect on that edge.

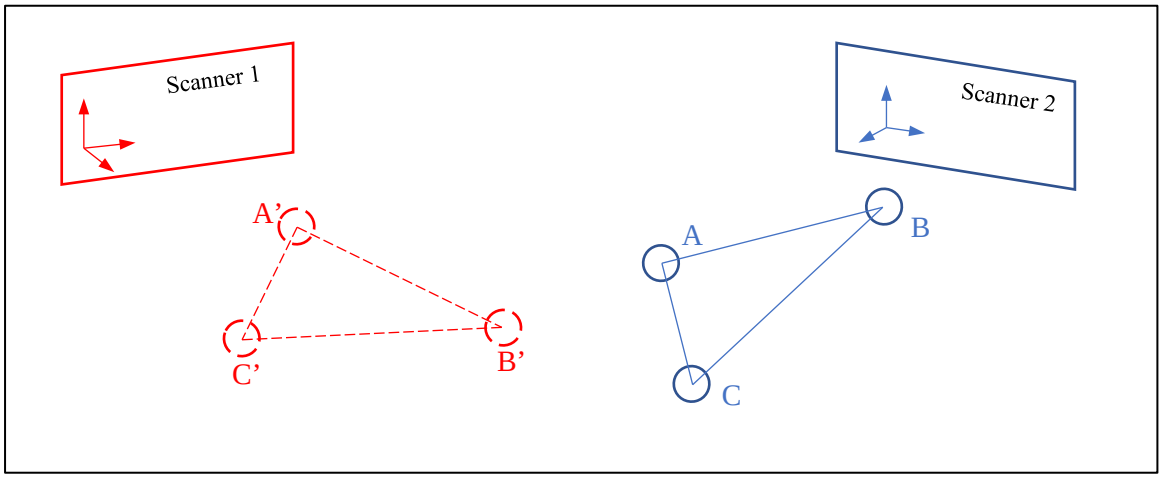

Figure 5-14 Spatial Relation of two Laser Profilometers (Scanner)

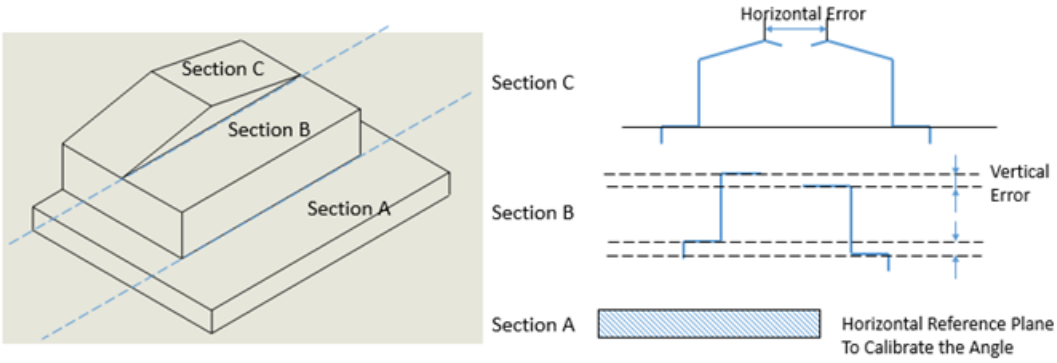

Figure 5-15 Schematic Diagram of a Test Part and Its Error Analysis

In order to rectify the orientation and the location error, there are 6 degrees of freedom between two coordinate frames. In this case at least three consensus points need to be identified to eliminate the 6 Degrees of Freedom (DoF) as shown in Figure 5-14. It is noted that finding a consensus point from the scanning result of two laser profilometers is not trivial, as all points are ordinary points without any attributes. In order to find consensus points in the point cloud data, the author proposed a ball centre method, in which three balls are placed in the scanning space and the ball centres could be used as the consensus points. This calibration procedure is shown in Figure 5-16 and consists of 5 steps. The first step in Figure 5-16a is to place four balls on the working bed of the HiVE. It is noted that any three balls of the four cannot be located on a line to avoid less of a constraint. The second step is to scan the four balls with both laser scanners (Figure 5-16b). The initial results from the scanner are associated with each frame number instead of position. Therefore, a mapping procedure is needed to map each frame to its corresponding location and orientation, as shown in Figure 5-16c. The consecutive step is to fit the ball centre in the scanned point cloud.

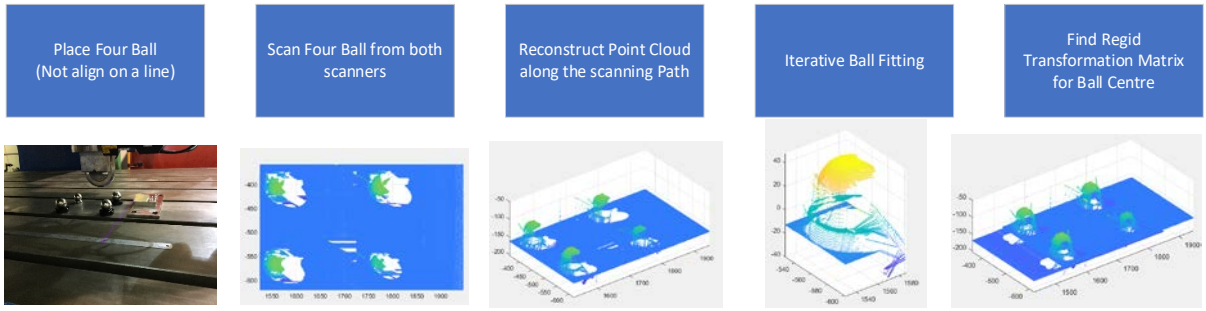

Figure 5-16 Raw Point Cloud Data for Profilometer Calibration Procedure

In order to fit the ball centre, the points on the ball surface require selection, and all unrelated points that are not on the ball surface need to be deleted. Hence, the ball fitting procedure has been implemented as follows:

(i) Crop one ball from the global point cloud (Figure 5-16d)

(ii) Remove unrelated points such as the base of the ball (As shown in Figure 5-16d, most ball surface points in yellow are on top part of the point cloud, lower part points are from ball base, which should be removed)

(iii) Use the Iterative Fitting Algorithm to fit the ball

The iterative fitting algorithm to fit the ball is used to obtain the ball centre and is based on the following equations.

$$(x-x_c)^2+(y-y_c)^2+(z-z_c)^2=R^2 \tag{5.4}$$

Where (x, y, z) is the coordinate of the point on the surface, and (x_c, y_c, z_c) is the ball centre coordinate to be calculated. Expanding equation 5.4 leads to the following equation (5.5):

$$2x_c\cdot x+2y_c\cdot y+2z_c\cdot z+(R^2-x_c^2-y_c^2-z_c^2)=x^2+y^2+z^2 \tag{5.5}$$

Then by substituting all scanned points on the ball surface into equation 5.5, generates equation 5.6

$$\begin{pmatrix} x_1 & y_1 & z_1 & 1 \\ x_2 & y_2 & z_2 & 1 \\ \vdots & & & \vdots \\ x_n & y_n & z_n & 1 \end{pmatrix} \bullet \begin{pmatrix} x_c \\ y_c \\ z_c \\ K \end{pmatrix} = \begin{pmatrix} x_1^2+y_1^2+z_1^2 & x_2^2+y_2^2+z_2^2 & \cdots & x_n^2+y_n^2+z_n^2 \end{pmatrix} \tag{5.6}$$

Where (x_n, y_n, z_n) is the coordinate of the points on the surface, (x_c, y_c, z_c) is the ball centre coordinate, and $K = R^2 - x_c^2 - y_c^2 - z_c^2$. In this case, equation 5.6 is in the standard form of AX = B, where the left matrixes of the equation 5.6 are A and X and the right matrix is B. All factors in matrices A and B are known. The only unknown factor is X. Since the scanned point cloud position contains inaccuracies and noises, therefore X in equation 5.6 may not be solvable. But, a best estimate of X can be solved through a projection method (Gilbert S. 1993).

$$\hat{X} = (A^T \cdot A)^{-1} A^T B \tag{5.7}$$

Where A is the surface points coordinates matrix as shown in left side of Equation 5.7, B is the same as the right side of Equation 5.7, and $\hat{X}$ is the best estimate of ball centre vector. Since some outlier points are still in the sampled point cloud set, they may induce large inaccuracies for the ball centre fitting. The author undertook an error analysis step to eliminate the error as following:

$$E = A\hat{X} - B \tag{5.8}$$

Where E is the error matrix. Consecutively, all points that have an error larger than the 1.5x standard variance of matrix E has been eliminated, and a new point cloud without eliminated points is generated and it is substituted into equation 5.4 and this whole procedure will be iteratively implemented 3 times to calculate a best estimate $\hat{X}$.

$$\hat{X} = \begin{pmatrix} \hat{x}_c \\ \hat{y}_c \\ \hat{z}_c \\ \hat{K} \end{pmatrix} \tag{5.9}$$

Based on equation 5.9 and the previous assumption $K = R^2 - x_c^2 - y_c^2 - z_c^2$, the estimated radius R of the ball can be obtained. Table 5-6 is a calibration test result from the left profilometer.

Table 5-6 Calibration Test Result from the Left Profilometer

	True Radius / mm	Measured Radius / mm	Relative Error
Ball 1	25.05	24.985	0.2%
Ball 2	25.15	25.345	0.7%
Ball 3	25.0	25.053	0.2%
Ball 4	20.50	20.614	0.5%

As shown in Table 5-6, each ball diameter is measured by a calliper, and for the reader's convenience the diameter has been converted to true radius. The measured radius is calculated from the calibration procedure. The error between the true radius and the measured radius can be regarded as an accuracy factor for the fitting algorithm. The next step is to find a rigid transformation between two set of ball centres as shown in Figure 5-16e.

In order to calculate, the best transformation matrix between two batch of points, a least squared Rigid Motion Algorithm has been applied to calculate the transformation matrix to translate one ball centre set to the other. The basic procedure is as following:

$$x_i = p_i - \overline{p}\,, y_i = q_i - \overline{q} \tag{5.10}$$

Where p_i represents the coordinates of the fixed ball centre set, and the q_i represents the coordinates of the moving ball centre set.

$$S = XY^{\mathrm{T}} \tag{5.11}$$

Where X and Y are matrices that have x_i and y_i as columns. Then apply singular value decomposition(SVD) to S:

$$S = U\Sigma \mathrm{V}^{\mathrm{T}} \tag{5.12}$$

The Final Rotation Matrix will be

$$R = VU^T \tag{5.13}$$

5.7 Summary

In this chapter, a hardware implementation for the WAAM monitoring system on the HiVE WAAM machine was outlined. This monitoring system is able to monitor the process parameters including the welding voltage, welding current, wire feed speed and gas flow. In addition, the monitoring system is able to monitor the profile of the part, the surface temperature of the part and the pressure in rolling the layers after deposition. The monitoring system has been integrated in the HiVE WAAM machine which enables the FANUC PLC to control the monitoring system to start monitoring or end monitoring in the process. All the signals were collected at 5Hz and synchronized to the position where they were collected.

Chapter 6

Results and Evaluations

6.1 Introduction

This chapter reports the results obtained from the WAAM monitoring system described in chapter 5. Three experiments have been defined to demonstrate the capability of the WAAM monitoring system. The first experiment validates the essential capabilities of the voltage and current sensor. In the second experiment the variation of the voltage and current in the process has been evaluated. The final experiment provides a complete method to process the point cloud data generated from the dual laser profilometer system.

After the monitoring system mounted on the real machine, the performance of system needed to be tested. The first experiment is used to validate the performance of the system. After validation, the second experiment was used to establish a WAAM process data analysis process. The third experiment is used to demonstrate the capability of the laser profilometer sensor. Because there is no one, using two inclined laser profilometer to extract geometric information of the WAAM part.

6.2 WAAM Experiments

To evaluate the WAAM monitoring system 3 different experiments were designed. The first experiment 1, is to evaluate the overall performance of the process sensors to ensure validation of the WAAM monitoring system. The second experiment 2, is to illustrate the range of outputs from the monitoring system to identify the variation in parameters for the various sensors. The

final experiment 3, focuses on the geometric monitoring of the deposited parts and specifically on identifying the heights and shape of components deposited via the WAAM process.

6.3 Experiment 1 – Initial Functioning Validation

In order to validate the functionality of the monitoring system, an initial functioning validation experiment was conducted on a wall with zig-zag path and 150mm in length and 25mm in height as shown in Figure 6-1. This experiment was carried out the HiVE Machine. In this experiment, sensor data, process data and point cloud data are recorded. This data includes the coordinate data, voltage data, current data, oxygen data. The aim of this experiment was to identify any potential problems in the developed multi-sensor system and validate the collection of data.

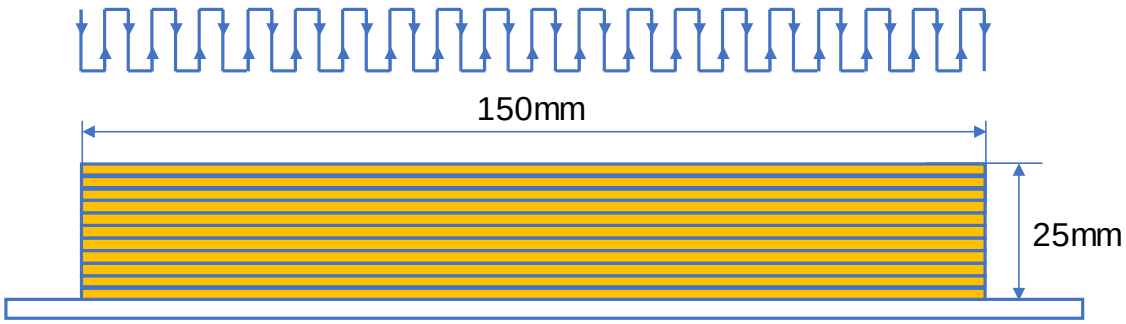

Figure 6-1 Schematic Diagram of Part Design for Experiment 1

6.3.1 Arc Voltage Data

The arc voltage data was collected from the voltage clamp, and the voltage clamp connected to the electrode directly. As shown in Figure 6-2a, the arc voltage is approximately 30Volts, and fluctuated with an increasing trend. Figure 6-2b, showed the frequency spectrum of the voltage data by applying a 660 points fast Fourier transform (FFT). The figure shows are two relatively high value components at about 0.007Hz and 0.34Hz corresponding to the increasing trend and the fluctuation accordingly. The high frequency fluctuation is due to the repeated zig-zag tool path. The height on side of the wall is commonly slightly lower than that in the middle.

This caused various airgap between the welder tip and the built component, which in turn caused resistance. Since in welding application, the welding current is constant to provide constant heat input, the voltage in turn varies along with the air gap. For the increasing trend of the voltage showing in Figure 6-2a, it is because the uneven bottom layer of the WAAM component. The distortion often causes the part to be tilted upwards at each end in the WAAM process. As a result, the decreased distance between the arc nozzle and the part caused this increasing trend.

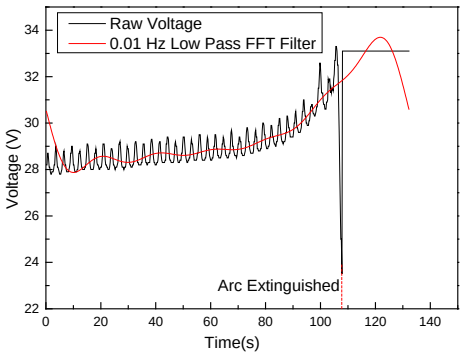

6-2 (a) Voltage Data for a single Layer

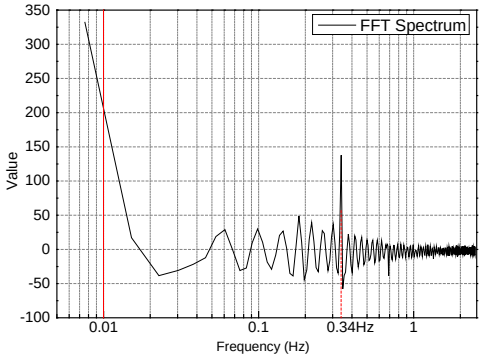

6-2 (b) FFT Frequency Spectrum for Voltage

Figure 6-2 Voltage Data for a single layer and its frequency spectrum

6.3.2 Current Signal

The current signal for a single layer is shown in Figure 6-3. The current is manually pre-set to a fixed 220 Amps. As shown in Figure 6-3a, there is an almost flat line at 210 amps with many spikes in the measured current signal. The fast Fourier Transform frequency spectrum is shown in Figure 6-3c. Apart from the frequencies lower than 0.05Hz, all the other frequency components vary between -2000 and 2000 Hz, which means the signal and noise is evenly spread on the spectrum and the noise cannot be filtered out with a frequency filter.

In order to eliminate the noise, a statistical analysis was applied to the current data before and after the arc extinguished as shown in Table 6-1. After the arc extinguished, the current should be zero, however the mean of the measurement result is -7.2 amps. This error is recognized as a zero-drifting error. After rectifying the zero-drifting error, the mean becomes

220.3 amps which is very close to the value initially set. Subsequently, the histogram of the error distribution is shown in Figure 6-4b. The horizontal axis represents the error between measurement value and mean. The vertical axis represents the counts of the errors in each range. Apart from the considerably large errors, most errors are in the range of -40 to 40 amps, and the distribution is approximated to a Gaussian distribution. Thus, a Kalman filter was used due to its good effect on filtering the Gaussian distribution error (Welch and Gary, 1995).

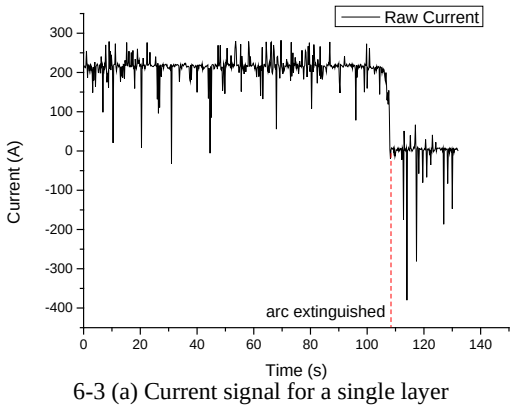

6-3 (a) Current signal for a single layer

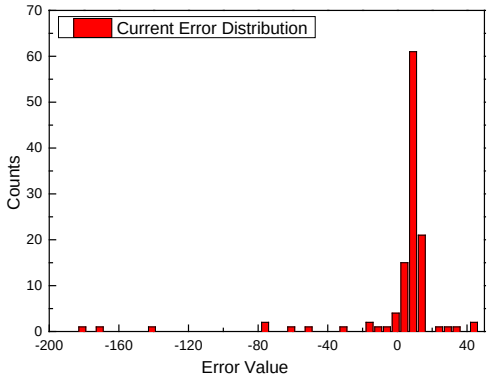

6-3 (b) histogram of current error distribution

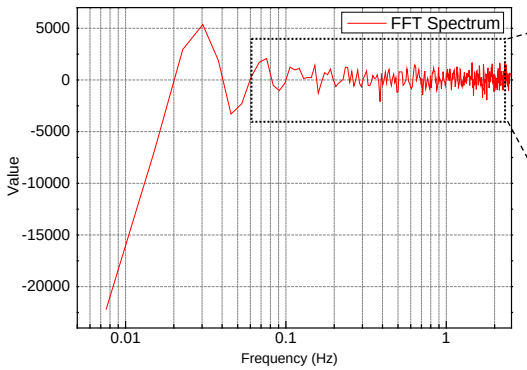

6-3 (c) FFT Current Frequency Spectrum

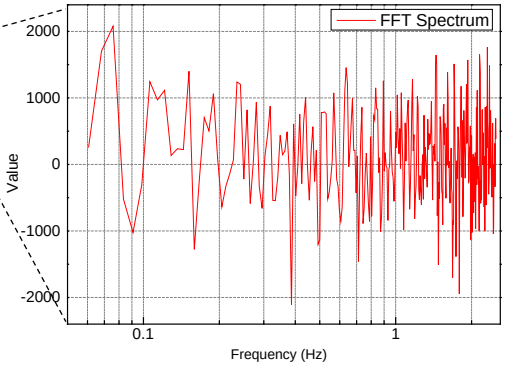

6-3 (d) Frequency Spectrum from 0.05Hz

Figure 6-3 Current value for a single laye4r and its frequency spectrum

Table 6-1 Current Mean Value Before and After Arc Extinguished

	Mean (Amps)	Standard Deviation
Current Data before arc extinguished	213.1	31.87
Current Data after arc extinguished	-7.2	53.20

The Kalman filter (Welch and Gary, 1995) is a mature algorithm used to estimate true value from a series of measurements with statistical noise over time. Essentially, the Kalman filter is a discrete time-varying least square estimator. The objective is to use the system

function to predict the next state, and then compensate the prediction value based upon the measurement value. The measurement results are assumed to be independent of the predicted values and subject to statistical noise. The Kalman filter comprises of two stages, namely, prediction and correction. The Kalman filter final estimated value is from the correction Equation 6-1.

Correction Equation: $\hat{x}_{k|k} = \hat{x}_{k|k-1} + K_k(z_k - H\hat{x}_{k|k-1})$ (6-1)

Where:

K_k is the Kalman gain value.

z_k is the measurement value.

H is the representation matrix.

$\hat{x}_{k|k-1}$ is the prediction value from the system function.

$\hat{x}_{k|k}$ is the corrected estimation based on Kalman filter.

The final estimated value $\hat{x}_{k|k}$ is obtained from a system predicted value $\hat{x}_{k|k-1}$ plus a correction item. In this eqation, the $\hat{x}_{k|k-1}$ is obtained from Equation 6-2 as written below. The measurement value $\boldsymbol{z_k}$, which is assumed to be a zero-mean error data with a variance of ***R,*** is collected from sensor.

Prediction: $\hat{x}_{k|k-1} = F_{k-1}\hat{x}_{k-1|k-1}$ (6-2)

Where:

$\hat{x}_{k-1|k-1}$ is the best estimation from the previous time-step ***k-1***;

$\hat{x}_{k|k-1}$ is the prediction value of time ***k*** from the system function;

F_{k-1} is the state transfer function based on system model.

All system models are a simplified representation of the real world and as such the prediction

will have some error associated with it. The variance of this error is named as Q. At each step, the system states will be measured by specific sensors.

The Kalman gain is calculated as below:

Kalman Gain $K_k = P_{k|k-1}H^T(HP_{k|k-1}H^T + R)^{-1}$ (6-3)

Predicted Covariance $P_{k|k-1} = F_{k-1}P_{k-1|k-1}F_{k-1}^T + Q$ (6-4)

Corrected Covariance $P_{k|k} = (I - K_k H)P_{k|k-1}$ (6-5)

Where:

$P_{k|k-1}$ is the predicted covariance

Q is the system error variance

R is the measurement error variance

$P_{k-1|k-1}$ is the previous covariance

$P_{k|k}$ is the estimated covariance

F_{k-1} is the state transfer function based on system model

I is the identity covariance

The basic idea behind the Kalman gain value is to minimize the errors with the variance Q and R. Readers may refer to Welch and Gary (1995) for more information on the Kalman filter. The Kalman filtering algorithm was applied to the raw current signal as shown in Figure 6-4a and the result is shown in Figure 6-4b. The arc current was set to 220amps and the filtered signal shows that the arc current is almost steady at 213 amps from 0s to 108s and after that, the arc current is steady at about -7amps which is a zero drift. As mentioned in Table 6-1, the zero-drifting error is about 7amps. By adding 7 amps zero drift, the measured value is around 220 amps which is equal to the set value.

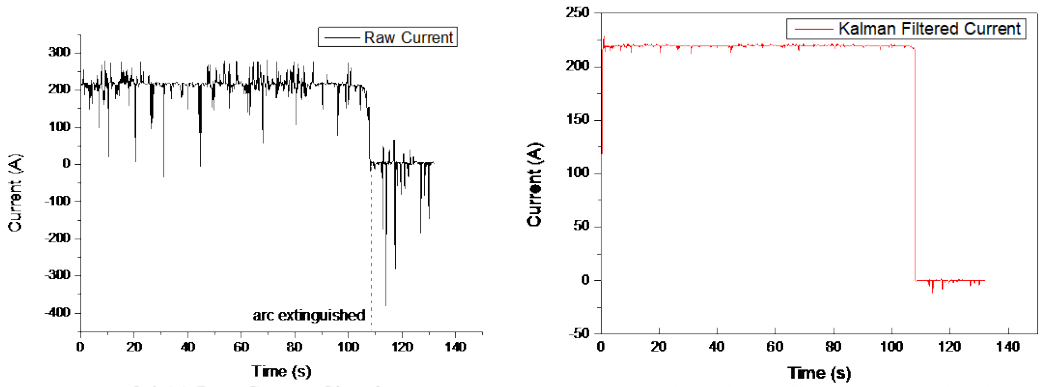

6-4 (a) Raw Current Signal

6-4 (b) Kalman Filtered Current Signal

Figure 6-4 Comparison between raw current signal and Kalman filtered signal

6.4 Experiment 2 - Process Data Experiment

In Experiment 1, the sensors have been validated to be functional. In this experiment, the aim is to observe and analyse the parameters' variation during a real WAAM part building process. The validation test was carried out on a 17-wall part depicted in Figure 6-5. This part was designed to have 17 identical walls with a length of 150mm, and a height of 100mm. These walls were used for machining experiment. Therefore, they were designed to be identical. The walls were rolled after each layer with a pressure of 60kN as shown in Figure 6-5. The width of each wall is 12mm.

In this experiment, the rectified voltage and current data was recorded. The voltage variation with respect to position is shown in Figure 6-6. Each dot in the figure stands for the voltage at the corresponding position of the wall. The colour of the dot represents the voltage value which varies from blue to red representing the voltage varying from 23 volts to 28 volts accordingly. The result is recorded at a frequency of 5Hz. Due to noise that occurred in the process, some of the out of range acquisition data has been filtered out which caused data to be missing which is shown as blank dots in Figure 6-6. The blue dots shown at the beginning and the end are 0 volts dot collected at arc ignition period. Figure 6-7a illustrates the voltage variation in wall 5 layer 31 with respect to position. It is noted that the voltage at the both ends is slightly higher

than in the middle part. This is because of the hump at the beginning and the end of the part. It decreased the distance between the welder tip and the part and caused a voltage increase. Figure 6-7b shows the voltage variation with respect to time. The voltage at the beginning is obviously higher than the following period. This is caused by the arc ignition.

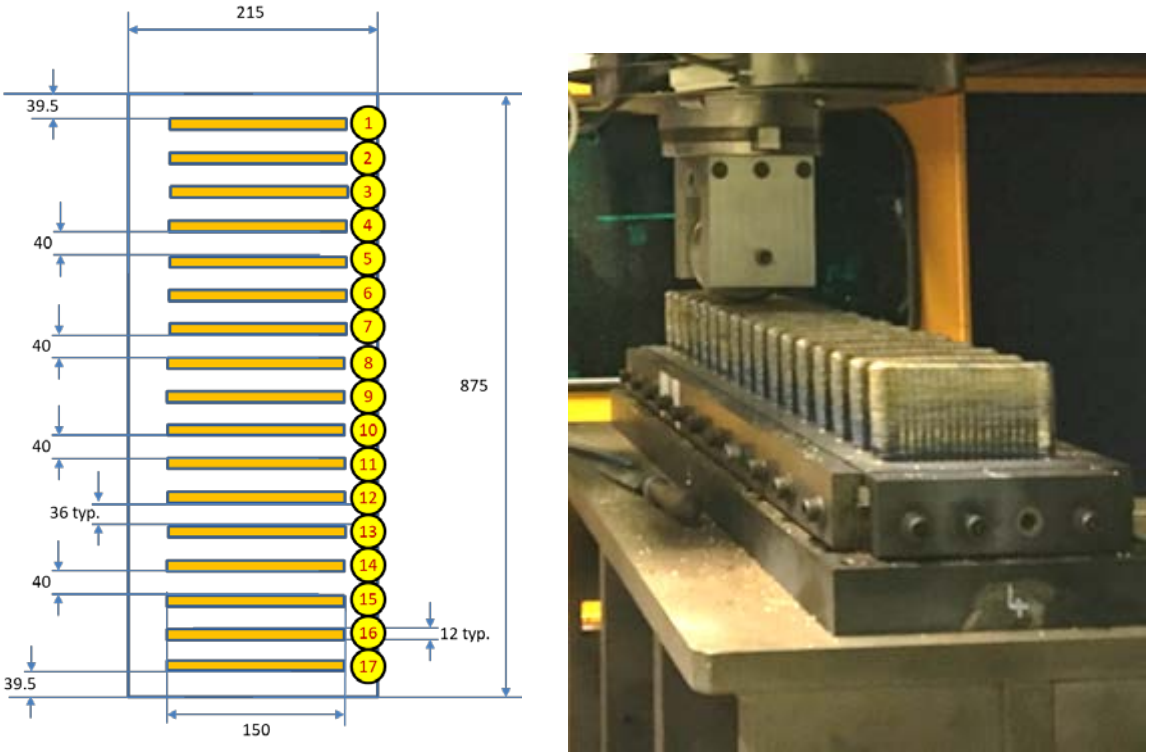

Figure 6-5 Experiment Set-up for 17 walls

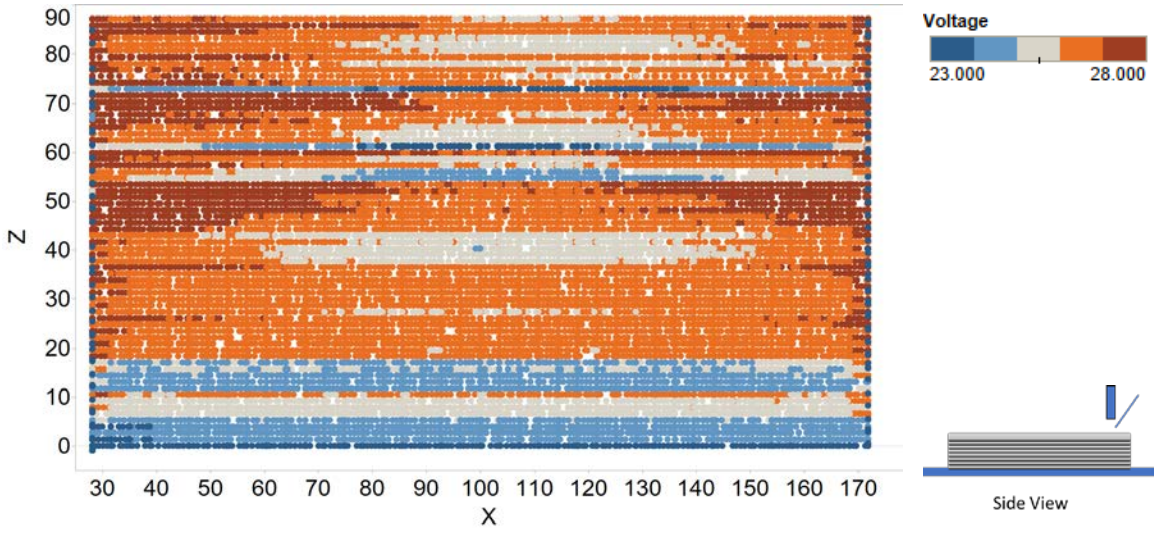

Figure 6-6 Voltage variation with respect to position

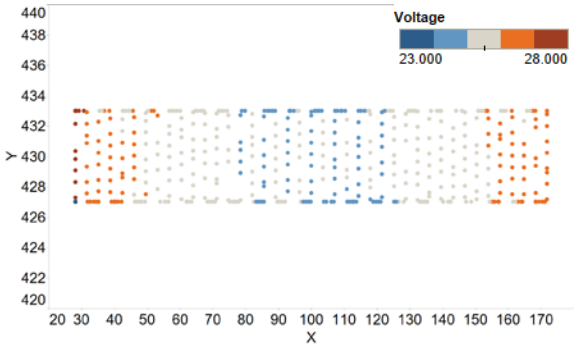

6-7 (a) Voltage variation with respect to position in Layer 31

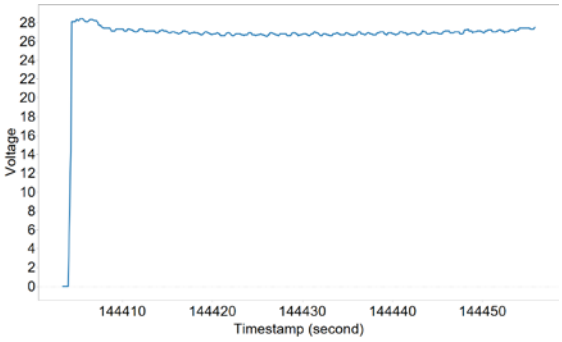

6-7 (b) Voltage variation over time in Layer 31

Figure 6-7 Voltage variation in layer 31

The current signal is precisely controlled by the welding power module to provide consist heat input. As shown in Figure 6-8a, the current variation in the wall 04 is illustrated. It is clear that the current is consistent over the whole production process of the part. It is noted that the blue dots at the beginning and the end are the arc ignition and extinguishing points. In order to investigate the current variation in a single layer, the current signal over time in Layer 21 of the Wall 04 is shown Figure 6-8b. The current signal is straight line after arc ignited in this case, which proves the current signal is very stable in Layer 21.

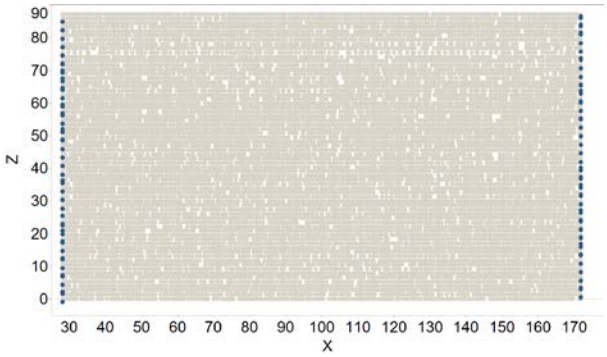

6-8 (a) Current variation with respect to position

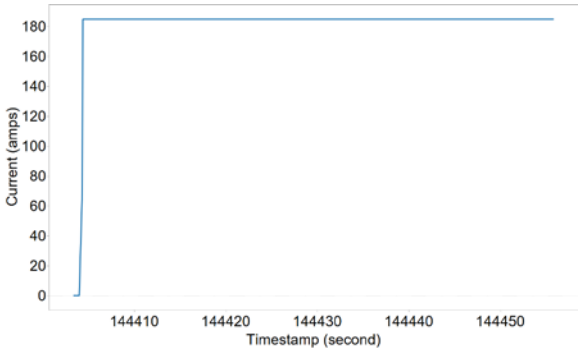

6-8 (b) Current signal in Layer 21

Figure 6-8 Current Data for Wall 04

6.5 Experiment 3 – Geometric Data Validation and Assessment

For the WAAM process, the geometric data is a direct reflection of the quality of the part. With the development of WAAM, users are expecting lower buy-to-fly ratios for the parts produced with higher dimensional accuracy. To achieve this expectation, applying a geometric sensor for the WAAM process is a necessity. As discussed in Chapter 5, the author applied two laser profilometers as the geometric sensor. The ultimate goal of the sensor is to obtain in-process geometric indicator parameters for WAAM part. In this research, all the WAAM built parts are single-bead and multi-bead walls, typical of the components required in industry, thus wall height was selected as the geometric indicators.

The complete point cloud processing pipeline is illustrated in the Figure 6-9. The pipeline starts with WAAM part scanning, following by frame relocation, noise filtering, point cloud sets registration, point cloud sets merging, voxel down-sampling, normal vector estimation, and surface segmentation. Scanning step occurs every time after one layer is deposited. In this step, the point clouds are collected and stored in frames. These frames of point cloud are then relocated according to the coordinated information collected along with each point cloud frame. Then, a point cloud statistical filter would apply to filter out outliner points. The point cloud sets from the left laser profilometer and right laser profilometer are aligned and registered based on calibrated transformation matrix. This matrix is obtained from a calibration process and is described in section 5.6.7. After registration, two point cloud sets are well aligned and merged into one point cloud. Then a voxel-based down sampling algorithm would apply to eliminate point density imbalance at the matching area. Then the normal vector of each point in the point cloud would be calculated. Based on the normal vector, the surfaces are separated to horizontal

planes and vertical planes. Then, the height and the width could be extracted from the top surface and the side surface.

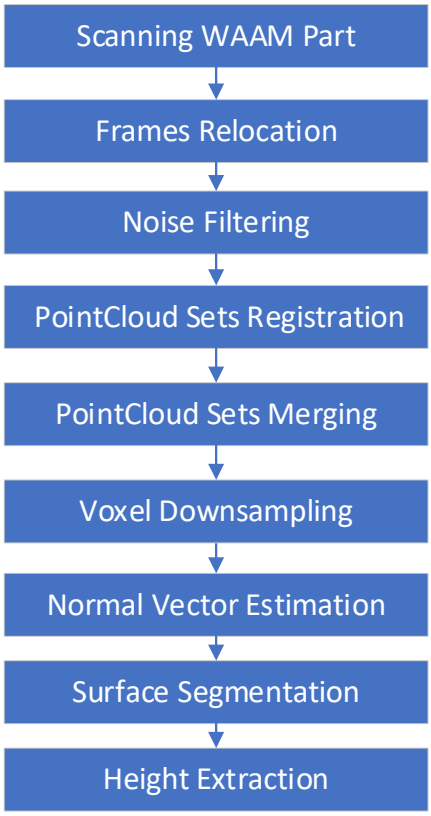

Figure 6-9 Complete Pipeline for Point Cloud Processing

i) Scanning the WAAM part:

Scanning step occurs right after each layer is deposited. The scanning result is stored in frames, and each frame contains 800 points of height information for a laser profilometer. As discussed in section 5.6.1, the scanner position and orientation information along with the scanning results from two laser profilometers are stored together in a file.

ii) Frames Relocation:

In order to obtain a point cloud model, the data stored in frames is relocated according to the machine coordinates and orientation. The relocation algorithm has been attached in Appendix. A relocated point cloud data is shown in Figure 6-10. The blue one is the point cloud generated

from the left laser profilometer and the yellow one is from the right laser profilometer. This represents which is a simple wall with a substrate. It is clear to see that each laser scanner is only able to obtain the points on its side. By combining two point cloud sets, a complete part point cloud model could be obtained.

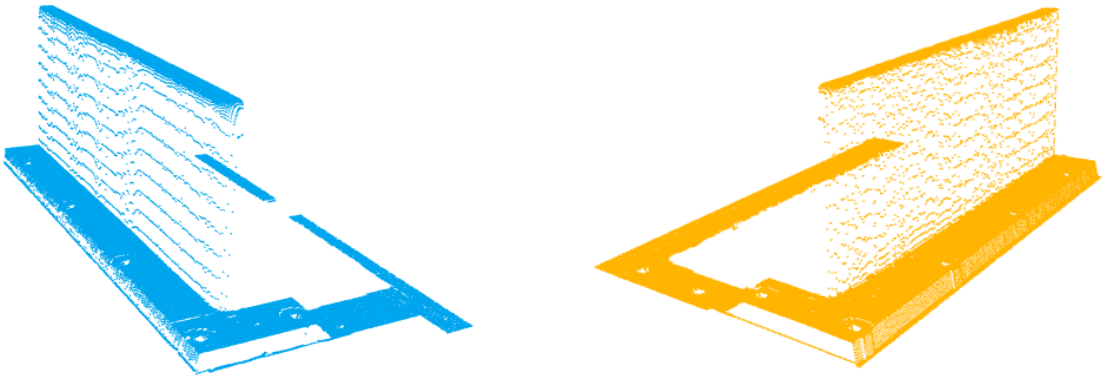

Figure 6-10 Relocated Point Cloud from left laser profilometer and right laser profilometer

iii) Noise Filtering:

Due to material reflection and environment light interference, laser profilometers may generate noise in the scanning process. To eliminate the outliner points from the model, a statistical filter (Zhou et al. 2018) has been applied to filter out these outliners.

iv) Point Cloud Sets Registration:

Though the point cloud sets from the left laser profilometer and right laser profilometer are both relocated, they are not aligned. The point cloud sets are referenced to their own coordinate framework with respect to its own laser profilometer and need to be re-aligned. In the point cloud processing area, this step is named registration. In order to precisely register two point cloud sets, a pre-calculated transformation matrix is applied on one set of point cloud data to make the two point clouds align. The transformation matrix is obtained from the calibration process introduced in section 5.6.7. The registered point cloud sets are shown in Figure 6-11. Also, in Figure 6-11a, the blue points are from the left point cloud set and the yellow points are

from the right point cloud set. The blank are in Figure 6-11a and Figure 6-11b was generated due to obstruction of each laser profilometer, but this part is not required as it belongs to the working table. The extra blue and yellow points on the leftmost and rightmost are also not required and also belongs to the working table.

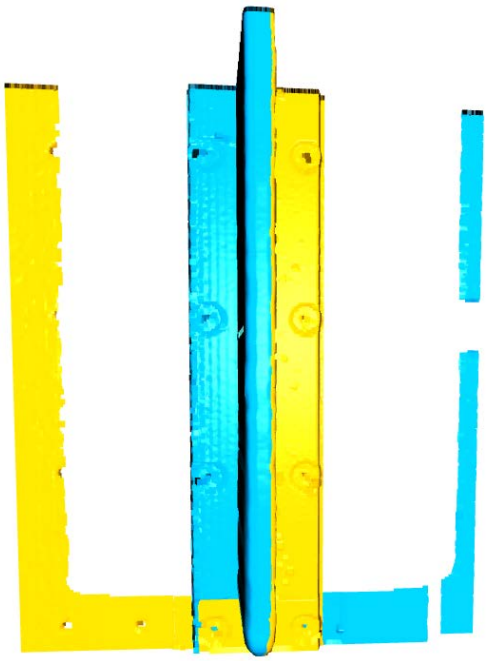

6-11 (a) Top View of the Registered Point Cloud

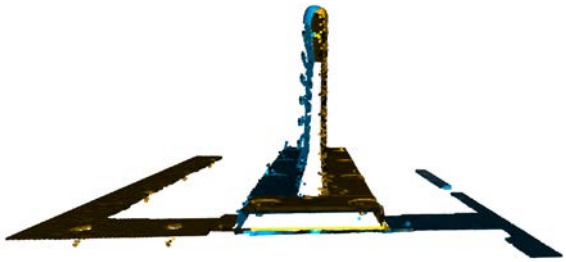

6-11 (b) Front View of the Registered Point Cloud

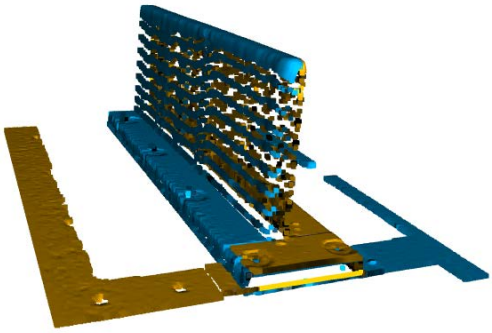

6-11 (c) Orthogonal View of the Point Cloud

Figure 6-11 Registered Point Cloud Sets

v) Point Cloud Sets Merging:

After point cloud registration, two point cloud sets were merged into one. This is a simple step, as it only combines the two sets of data into a uniform point cloud set.

vi) Voxel Down Sampling:

Since the two point cloud sets coincide in the middle of the part, the point density is higher than other area. This will induce an imbalance problem in the following steps. A voxel based down sampling method has been applied to smooth out the point density.

vii) Normal Vector Estimation:

Normal vector calculation is particular important in point cloud processing. It could be used for segmentation, reconstruction, feature detection etc. In this research, a normal vector has been used to identify the horizontal surface and vertical surface of the part. For each points, 30 nearest neighbour points are selected to estimate its normal vector. The common algorithm for estimating the normal vector is based on eigenvector analysis of a covariance matrix created from the 30 nearest neighbour points (Rusu, R.B.. 2010). The point cloud models without normal vector and with the normal vectors are shown in Figure 6-12.

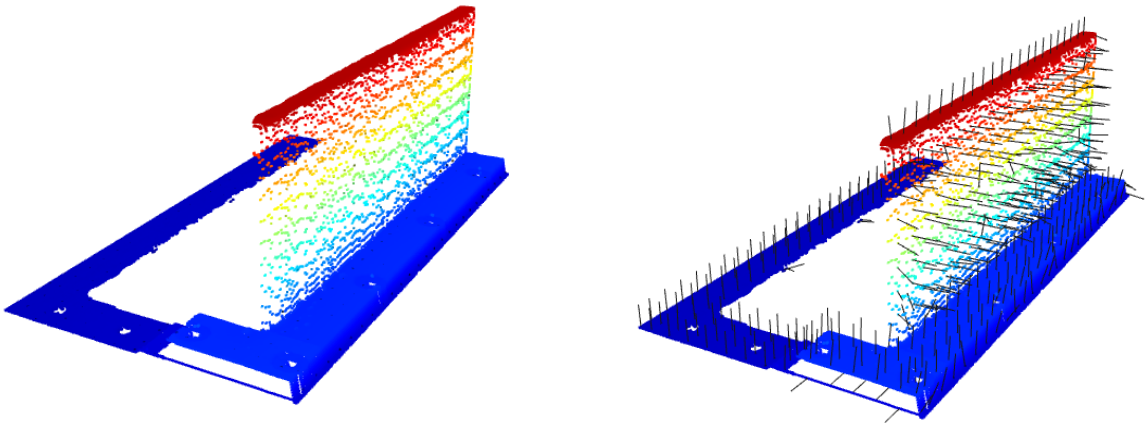

(a) without normal vectors (b) with normal vectors

Figure 6-12 Point Cloud Normal Vector Estimation

viii) Surface Segmentation

In this research, all the parts are vertical walls which are typical of industrial WAAM parts. Therefore, the author presumes that there only exists horizontal planes and vertical planes in the point cloud data. Hence, any normal vector with an angle less than 20 degree to the z-axis is identified as from the horizontal plane. Those normal vectors with an angle from 70 to 110 degree to the z-axis are identified as from the vertical plane. This simple method has been proved to have an excellent performance as shown in Figure 6-13. All horizontal planes are successfully extracted from the point cloud and is shown in Figure 6-13a and vertical planes

are shown in Figure 6-13b. It is noted that not all planes belong to the wall part, some planes at the bottom on the substrate or working table are extracted as well. These planes from the substrate and the working table could be removed by removing any points lower than the substrate plane.

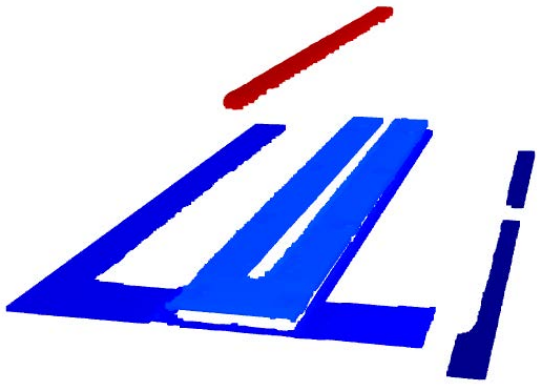

6-13(a) Extracted Horizontal Plane

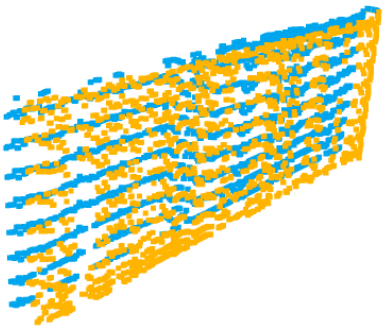

6-13(b) Extracted Vertical Plane

Figure 6-13 Extracted horizontal planes and vertical planes

ix) Height Extraction

The top surface of the wall in Figure 6-13 has been extracted as shown in Figure 6-14a. The maximum height of each cross-section plane is extracted and is defined as the height of the wall. The height variation of the wall is shown in Figure 6-14b. In order to see the height variation in a single layer, an enlarged chart is shown in Figure 6-14c. The height variation of this example layer is around 2mm. The height of the part increases from the beginning of the wall to the end. Due to the bead shape, the height decreases at the end of the part. The accuracy of the result is 0.01 mm.

6-14 (a) Top surface of a wall part

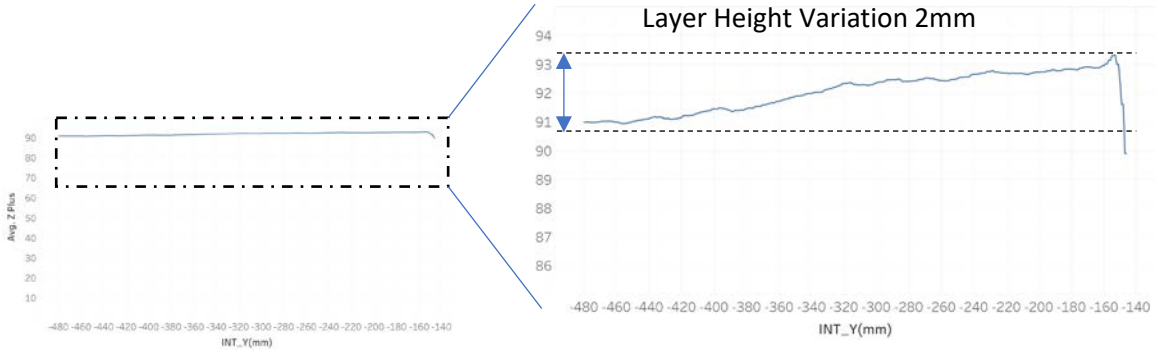

6-14 (b) the height variation across the wall

6-14 (c) enlarged view of 6-14(b)

Figure 6-14 Height variation of a WAAM wall part

6.5.1 Multiple-layer Height Variation

In order to test the robustness of the height monitoring method shown in Figure 6-9 described above, a WAAM part has been built with its first 9 layers being measured as shown in Figure 6-15a. Layer 1 of the part is scanned, but the first layer is too low that it is not easy to separate the top surface and the substrate and the result is intentionally excluded. The part scanning result for layer 2 ~ layer 9 is shown in Figure 6-15b. The lines in different colours represent the height variation in each different layer. The average height difference between layers is approximately 1.1mm.

6-15 (a) WAAM Part for Height Evaluation Test

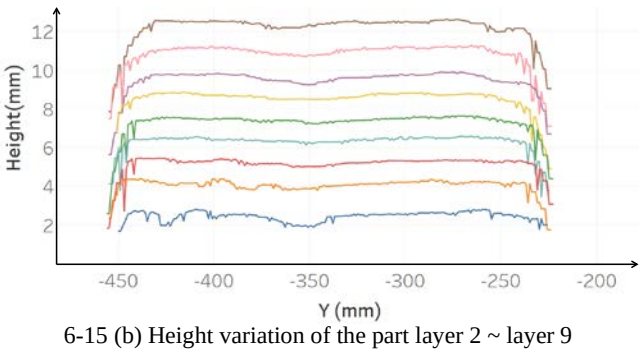

6-15 (b) Height variation of the part layer 2 ~ layer 9

Figure 6-15 Height Variation for layer 2 ~ layer 9 of a WAAM part

6.6 Summary

In this chapter, three types of data namely point-cloud data, voltage data and current data collected from the WAAM monitoring system have been reported. In order to identify the semantics of the point cloud data, a series of point cloud manipulation and algorithms have been applied. The final result shows that, the point cloud was able to identify the height at an accuracy of 0.01 mm

Chapter 7

Discussion

7.1 Introduction

This chapter brings together a discussion of the research based on the areas of investigation identified in chapter 3. The goal is to relate the research to the literature to identify novel aspects and also compare the research with other competitive approaches.

7.2 Review of the WAAM literature

The author has identified major monitoring parameters and its categorization (See Section 3.4.1). In WAAM area, a complete monitoring method hasn't been proposed before. The author investigated monitoring system in similar areas such as wire laser additive manufacturing, electron-beam freeform fabrication, and welding. In WAAM process monitoring, single articles only focus on single bead wall monitoring (Zhang et al. 2006, Xiong et al. 2010, 2011). The monitoring for multi-bead wall and complex part is less reported (Han et al. 2018). To date there has been little work undertaken in developing a holistic monitoring system for DED processes. The main work reported as outlined in chapter 2, has been by Xiong et al. (2015, 2016) and Bonaccorso (2009). The requirements for these systems are not clearly defined in the papers though they do enable geometry, current and voltage to be monitored. The author's work has established the way to reliably monitor the process parameters and geometric shape of the part in real-time as reported in Chapter 5.

As described in 2.4.2, there are three major heat sources identified, namely GMAW, GTAW and PAW that are used in the WAAM process. For titanium alloys and some other high melting

point temperature alloys these are normally deposited by GTAW and Plasma sources, this is due to GTAW and PAW providing a high temperature welding torch around 16,000-20,000 ℃. For other materials such as steel an aluminium which are more commonly deposited using GMAW at lower temperature, it does not need a separate wire feeding device which is commonly used in GTAW and Plasma. In addition, in some low heat input GMAW processes, such as a CMT welder it shows great potential for controlling the heat induced residual stress and distortion (Martina et al. 2012).

Currently, the accuracy of the WAAM process is typically around 1mm (TWI 2019). This is due to a lack of a geometric monitoring method during the deposition process and the lack of a closed loop control system. In welding and WAAM applications, the traditional parameter monitoring (Węglowski, 2012) is related to monitoring process parameters including arc voltage, arc current, travelling speed and wire feed speed. A large number of authors are recognised for modelling of these parameter types (Bonaccorso et al. 2009, Węglowski et al., 2012 Xu et al. 2018). The author has taken this as the their base position and added additional sensors to form the multi-sensor system for WAAM.

7.3 Specification and design of a WAAM monitoring framework

The author has proposed major process performance indicators and designed a multi-sensor framework for WAAM monitoring as described in chapter 4. The framework has been specifically designed for the WAAM process, providing the ability to monitor the geometry in real-time, with the mapping of performance indicators to enable sensor requirements. The framework incorporates process sensors, environment monitoring sensors and geometric monitoring sensors. All sensing data has been unified under one coordinate framework. This has extended the state of the art is WAAM monitoring through unifying the performance parameters and process parameters in to one coordinate system and enable researchers to study

the relationship between process parameters and WAAM part geometry. This framework has abstracted the monitoring process to 5 layers namely the sensor layer, the signal layer, the feature layer, the decision-making layer and the output layer. This enables an interchangeable and flexible approach to the selection of the sensors and the adaptability of the framework to be considered for other DED processes.

7.4 WAAM monitoring system evaluation

The literature provides examples from researchers who have demonstrated WAAM monitoring systems (Bonaccorso et al., 2011a, Xiong et al. 2015, Chen, B 2015) which prove that the systems function. Though, these provide functional proof of the monitoring system none of the current systems compared the process capability and parts produced as illustrated in chapter 6, in terms of accuracy and process parameters.

The author realised a multi-sensor system based on the conceptional design in chapter 4. This consists of 7 sensors which are in three sub-systems as described in section 5.4, namely heat monitoring sub-system, ii) bead geometry control sub-system, and iii) environmental monitoring sub-system. These sub-systems enabled a holistic process monitoring capability which has been successfully implemented on a large-scale WAAM manufacturing system. A critical part of the work is the sensor selection and the specific sensors implemented in terms of the functional capabilities, as outlined in section 5.3.

The major focus of monitoring systems in the literature has always been the height of the WAAM components as it is in this research. Two types of sensors are typically used in geometric data monitoring, namely passive optical monitoring and active optical monitoring. In the subset of passive optical monitoring, a camera has been the most commonly used sensor for monitoring geometric features. Xiong et al.(2013) realized the height and width detection for WAAM parts using two cameras. However, due to the camera obtaining the height and

width by capturing the width and height of the bead, it is challenging for this method to obtain these features on a multi-bead wall. and height are extracted and analysed.

As an alternative approach, the author has applied an active optical sensor namely dual laser profilometers to measure and monitor the shape of the WAAM produced part. The calibration method has been proposed and evaluated based on the calibration ball. To date, point cloud processing method on WAAM has not been clearly defined. The author proposed a pipeline to process the point cloud data. Using this method, it is able to measure the height and shape of the WAAM walls produced to an accuracy of 0.01 mm.

Measuring the height of the WAAM wall has always been challenging, due to the interference of the arc light emission. There are a few systems that achieved online height monitoring, i.e. the computer vision based system from Xiong et al. (2015) and the interferometer sensor system from Kissinger et al. 2019. A system from Xiong et al. (2016) utilizes a high contrast image to extract the molten bead height. This method only works for a single bead wall, but for a multi-bead wall, the camera view may be obstructed by the existing part. Another system from Kissinger et al. (2019) only monitors the height of a point, whereas the author proposed monitoring system that is able to monitor the entire top surface of a part.

7.5 Discussion of the results

Experiments have been designed to prove the capability of the WAAM monitoring system described in Chapter 5. These experiments show that the system is able to produce repeatable quality assured WAAM components.

The first experiment validates the essential capabilities of the voltage and current sensors which are essential for monitoring the het input of the WAAM process and can be used as an implicit indicator for arc length and height of the WAAM part. The electro-magnetic interference has been recognised by the author and reported in 6.3. Frequency spectrum

analysis has also been carried out on the voltage and current signal. The voltage signal shows two separate frequencies, namely a low frequency with increasing trend and also a high frequency due to oscillating toolpath. The current signal incorporates a statistical noise, spread out evenly across the spectrum which was difficult to be removed. A Kalman filtering method was applied and proved to be highly effective in filtering noise of up to 250 Amps.

The second experiment was designed to monitor and analyse the performance of the WAAM machine. A value distribution illustration method has been proposed and applied on voltage signal and current signal. The voltage signal varied across the whole building process, however it did not show any discontinuity which is expected. The current signal was precisely controlled by the powered module and the measured output was also constant throughout the process apart from the beginning and the end because of the arc ignition and termination.

The final experiment 3 provides a complete method to process the point cloud data generated from the dual laser profilometer system. It is noted that in order to utilise the dual laser profilometer system, a calibration process needs to be carried out in advance to calculate the relative position between two laser profilometers. The calibration process has been introduced in section 5.5.6. The height extraction process for a WAAM part has been described and evaluated. According to the evaluation, the accuracy of this method has been shown to be 0.01 mm and the layer height variation in a single layer is between 0~2 mm.

Chapter 8

Conclusions & Future work

8.1 Conclusions

(i) A monitoring framework has been specified and designed and implemented consisting of a number of different sensors to monitor the performance of the WAAM processes. This framework has shown that the WAAM process can be monitored based on the critical performance parameters that affect the quality of the built parts.

(ii) A WAAM monitoring system has been developed and tested and shown to have the ability to monitor, record and analyse the major output of the WAAM process to a high degree of detail. This monitoring system has been shown to provide rapid feedback at 5Hz that enables the WAAM process to be adjusted in real time.

(iii) To implement the monitoring system a new file format has been defined and used to unify the deposition process data and post deposition measurement data. This enables researchers to study the relationship between process parameters and WAAM part geometry.

(iv) A calibration method has been designed and implemented for a dual laser profilometer system to accurately measure the WAAM component height during process to an accuracy of 0.01mm. As the height of each layer is approximately 1.5mm this provides a highly accurate method to measure in-situ wall height.

(v) A number of experiments have been devised to enable a WAAM monitoring system to be evaluated. These scenarios consist of a test for dimensional accuracy of laser

profilometer and a second scenario used to evaluate calibration performance using a test block with several features for measurement.

(vi) A voltage analysis method has been developed and implemented to evaluate the voltage clamp sensor. The analysis method shows the variation of the voltage at low frequency and high frequency fluctuation during the WAAM deposition process.

(vii) A new point cloud processing pipeline has been established to extract features of the built WAAM parts, such as the height, width, top surface and side surface dimensions to an accuracy of 0.01mm. This was used for post process analysis of the WAAM produced parts but could also be used for real time compensation for geometric compensation.

(viii) A voltage mapping of the WAAM process has been created and implemented to show the variation of the voltage against the welding path. This analysis provides an extremely valuable voltage map of each welded layer deposited to show the height variation reflected on voltage changes for each individual component.

8.2 Contribution to Knowledge

This research provides a new framework for the monitoring of WAAM based processes consisting of a number of sensors which are integrated to enable comprehensive system monitoring of a WAAM based machine. The WAAM monitoring system has been tested and evaluated for producing different types of components and the results have shown that the system can effectively enable quality components to be produced and can be used to identify different types of issues during production process.

8.3 Further work

8.3.1 Short term work

(i) The WAAM monitoring of the built side wall profiles requires improvement as the resolution of the laser profilometers is approximately only 0.5mm, which does not reflect the actual waviness of the side wall. The resolution of the current laser profilometer as described in section 5.5 needs to be improved to approximately 0.1mm to provide enough measurement accuracy on vertical direction.

(ii) The current laser profilometer is for general purpose usage which is incompatible to the high light emission and heat radiation in welding application. Because of this, the current process only enables after deposition geometric measurement. The laser profilometer should be replaced with a welding tracking sensor which is the same type of sensor but is able to work along with welding torch.

8.3.2 Longer term work

(i) The WAAM process parameters were initially defined by the industrial partners of the Innovate UK RAWFEED project based on historical and empirical data. There is a need to further investigate the best process parameters for the WAAM process based on the experiments. These process parameters need to be modified based on the process monitoring system results in real-time so the system can be considered a process control system.

(ii) Since the author has proposed a method to extract the top surface dimension of the built part during the WAAM process. This method enables the establishment of a highly accurate WAAM wall model, which would be highly valuable for WAAM modelling and simulation.

(iii) The author has proposed a reliable process monitoring method which could provide accurate dimensions of the part. This method can use these dimensions in the future as feedback to realize a WAAM closed loop control and compensation system.

(iv) The sensors that have been used for the WAAM monitoring system, have been selected based on their use in welding applications and generic purposes. In order to provide specifically designed WAAM geometric sensor which would enable measurement of both the side and top surface of the built components.

(v) As the framework is based on a generic requirement of WAAM process, the research should be evaluated on other WAAM machines and other similar processes such as laser cladding and electron-beam DED.

(vi) Identify the relationship between current, voltage and profile of the part, and provide a method to determine proper voltage and current.

8.4 Reflections and Challenges

At the beginning of this research, the knowledge for WAAM process monitoring and related sensors was limited. The equipment used in this research was a generic welding device. The WAAM process required the welding power module to adjust the voltage and current in the process, which was not well supported by generic welding machine. As the development process evolved, parts with larger sizes (i.e. 50mm height and 20mm width) and more layers were deposited (i.e. 40 layers). The tremendous heat accumulation was unexpected and raised new challenges for process plan and monitoring. The ad-hoc solution is to increase the thickness of the baseplate, though this can bear higher residual stresses in the part.

The WAAM process parameters were initially defined by the industrial partners of the RAWFEED project based historical and empirical data. This part of research will be added to future work. There is a need to further investigate the best process parameters for the WAAM

process based on the experiments. These process parameters need to be modified based on the process monitoring system results in real-time so the system can be considered a process control system.

References

Aiyiti, W., W. Zhao, B. Lu, and Y. Tang. 2012. Investigation of the Overlapping Parameters of MPAW-Based Rapid Prototyping. doi:10.1108/13552540610670744.

Almeida, P. M. S.. 2012. Process Control and Development in Wire and Arc Additive Manufacturing, No. April: 1–467.

Anzehaee, M. M., and M. Haeri. 2011. We.lding current and arc voltage control in a GMAW process using ARMarkov based MPC. Control Engineering Practice 19, no. 12 (2011): 1408-1422.

Ayres, P. S., D. P. Edmonds, D. D. Hartwig, D. E. Merker, and C. M. Weber. 1988. Method and Apparatus for Controlling Weld Bead Shape to Eliminate Microfissure Defects When Shape Melting Austenitic Materials, no. 19.

Baker, R.. 1920. Method of Making Decorative Articles. *US Patent*, 1–3. https://drive.google.com/viewerng/viewer?url=patentimages.storage.googleapis.com/pdfs/US1533300.pdf.

Baufeld, B., O. V. D. Biest, and R. Gault. 2010. Additive Manufacturing of Ti-6Al-4V Components by Shaped Metal Deposition: Microstructure and Mechanical Properties. *Materials and Design* 31 (SUPPL. 1). Elsevier Ltd: S106–11. doi:10.1016/j.matdes.2009.11.032.

Baufeld, B., O. V. D. Biest, and S. Dillien. 2010. Texture and Crystal Orientation in Ti-6Al-4V Builds Fabricated by Shaped Metal Deposition. *Metallurgical and Materials Transactions A: Physical Metallurgy and Materials Science* 41 (8): 1917–27. doi:10.1007/s11661-010-0255-x.

Baufeld, Bernd, O. V. D. Biest, R. Gault, and K. Ridgway. 2011. Manufacturing Ti-6Al-4V Components by Shaped Metal Deposition: Microstructure and Mechanical Properties. *IOP Conference Series: Materials Science and Engineering* 26: 012001. doi:10.1088/1757-899X/26/1/012001.

Baufeld, Bernd, Erhard Brandl, and Omer Van der Biest. Wire based additive layer manufacturing: Comparison of microstructure and mechanical properties of Ti–6Al–4V components fabricated by laser-beam deposition and shaped metal deposition. *Journal of Materials Processing Technology* 211, no. 6 (2011): 1146-1158.

Bonaccorso, F., C. Bruno, L. Cantelli, D. Longo, and G/ Muscato. 2009. Control of a Shaped Metal Deposition Process. *Physics Conference (PHYSCON)*, 1–5.

Bonaccorso, F., L. Cantelli, and G. Muscato. An arc welding robot control for a shaped metal deposition plant: Modular software interface and sensors. IEEE Transactions on Industrial Electronics 58, no. 8 (2011): 3126-3132.

Bonaccorso, F., L. Cantelli, and G. Muscato. 2011. Arc Welding Control for Shaped Metal Deposition Process. *IFAC Proceedings Volumes (IFAC-PapersOnline)* 18 (PART 1): 11636–41. doi:10.3182/20110828-6-IT-1002.01575.

BSI. 2015. BSI Standards Publication Additive Manufacturing — General Principles Part 2 : Overview of Process Categories and Feedstock.

Chen, B., J. Wang, and S. Chen. 2010. A Study on Application of Multi-sensor Information Fusion in Pulsed GTAW. *Industrial Robot: An International Journal* 37 (2): 168–76. doi:10.1108/01439911011018948.

Chen, B., J. Wang, and S. Chen. 2010. Prediction of Pulsed GTAW Penetration Status Based on BP Neural Network and D-S Evidence Theory Information Fusion. *International Journal of Advanced Manufacturing Technology* 48 (1–4): 83–94. doi:10.1007/s00170-009-2258-6.

Chen, S.. On intelligentized welding manufacturing. In Robotic Welding, Intelligence and Automation, pp. 3-34. Springer, Cham, 2015.

Chen, Z., J. Chen, Z. Feng, and Y. Zhang. 2016. In Situ Strain Monitoring in Gas Tungsten Arc Welding Processes. *2016 IEEE International Conference on Advanced Intelligent Mechatronics (AIM)*, 800–804. doi:10.1109/AIM.2016.7576866.

Colegrove, P. A., H. E. Coules, J. Fairman, F. Martina, T. Kashoob, H. Mamash, and L. D. Cozzolino. 2013. Microstructure and Residual Stress Improvement in Wire and Arc Additively Manufactured Parts through High-Pressure Rolling. *Journal of Materials Processing Technology* 213 (10). Elsevier B.V.: 1782–91. doi:10.1016/j.jmatprotec.2013.04.012.

Colegrove, P. A., F. Martina, M. J. Roy, B. A. Szost, S. Terzi, S. W. Williams, P. J. Withers, and D. Jarvis. High pressure interpass rolling of wire+ arc additively manufactured titanium components. *Advanced Materials Research*, vol. 996, pp. 694-700. Trans Tech Publications Ltd, 2014.

Ding, D., Z. Pan, D. Cuiuri, H. Li, N. Larkin, and S. V. Duin. 2016. Automatic multi-direction slicing algorithms for wire based additive manufacturing. Robotics and Computer-Integrated Manufacturing 37 (2016): 139-150.

Ding, D., Z. Pan, D. Cuiuri, and H. Li. 2015. A Multi-Bead Overlapping Model for Robotic Wire and Arc Additive Manufacturing (WAAM). Robotics and Computer Integrated Manufacturing 31. Elsevier: 101–10. doi:10.1016/j.rcim.2014.08.008.

Ding, D., Z. Pan, D. Cuiuri, and H. Li. 2015. A Practical Path Planning Methodology for Wire and Arc Additive Manufacturing of Thin-Walled Structures. *Robotics and Computer Integrated Manufacturing* 34. Elsevier: 8–19. doi:10.1016/j.rcim.2015.01.003.

Ding, D., Z. Pan, D. Cuiuri, and H. Li. 2015. Wire-Feed Additive Manufacturing of Metal Components : Technologies , Developments and Future Interests, 465–81. doi:10.1007/s00170-015-7077-3..

Ding, D., Z. Pan, D. Cuiuri, H. Li, and N. Larkin. 2016. Adaptive Path Planning for Wire-Feed Additive Manufacturing Using Medial Axis Transformation. *Journal of Cleaner Production* 133. Elsevier Ltd: 942–52. doi:10.1016/j.jclepro.2016.06.036.

Ding, Feng, Xiaoping Peter Liu, and Guangjun Liu. Identification methods for Hammerstein nonlinear systems. Digital Signal Processing 21, no. 2 (2011): 215-238.

Ding, J, P. Colegrove, J. Mehnen, and S. Williams. 2014. A Computationally Efficient Finite Element Model of Wire and Arc Additive Manufacture, 227–36. doi:10.1007/s00170-013-5261-x.

Ding, J., P. Colegrove, F. Martina, S. Williams, R. Wiktorowicz, and M.R. Palt. 2015. Development of a Laminar Flow Local Shielding Device for Wire+arc Additive Manufacture. *Journal of Materials Processing Technology* 226. Elsevier B.V.: 99–105. doi:10.1016/j.jmatprotec.2015.07.005.

Ding, J., P. Colegrove, J. Mehnen, S. Ganguly, P. M.Sequeira Sequeira Almeida, F. Wang, and S. Williams. 2011. Thermo-Mechanical Analysis of Wire and Arc Additive Layer Manufacturing Process on Large Multi-Layer Parts. *Computational Materials Science* 50 (12). Elsevier B.V.: 3315–22. doi:10.1016/j.commatsci.2011.06.023.

Ding, J., 2012. Thermo-Mechanical Analysis of Wire and Arc Additive Manufacturing Process.

Donoghue, J., A. A. Antonysamy, F. Martina, P. A. Colegrove, S.W. Williams, and P. B. Prangnell. The effectiveness of combining rolling deformation with Wire–Arc Additive Manufacture on β-grain refinement and texture modification in Ti–6Al–4V. *Materials Characterization* 114 (2016): 103-114.

DoPont, J. N., and A. R. Marder. 1995. Thermal Efficiency of Arc Welding Processes, no. December.

Doumanidis, C., and Y. M. Kwak. 2002. Multivariable Adaptive Control of the Bead Profile Geometry in Gas Metal Arc Welding with Thermal Scanning. *International Journal of Pressure Vessels and Piping* 79 (4): 251–62. doi:10.1016/S0308-0161(02)00024-8.

Doyle, T. E., D. P. Edmonds, M. D. McAninch, and P. M. Ryan. 1989. Method and Apparatus for Building a Workpiece by Deposit Welding, no. 19.

Escobar-Palafox, G., R. Gault, and K. Ridgway. 2011. Preliminary Empirical Models for Predicting Shrinkage, Part Geometry and Metallurgical Aspects of Ti-6Al-4V Shaped Metal Deposition Builds. *IOP Conference Series: Materials Science and Engineering* 26 (1): 1–8. doi:10.1088/1757-899X/26/1/012002.

Escobar-Palafox, G., R. Gault, and K. Ridgway. 2011. Robotic Manufacturing by Shaped Metal Deposition: State of the Art. *Industrial Robot: An International Journal* 38 (6): 622–28. doi:10.1108/01439911111179138.

Feng, J., L. Li, Y. Chen, Z. Lei, H. Qin, and Y. Li. 2012. Effects of Welding Velocity on the Impact Behavior of Droplets in Gas Metal Arc Welding. Journal of Materials Processing Technology 212 (11): 2163–72. https://doi.org/10.1016/j.jmatprotec.2012.02.016.

Font Comas, T., C. Diao, J. Ding, S. Williams, and Yifan Zhao. 2017. A Passive Imaging System for Geometry Measurement for the Plasma Arc Welding Process. *IEEE Transactions on Industrial Electronics* 64 (9): 1–1. doi:10.1109/TIE.2017.2686349.

Geng, H., J. Li, J. Xiong, X. Lin, and F. Zhang. 2017. Optimization of Wire Feed for GTAW Based Additive Manufacturing. *Journal of Materials Processing Technology* 243. Elsevier B.V.: 40–47. doi:10.1016/j.jmatprotec.2016.11.027.

Geomagic. 2019. Available online: https://uk.3dsystems.com/software#design-software (Accessed on 13 November 2019)

Gockel, J., and J. Beuth. 2013. Understanding Ti-6Al-4V Microstructure Control in Additive Manufacturing via Process Maps. *Solid Freeform Fabrication Symposium*, 666. doi:10.1007/s11837-005-0029-x.

Gockel, J., J. Beuth, and K. Taminger. 2014. Integrated Control of Solidification Microstructure and Melt Pool Dimensions in Electron Beam Wire Feed Additive Manufacturing of Ti-6al-4v. *Additive Manufacturing* 1. Elsevier B.V.: 119–26. doi:10.1016/j.addma.2014.09.004.

Gockel, J., L. Sheridan, S. P. Narra, N. W. Klingbeil, and J. Beuth. 2017. Trends in Solidification Grain Size and Morphology for Additive Manufacturing of Ti-6Al-4V. *Jom* 69 (12). Springer US: 2706–10. doi:10.1007/s11837-017-2601-6.

Gu, H, and W W Duley. 1996. A Statistical Approach to Acoustic Monitoring of Laser Welding. *Journal of Physics D: Applied Physics* 29 (3): 556–60. doi:10.1088/0022-3727/29/3/011.

Han, Qinglin, Y. Li, and G. Zhang. 2018. Online Control of Deposited Geometry of Multi-Layer Multi-Bead Structure for Wire and Arc Additive Manufacturing, 85–93. doi:10.1007/978-981-10-5355-9.

Heralic´, A., A. Christiansson, and B. Lennartson. 2012. Height Control of Laser Metal-Wire Deposition Based on Iterative Learning Control and 3D Scanning 50: 1230–41. doi:10.1016/j.optlaseng.2012.03.016.

Ho, A., H. Zhao, J.W. Fellowes, F. Martina, A.E. Davis and P.B. Prangnell. 2019. On the origin of microstructural banding in Ti-6Al4V wire-arc based high deposition rate additive manufacturing. Acta Materialia, 166, pp.306-323.

Huang, R-S., L-M. Liu, and G. Song. 2007. Infrared temperature measurement and interference analysis of magnesium alloys in hybrid laser-TIG welding process. Materials Science and Engineering: A 447, no. 1-2 (2007): 239-243.

Kazanas, P., P. Deherkar, P. Almeida, H. Lockett, and S. Williams. 2012. Fabrication of Geometrical Features Using Wire and Arc Additive Manufacture. Proceedings of the Institution of Mechanical Engineers, Part B: Journal of Engineering Manufacture 226 (6): 1042–51. doi:10.1177/0954405412437126.

Kissinger, T., B. Gomis, J. Ding, S. W. Williams, and R. P. Tatam. 2019 Measurements of Wire+ Arc additive manufacturing layer heights during arc operation using coherent range-

resolved interferometry (CO-RRI). Joint Special Interest Group meeting between euspen and ASPE Advancing Precision in Additive Manufacturing

Li, W., Y. Ji, J. Wu, and J. Wang. 2015. A Modified Welding Image Feature Extraction Algorithm for Rotating Arc Narrow Gap MAG Welding. *Industrial Robot* 42 (3): 222–27. doi:10.1108/IR-11-2014-0407.

Lü, F., H. Chen, C. Fan, and S. Chen. 2010. A Novel Control Algorithm for Weld Pool Control. *Industrial Robot: An International Journal* 37 (1): 89–96. doi:10.1108/01439911011009993.

Lv, N., and S. Chen. 2011. Investigation on Acoustic Signals for On-Line Monitoring of Welding. *Robotic Welding, Intelligence and Automation*, 235–43.

Martina, F., J. Mehnen, S. W. Williams, P. Colegrove, and F. Wang. 2012. Investigation of the Benefits of Plasma Deposition for the Additive Layer Manufacture of Ti-6Al-4V. *Journal of Materials Processing Technology* 212 (6). Elsevier B.V.: 1377–86. doi:10.1016/j.jmatprotec.2012.02.002.

Martina, F.. 2014. Investigation of Methods to Manipulate Geometry, Microstructure and Mechanical Properties in Titanium Large Scale Wire+Arc Additive Manufacturing, 178. https://dspace.lib.cranfield.ac.uk/bitstream/1826/9270/1/Martina_Filomeno_Thesis_2014.pdf.

Martina, F., S. W. Williams, F. Martina, A. C. Addison, J. Ding, G. Pardal, and P. Colegrove. 2015. Wire + Arc Additive Manufacturing Wire þ Arc Additive Manufacturing, no. MAY. doi:10.1179/1743284715Y.0000000073.

Mazak. 2018. Variaxis j-600AM. Available online: https://www.mazakusa.com/news-events/news-releases/new-variaxis-j-600am-grows-the-mazak-additive-series/ (Accessed on 13 November 2019)

Metal AM. 2018 Boeing and Norsk Titanium recognised for metal additively manufactured structural components Available on: http://www.metal-am.com/boeing-norsk-titanium-recognised-metal-additively-manufactured-structural-components/

Micro-Epsilon. 2018. Catalogue thermoMETER. Micro-Epsilon Website. Available on: https://www.micro-epsilon.co.uk/temperature-sensors/thermoMETER_CT_basic/

Moore, K. L., D. S. Naidu, and S. Ozcelik. 2003. Modeling, sensing and control of gas metal arc welding. Kidlington (UK): Elsevier Science Ltd (2003).

Mughal, M.P., H. Fawad, R.A. Mufti, and M. Siddique. 2005. Deformation modelling in layered manufacturing of metallic parts using gas metal arc welding: effect of process parameters. Modelling and Simulation in Materials Science and Engineering, 13(7), p.1187.

Muscato, G., V. A Doria, G. Spampinato, Viale A Doria, Luciano Cantelli, and Viale A Doria. 2008. A Closed Loop Welding Controller for a Rapid Manufacturing Process, 1080–83.

Nippes, E. F. 1983 Metals Handbook; Vol. 6, Welding, Brazing and Soldering. American Society for Metals, 1983, (1983): 1152.

Norsk Titanium. 2017. Norsk Titanium Marks Milestone in U.S. Production Norsk Titanium Website. Available on: https://www.norsktitanium.com/media/press/norsk-titanium-marks-milestone-in-u-s-production

Ogawa, Y. 2011. High Speed Imaging Technique Part 1 – High Speed Imaging of Arc Welding Phenomena. *Science and Technology of Welding and Joining* 16 (1): 33–43. doi:10.1179/136217110X12785889549903.

Ogawa, Y. 2011. High Speed Imaging Technique Part 2 - High Speed Imaging of Power Beam Welding Phenomena. *Science and Technology of Welding and Joining* 16 (1): 33–43. doi:10.1179/136217110X12785889549903.

Ogawa, Yoji. 2012. Visual Analysis of Welding Processes. R. Kovacevic, INTEC (2012): 277-304.

Pan, B., K. Qian, H. Xie, and A. Asundi. 2009. Two-Dimensional Digital Image Correlation for in-Plane Displacement and Strain Measurement: A Review. *Measurement Science and Technology* 20 (6). doi:10.1088/0957-0233/20/6/062001.

Polajnar, I., Z. Bergant, and J. Grum. 2013. ARC Welding Process Monitoring by Audible Sound. *12th International Conference of the Slovenian Society for Non-Destructive Testing: Application of Contemporary Non-Destructive Testing in Engineering, ICNDT 2013 - Conference Proceedings*, 613–20.

Rhino. 2019. Available online: https://www.rhino3d.com/ (Accessed on 13 November 2019)

Rusu, R.B.. 2010. Semantic 3d object maps for everyday manipulation in human living environments. KI-Künstliche Intelligenz 24, no. 4 (2010): 345-348.

Rusu, R.B. and S. Cousins. 2011. 3d is here: Point cloud library (pcl). In 2011 IEEE international conference on robotics and automation (pp. 1-4). IEEE.

Saeed, G, and Y. M. Zhang. 2003. Mathematical Formulation and Simulation of Specular Reflection Based Measurement System for Gas Tungsten Arc Weld Pool Surface. *Measurement Science & Technology* 14 (9): 1671–82. doi:Pii S0957-0233(03)62385-4\rDoi 10.1088/0957-0233/14/9/319.

Saeed, G., and Y. M. Zhang. 2007. Weld Pool Surface Depth Measurement Using a Calibrated Camera and Structured Light. *Measurement Science and Technology* 18 (8): 2570–78. doi:10.1088/0957-0233/18/8/033.

Saeed, G., M. Lou, and Y. M. Zhang. 2004. Computation of 3D Weld Pool Surface from the Slope Field and Point Tracking of Laser Beams. *Measurement Science and Technology* 15 (2): 389–403. doi:10.1088/0957-0233/15/2/012.

Segerstark, A., J. Andersson, and L. Svensson. 2017. Evaluation of a Temperature Measurement Method Developed for Laser Metal Deposition. *Science and Technology of Welding and Joining* 22 (1). Taylor & Francis: 1–6. doi:10.1080/13621718.2016.1169363.

Strang, G. 1993. Introduction to linear algebra (Vol. 3). Wellesley, MA: Wellesley-Cambridge Press.

Sorkine, O., 2009. Least-squares rigid motion using SVD. Technical notes, 120(3), p.52.

Spencer, J. D., P. M. Dickens, and C. M. Wykes. 1998. Rapid prototyping of metal parts by three-dimensional welding. Proceedings of the Institution of Mechanical Engineers, Part B: Journal of Engineering Manufacture 212, no. 3 (1998): 175-182.

Taminger, K. M., and R. A. Hafley. Electron beam freeform fabrication for cost effective near-net shape manufacturing. (2006).

Taminger, K. M., and R. A. Hafley. 2003. Electron Beam Freeform Fabrication: A Rapid Metal Deposition Process. *Proceedings of the 3rd Annual Automotive Composites Conference*, 9–10.

Thomas, D. S., and S. W. Gilbert. Costs and cost effectiveness of additive manufacturing, NIST Special Publication 1176 (2014): 12.

TWI, 2019, Additive Manufacture of Complex Components using CMT, TWI, UK, web-address: https://www.twi-global.com/media-and-events/insights/additive-manufacture-of-aluminium-alloy-components-using-the-cold-metal-transfer-cmt-process, accessed 19/11/2019.

Unocic, R.R. R, and J.N. N DuPont. 2004. Process Efficiency Measurements in the Laser Engineered Net Shaping Process. *Metallurgical and Materials Transactions B* 35 (February): 143–52. doi:10.1007/s11663-004-0104-7.

Van Herwaarden, A.W. and P.M. Sarro.1986. Thermal sensors based on the Seebeck effect. Sensors and Actuators, 10(3-4), pp.321-346.

Wang, J. F., B. Chen, H. B. Chen, and S. B. Chen. 2009. Analysis of Arc Sound Characteristics for Gas Tungsten Argon Welding. *Sensor Review* 29 (3): 240–49. doi:10.1108/02602280910967657.

Węglowski, M.S., 2012. Monitoring of arc welding process based on arc light emission. Welding Processes, p.305.

Williams, S. W., F. Martina, A. C. Addison, J. Ding, G. Pardal, and P. Colegrove. 2015. Wire + Arc Additive Manufacturing. *Materials Science and Technology* 0836 (March): 1743284715Y.000. doi:10.1179/1743284715Y.0000000073.

Wu, B., D. Ding, Z. Pan, D. Cuiuri, H. Li, J. Han, and Z. Fei. 2017. Effects of Heat Accumulation on the Arc Characteristics and Metal Transfer Behavior in Wire Arc Additive Manufacturing of Ti6Al4V. Journal of Materials Processing Technology 250 (December 2016). Elsevier: 304–12. doi:10.1016/j.jmatprotec.2017.07.037.

Wu, C. S., L. Wang, W. J. Ren, and X. Y. Zhang. 2014. Plasma Arc Welding: Process, Sensing, Control and Modeling. *Journal of Manufacturing Processes* 16 (1): 74–85. doi:10.1016/j.jmapro.2013.06.004.

Wu, C.S. 2008. Weld Pool Surface Monitoring. *Real-Time Weld Process Monitoring*, 213–37. doi:10.1533/9781845694401.2.213.

Wu, L., and G. J. Zhang. 2008. Weld Profile Monitoring. *Real-Time Weld Process Monitoring*, 164–85. doi:10.1533/9781845694401.2.164.

Wu, Q., J. Lu, C. Liu, H. Fan, X. Shi, J. Fu, and S. Ma. 2017. Effect of Molten Pool Size on Microstructure and Tensile Properties of Wire Arc Additive Manufacturing of Ti-6Al-4V Alloy. *Materials* 10 (7): 1–11. doi:10.3390/ma10070749.

Wu, Q., J. Lu, C. Liu, X. Shi, Q. Ma, S. Tang, H. Fan, and S. Ma. 2017. Obtaining Uniform Deposition with Variable Wire Feeding Direction during Wire-Feed Additive Manufacturing. *Materials and Manufacturing Processes* 32 (16). Taylor & Francis: 1881–86. doi:10.1080/10426914.2017.1364860.

Xiong, J., and G. Zhang. 2013. Online Measurement of Bead Geometry in GMAW-Based Additive Manufacturing Using Passive Vision. *Measurement Science and Technology* 24 (11): 115103. doi:10.1088/0957-0233/24/11/115103.

Xiong, J., and G. Zhang. 2014. Adaptive Control of Deposited Height in GMAW-Based Layer Additive Manufacturing. *Journal of Materials Processing Technology* 214 (4). Elsevier B.V.: 962–68. doi:10.1016/j.jmatprotec.2013.11.014.

Xiong, J., G. Zhang, and W. Zhang. 2015. Forming Appearance Analysis in Multi-Layer Single-Pass GMAW-Based Additive Manufacturing, 1767–76. doi:10.1007/s00170-015-7112-4.

Xiong, J., G. Zhang, H. Gao, and L. Wu. 2013. Modeling of Bead Section Profile and Overlapping Beads with Experimental Validation for Robotic GMAW-Based Rapid Manufacturing. *Robotics and Computer-Integrated Manufacturing* 29 (2). Elsevier: 417–23. doi:10.1016/j.rcim.2012.09.011.

Xiong, J., G. Zhang, J. Hu, and L. Wu. 2014. Bead Geometry Prediction for Robotic GMAW-Based Rapid Manufacturing through a Neural Network and a Second-Order Regression Analysis. *Journal of Intelligent Manufacturing* 25 (1): 157–63. doi:10.1007/s10845-012-0682-1.

Xiong, J., G. Zhang, J. Hu, and Y. Li. 2013. Forecasting Process Parameters for GMAW-Based Rapid Manufacturing Using Closed-Loop Iteration Based on Neural Network, 743–51. doi:10.1007/s00170-013-5038-2.

Xiong, J., G. Zhang, Z. Qiu, and Y. Li. 2013. Vision-Sensing and Bead Width Control of a Single-Bead Multi-Layer Part: Material and Energy Savings in GMAW-Based Rapid Manufacturing. *Journal of Cleaner Production* 41. Elsevier Ltd: 82–88. doi:10.1016/j.jclepro.2012.10.009.

Xiong, J., Y. Lei, H. Chen, and G. Zhang. 2017. Fabrication of Inclined Thin-Walled Parts in Multi-Layer Single-Pass GMAW-Based Additive Manufacturing with Flat Position Deposition. *Journal of Materials Processing Technology* 240. Elsevier B.V.: 397–403. doi:10.1016/j.jmatprotec.2016.10.019.

Xiong, J., Z. Yin, and W. Zhang. 2016. Closed-Loop Control of Variable Layer Width for Thin-Walled Parts in Wire and Arc Additive Manufacturing. *Journal of Materials Processing Technology* 233. Elsevier B.V.: 100–106. doi:10.1016/j.jmatprotec.2016.02.021.

Xu, F., Dhokia, V., Colegrove, P., McAndrew, A., Williams, S., Henstridge, A. and Newman, S.T., 2018. Realisation of a multi-sensor framework for process monitoring of the wire arc additive manufacturing in producing Ti-6Al-4V parts. International Journal of Computer Integrated Manufacturing, 31(8), pp.785-798.

Xu, Y., J. Zhong, M. Ding, H. Chen, and S. Chen. 2012. The Acquisition and Processing of Real-Time Information for Height Tracking of Robotic GTAW Process by Arc Sensor. *International Journal of Advanced Manufacturing Technology*, 1031–43. doi:10.1007/s00170-012-4237-6.

Yang, X., G. Yan, Y. Xiu, Z. Yang, G. Wang, W. Liu, S. Li, and W. Jiang. 2019. Welding Temperature Distribution and Residual Stresses in Thick Welded Plates of SA738Gr. B Through Experimental Measurements and Finite Element Analysis. Materials 12, no. 15 (2019): 2436.

Yilmaz, O., and A. A. Ugla. 2017. Microstructure Characterization of SS308LSi Components Manufactured by GTAW-Based Additive Manufacturing: Shaped Metal Deposition Using Pulsed Current Arc. *International Journal of Advanced Manufacturing Technology* 89 (1–4). The International Journal of Advanced Manufacturing Technology: 13–25. doi:10.1007/s00170-016-9053-y.

Zhang, F., K. Yu, K. Zhang, Y. Liu, K. Xu, and Y. Liu. An emissivity measurement apparatus for near infrared spectrum. Infrared Physics & Technology 73 (2015): 275-280.

Zhang, G., Z. Yan, and L. Wu. 2006. Reconstructing a Three-Dimensional P-GMAW Weld Pool Shape from a Two-Dimensional Visual Image. *Measurement Science and Technology* 17 (7): 1877–82. doi:10.1088/0957-0233/17/7/028.

Zhang, W., X. Wang, and Y. Zhang. 2013. Analytical Real-Time Measurement of a Three-Dimensional Weld Pool Surface. *Measurement Science and Technology* 24 (11). doi:10.1088/0957-0233/24/11/115011.

Zhang, W., X. Zhang, and Y. Zhang. 2015. Robust Pattern Recognition for Measurement of Three Dimensional Weld Pool Surface in GTAW. *Journal of Intelligent Manufacturing* 26 (4). Springer US: 659–76. doi:10.1007/s10845-013-0825-z.

Zhang, Z., X. Chen, H. Chen, J. Zhong, and S. Chen. 2014. Online Welding Quality Monitoring Based on Feature Extraction of Arc Voltage Signal. *International Journal of Advanced Manufacturing Technology* 70 (9–12): 1661–71. doi:10.1007/s00170-013-5402-2.

Zhou, Q., J. Park, and V. Koltun. 2018. Open3D: A modern library for 3D data processing. arXiv preprint arXiv:1801.09847 (2018).

Appendix A Publications

Journal Papers

2018 **F. Xu,** V. Dhokia, P. Colegrove, A. McAndrew, S. Williams, *A. Henstridge and S.T. Newman. Realization of A Multi-Sensor Framework for Process Monitoring of the Wire Arc Additive Manufacturing in Producing Ti6Al4V Parts.* International Journal of Computer Integrated Manufacturing. 2018.

Conference Papers

2017 C.R. Cunningham, S. Wikshåland, **F. Xu**, N. Kemakolam, A.Shokrani, V. Dhokia, and S.T. Newman. *Cost Modelling and Sensitivity Analysis of Wire and Arc Additive Manufacturing. Procedia Manufacturing*. 2017, 11: 650-657

2016 **F. Xu**, N. Madhavan, V. Dhokia, A.R. McAndrew, P. Colegrove, S. Williams, *A. Henstridge and S.T. Newman, Multi-Sensor System for Wire-Fed Additive Manufacture of Titanium Alloys*. Proceedings of Flexible Automation and Intelligent Manufacturing. 2016.